Universität Zürich[UZH]

Geographisches Institut

Persistence of a Low-Altitude Alpine Glacier: The Influence of Avalanches, Shading, and Debris

GEO 511 Master's Thesis

Author: Mattia Salvi, 20-709-770

Supervised by: Dr. Martin Lüthi

Faculty representative: Prof. Dr. Andreas Vieli

29.08.2025

Abstract

In the Swiss Alps, an exceptional glacier – the Clariden-N Glacier – persists under extreme conditions. Near Klausen Pass and north of the Clariden, this glacier is situated with an average altitude far lower than typical for the region or the European Alps (~2220 m a.s.l. in 2022). And despite this low altitude, it has persisted far longer than regional climate conditions would suggest. This thesis investigates three processes that might allow its persistence and reconstructs its past, present, and future evolution.

A combination of glaciological stake observations (2023–2025), geodetic DEM differencing (2013–2022), process-based analyses (avalanche input, topographic shading, debris cover), and a calibrated 1-D shallow-ice approximation flowline model was applied. The geodetic mass balance yielded a glacier-wide loss of −0.74 ± 0.05 m w.e. a^{-1}, while glaciological measurements recorded maximum local ablation of −2.19 ± 0.17 m w.e. a^{-1}. Avalanche mapping from more than 7000 hourly images over nearly two years showed deposition on 60% of the observed glacier surface. Topographic shading was found to reduce potential incoming shortwave radiation by ~37% (~751 kWh m^{-2} a^{-1}). Debris cover measurements confirmed a strong insulating effect on the tongue. Model calibration reproduced the 2022 glacier length within 9–27 m across configurations, though past retreat rates were underestimated, probably due to the absence of frontal-ablation processes.

The results indicate that the persistence of Clariden-N Glacier is explained by a unique interplay of frequent avalanche supply in proximity to the headwalls, extensive debris insulation on most surfaces, and strong topographic shading increasing towards the headwall, which together counteract otherwise unfavourable climatic conditions. Nevertheless, simulations and field evidence point to its imminent extinction within the next 20–30 years, with only avalanche-fed remnants near the headwall surviving somewhat longer. With that, the water reservoir for the lake will be gone and altering the hydrological system of the lake and stream below.

This study highlights the resilience of low-altitude glaciers in complex settings and emphasises the necessity to improve the understanding of avalanche feeding, debris cover, topographic shading, and lake interactions on the glacier mass balance. Studying such outliers provides valuable insights for improving projections of glacier change in a rapidly warming world.

Zämmefassig

Ih de Schwiizer Alpe, nöd wiit vom Klausenpass und grad nördlich vom Clariden, liht en ganz bsundrige Gletscher – dä Clariden-Nord Gletscher. Sini durchschnittlichi Höchi isch so viel tüfer als alles andere was mer us der Region oder de Alpe kennt. Und trotzdem, gits ihn hüt no und er hebt sich trotz em wärmer werdende Klima überraschen guet. I dere Arbeit wird ahgluegt, weli Prozess entscheidend sind, damit de Gletscher überhaupt chan existiere. Es wird au untersuecht was für eh Entwicklig er ih de Vergangeheit duregmach het, wo er hüt stoht und wies ihm de Zuekunft ergoh wird.

Für das sind vo 2023 bis 2025 Messige direkt ufem Gletscher gmacht worde zum die maximali Schmelzi zbestimme. Usserdem, isch en geodätischi Höhenmodell-Vergliich (2013–2022), ä Prozessanalysä (Lawine, Schatte, Schuttbedeckig) und es 1-D Modell ahgwendet worde. Di geodätisch Massebilanz zeigt en Verlust vo öppe −0.74 ± 0.05 m w.e. pro Jahr, während die direkte Messige e maximali Schmelzi vo −2.19 ± 0.17 m w.e. pro Jahr zeigt händ. D Lawine-Analyse mit über 7000 Bilde us zwei Johr het zeigt, dass 60% vo de Gletscherflächi Lawinenschnee becho hät. De Schatte het d Sonnästrahlig um rund 37% (751 kWh pro m² im Johr) reduziert. D Schuttdeckig isch mächtig und zeigt en starche Isolations-Effekt. S Gletschermodell het d Längi usem johr 2022 sehr guet chöne nohbilde (uf öppe 9–27 Meter Abweichig), aber het d Entwicklig zwüsched 1951 und 2022 sehr unterschätzt, was wahrschindlich do dra liiht, dass d Interaktion mit dem Gleschsee nöd berücksigt worde isch.

D Resultat zeiged: dä Clariden-N Gletscher bliibt no en moment bestoh. Das liiht hauptsächlich am Zemespiel zwüsched viel Lawineschnee, de dicke Schuttschicht und am grosse Schattewurf vom Claride. Zeme kämpfed die Effekt gege s ungünstige Klima. D Modelle und d Beobachtige zeiged aber au, dass ih 20 bis 30 Jahr de Gletscher wäg isch und viellicht nur no en chline Reste wo no vo paar Lawinen gfüetteret wird übrig bliebt. Mit dem verschwindet au dä Wasserspeicher für s Griessseeli, was d Hydrologie vom See und de Bäch unterhalb verändere wird.

D Arbeit zeigt, dass tüf liegendi Gletscher ih komplexe Umgebige sehr widerständig sind. D Arbeit zeigt au wie wichitg Lawinä, Schuttschicht, Schattewurf und See-Interaktione für d Gletschermassebilanz sind. So spezielli Gletscher z studiere bringt wertvolli Erkennntnis für d Zuekunft vo allne Gletscher uf üsere Welt.

Acknowledgement

I would like to express my gratitude to all the people who have contributed and supported the realisation of this work.

I am very thankful to my supervisor Dr. Martin Lüthi, for giving me the opportunity to design and carry out this project with even more creative freedom than I had ever hoped for. The initial field visits and your passion is what made me hooked and motivated. Your guidance and advice turned what could have been mere hiking excursions into a meaningful thesis. I also want to thank Boris Ouvry for his great help and guidance with the photogrammetry work and Jana for lending me her camera. Although the photogrammetry part did not ultimately make it into the thesis, the experience and learnings were very enjoyable. A great pleasure was having Andrin Hauser's pioneering work on and off the glacier as the basis for various parts of this work. My gratitude also goes to all other people at the GIUZ who offered me their help. Further, I am grateful for the Canton of Uri for providing the camera footage of the Griessseeli. I am also very grateful to my good friend Lukas for accompanying me on several trips, for carrying a boat to the frozen lake and for sharing the fascination for this amazing place. Finally, I am glad to have had the companionship and motivation from everyone joining me in library sessions.

Table of contents

List of abbreviations

AAR	Accumulation-area ratio
DEM	Digital elevation model
ELA	Equilibrium-line altitude
GIUZ	Geographical Institute University Zürich
GPR	Ground-penetrating radar
InSAR	Interferometric Synthetic Aperture Radar
LIA	Little Ice Age
PDD	Positive degree-day
PDDF	Positive degree-day factor
RGI	Randolph Glacier Inventory
SIA	Shallow Ice Approximation
SLF	WSL Institute for Snow and Avalanche Research
SMB	Surface Mass Balance
WSL	Swiss Federal Institute for Forest, Snow and Landscape Research
WGMS	World Glacier Monitoring Service

List of figures

List of tables

1 Introduction

Glaciers are among the most visible indicators of climate change, and their retreat has become a symbol of the ongoing transformation of alpine environments. While many glaciers are in rapid decline, certain glaciers persist despite seemingly unfavourable climatic conditions. This thesis focuses on one such example: the Clariden-N Glacier in the Swiss Alps. This chapter introduces the motivation for this study, outlines its relevance within the broader scientific context, defines the main research objectives, and presents the structure of the thesis.

1.1 Motivation

Whenever people talk about having a passion for glaciology, they are often met with the humorous remark that the need for glaciologists may soon be obsolete, as global warming is set to bring an end to glaciers. While the statement may become repetitive, there is some merit to it. It is true that glaciers across the globe are undergoing accelerated mass loss, and without appropriate measures these losses will continue for decades and centuries (Zekollari et al., 2024). In fact, some glaciers have already melted or shrunk to an extent where they are considered extinct, like the famous Icelandic glacier Okjökull or the Pizol Glacier in Switzerland (GLIMS, n.d.). Until 2100 nearly all glaciers of the European Alps will be vanished if the world cannot follow the Paris Agreement and keep the global average temperature increase 2°C above pre-industrial levels (Zekollari et al., 2024).

Any glaciers that, in the face of changing conditions, perform exceptionally, tend to attract particular attention in media and science. However, this is mainly applicable to larger glaciers. Smaller glaciers are often given less attention and thus are less frequently studied (Huss & Fischer, 2016). One reason might be their seeming individual irrelevance due to their small contribution to global glacier ice volume. However, these smaller glaciers can still play an important role due to their sheer abundance, their role in the local hydrological system (Huss & Fischer, 2016), and might hide important knowledge about glacier behaviour under extreme conditions.

> ***Extreme conditions*** *refer to environmental and climatic scenarios which are unfavorable for a glacier to maintain equilibrium, stressing a strong retreat or complete extinction. Scenarios can include exceptionally high temperatures, low precipitation or low altitude.*

A particularly fascinating example is the Clariden-N Glacier in the Swiss Alps, which is characterised by its exceptionally low mean altitude (in 2022: ~2220 m a.s.l.) while maintaining a considerable size (in 2022: ~0.87 km^2). Given its altitude, its existence raises fundamental questions: Why can this glacier survive under climatically unfavourable conditions? What specific processes and conditions contribute to its continued existence? In addition to the exceptionally low altitude, the geomorphological environment the Clariden-N Glacier is located in is complex and may harbour reasons for the existence of the glacier. The surrounding area is characterised by steep rock faces, which indicates a high level of avalanche activity, and the glacier surface is largely covered by debris. Such conditions – debris cover and avalanche supply – influence the behaviour of glacier dynamics heavily and can cause great variations in glacier mass balances (D. Benn & Evans, 2010; Kneib et al., 2024). Nevertheless, these processes are far from being entirely understood and are certainly not adequately represented in glacier modelling (cf. Kneib et al., 2024).

Despite these extraordinary circumstances, the Clariden-N Glacier has hardly been subject to scientific research (an exception: Hauser, 2024). A look at the numerous alpine natural disasters that have occurred in Switzerland in recent years shows that the extent and frequency of extreme events are alarming. The disasters in Blatten (2025) underscores the great and often underestimated impact that even small glaciers can exert. For this reason, it is essential to gain a more comprehensive understanding of glacier behaviour under extreme conditions.

Understanding why and how the Clariden-N Glacier persists under climatically hostile conditions offers valuable insights into glacier resilience in a warming world. As climate change continues to reshape alpine environments, identifying the processes that allow low-altitude glaciers to survive can also strengthen water resource planning and future projections of glacier evolution. Studying such “outliers” contributes to a more detailed picture of glacier-climate interactions, which is crucial for improving the accuracy of glacier models under increasingly extreme climatic scenarios.

1.2 Relevance and research gap

The study object is the Clariden-N Glacier because of several aspects that make it interesting for this work. The most important characteristics regarding the relevance of this glacier are shown in Table 1: (1) low altitude, (2) high rock faces, (3) debris cover and (4) north-facing.

These characteristics are not only prominent, but they are also thought to allow, enhance or weaken certain processes that may be relevant for the dynamics of the Clariden-N Glacier.

Table 1: Specifically noticeable characteristics and related processes of Clariden-N Glacier and its surrounding. The triangles pointing upwards/downwards indicate an expected increase/decrease of the processes caused by the characteristic feature.

Characteristic		Process
Low altitude		Temperature ▲
High headwall	→	Avalanches ▲ / shadowing ▲
Debris cover		Insulation / melt ▲▼
North-facing		Snow drift ▲ / shadowing ▲

Low altitude is typically unfavourable for a mountain glacier, as it corresponds to a climatic environment characterised by higher temperatures (cf. Chapter 5.1). Ultimately, higher ambient temperatures increase surface melt(cf. Braithwaite, 1995) . The persistence of a glacier at such altitude therefore raises questions about compensating factors that must be balancing this climatic disadvantage. Studying how the Clariden-N Glacier persists at such low altitude can shed light on these questions.

High headwalls surrounding the accumulation area create ideal conditions for frequent snow or ice avalanches, which can significantly contribute to accumulation. Under the presence of unstable rock, rockfall originating from the headwalls can result in supraglacial debris cover which, if thick enough, insulates the ice (D. Benn & Evans, 2010). In addition, the steep topography may lead to pronounced shadowing effects, reducing incoming solar radiation and thus melt (cf. Florentine et al., 2018). These topographic influences are often oversimplified or ignored in mass balance modelling (Kneib et al., 2024).

Debris cover is widespread on the Clariden-N Glacier's surface and can either enhance melt through lower albedo for thin debris layers or insulate the ice and substantially reduce melt rates for thick debris layers (Østrem, 1959). The spatial variability and dynamic evolution of debris thickness make this process difficult to quantify, especially in models that assume uniform surface conditions (Foster et al., 2012).

North-facing orientation can lead to lower insolation due to topographic shading, which reduces melt (Arnold et al., 2006). However, orientation can also enhance snow redistribution through wind-driven processes like snow drift, increasing accumulation in sheltered zones

(Winstral et al., 2002). These complex interactions are rarely well constrained. Studying the Clariden-N Glacier can enhance the understanding of the effect the north-facing orientation has on glacier mass balance.

In combination, these characteristics create a setting that is far from standard and may promote glacier persistence through a unique balance of mass gain and loss processes. Despite this, small glaciers in complex environments such as Clariden-N have received less scientific attention compared to their bigger counterparts, where most models and observations are focused on. As a result, key processes such as avalanche input, debris cover effects, and topographic shading are underrepresented or poorly parameterized in glacier models (Kneib et al., 2024). These gaps in understanding will be explored further in the literature review, Chapter 3.

1.3 Aim and research questions

The aim of this Master's thesis is to analyse and understand the persistence of the Clariden-N Glacier despite its unfavourable climatic setting. The focus lies on identifying which processes contribute to the glacier's continued existence, and how these processes interact. To achieve this, the study follows two complementary objectives. First, the local conditions and processes relevant to the glacier's mass balance will be identified, investigated, and analysed. Second, an assessment of the possible influence of these processes on the mass balance of the Clariden-N Glacier is conducted to estimate their contribution.

The research questions form the basis for research into how localised, process-based factors can enable the persistence of glaciers in otherwise unsustainable environments. The research questions guiding this study are therefore as follows:

[R1] What climatic conditions are required to reproduce the current extent of the Clariden-N Glacier in a mass balance model?

[R2] Which specific processes and environmental characteristics contribute to the persistence and evolution of the Clariden-N Glacier under climatically unfavourable conditions?

[R3] To what extent do avalanche deposition, debris cover, and topographic shading contribute to the mass balance of the Clariden-N Glacier?

[R4] How will the Clariden-N Glacier evolve in the future?

1.4 Thesis structure

This thesis is structured into seven chapters. Chapter 1 has already depicted the motivation for the work, explained the relevance of the study, and stated the aim of the thesis. In Chapter 2 the study area is introduced, with a focus on the glaciology, local climate, geology, and hydrology. Chapter 3 provides a review of state-of-the-art literature on thesis-relevant topics including mass balance modelling, avalanche-fed, and debris-covered glaciers. In Chapter 4 the methods are explained in detail to allow for reproducibility of the results, which are presented in the following Chapter 5. The discussion critically reflects on the data quality, the results, the research approach, and underlying uncertainties, and puts them into a broader scientific context. The final Chapter 7 concludes the thesis by answering the research questions, showing the limits of the research and offering perspectives for future research.

2 Study site

This chapter gives an overview of the study area to help the reader better understand the environment in which the glacier is situated. Information is provided about the glacier itself, the hydrological system, the local climate, and the geological and geographical setting.

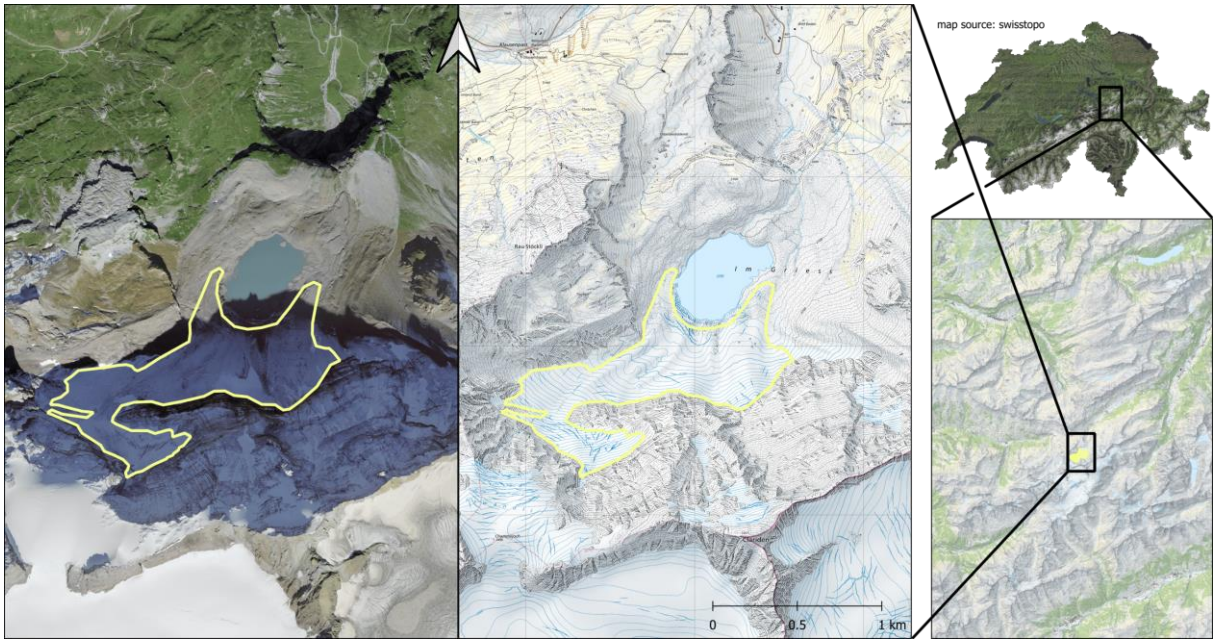

Figure 1: Study area with Clariden-N Glacier 2025 outlined in yellow.

2.1 Clariden-N Glacier

The study area is located near the Urnerboden, directly south of the Klausen Pass in the Canton of Uri (Figure 1). The glacier, locally referred to as “Griessgletscher”, “Claridennordfirn” or “Claridengletscher” hereby referred to as the Clariden-N Glacier (N standing for North), occupies a cirque-like basin at the foot of the Clariden north wall. These surrounding headwalls rise about one thousand metres above the ice surface. The highest parts of the glacier reach elevations of about 2,600 m a.s.l. Immediately in front of the glacier lies the proglacial lake Griessseeli, situated at an altitude of 2,098 m a.s.l. The lake has formed over the last four decades and has continues expanded due to the ongoing retreat of the glacier terminus. Since

2024 the glacier has mostly lost contact with the lake and in 2025 no point of contact could be seen. The exact topography of the lakebed remains unknown, as a bathymetric survey in fall 2024 failed due to planning issues and was never rescheduled since.

Location	Swiss Alps, Canton of Uri, Klausen Pass, Urnerboden
Coordinates (EPSG:2056)	2'708'819, 1'189'871
Alternative names	Griess Glacier, Clariden Glacier, Clariden Nordfirn (de), Claridengletscher (de)
Glacier type	Cirque glacier
Glacier area*	720'000 m^2
Altitude range*	2098 - ~2500 m a.s.l.
Mean annual precipitation**	2'410 mm
Main drainage	Fätschbach, KKL Limmernsee
Ice thickness change**	~ -1.8 m yr^{-1}

* Information pulled from Chapter 5.1
** Information pulled from Hauser (2024)

Due to the proximity to the Klausen Pass, the area is a popular tourist destination and invites visitors to take a short hike to the proglacial lake. Less well known are the glacier caves on the east side of the Clariden-N Glacier. There is a complex cave system carved out by subglacial streams which opens when the snow melts during summer. Most caves are several metres in diametre, but the "Klausen Grotto" is far bigger with a diametre greater than 12 m at some point. Sadly, it was mostly destroyed on 14 June 2025 as a consequence of a rockfall. Further information on the Klausen Grotto can be found in the Appendix B.

2.2 Climate

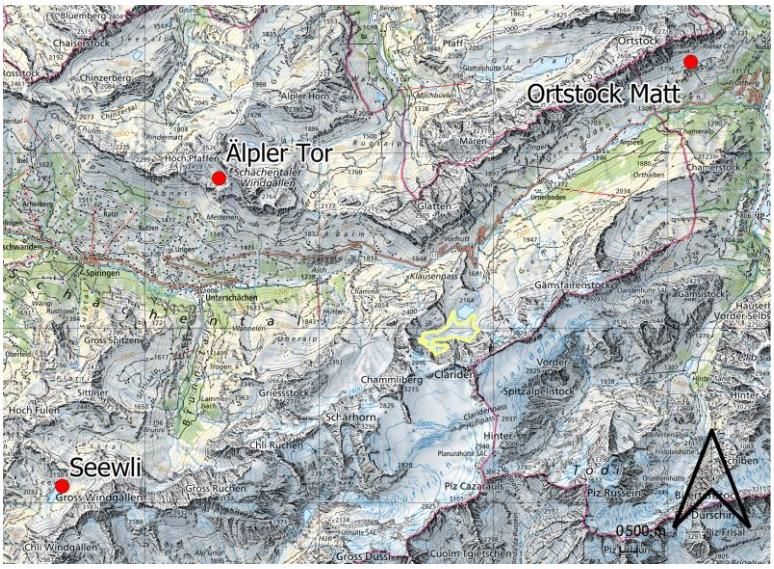

Figure 2: SLF IMIS stations.

Site-specific meteorological records are limited. Precipitation totals from a pluviometre located on the Tierälpli plateau at 2352 m a.s.l., which is within the same geomorphological area as the glacier, was analysed by Hauser (2024) for the period from 1964 to 2022, and he reported the

mean annual precipitation to be 2410 mm. A comparison of three IMIS snow stations nearby provides a relatively good approximation of the existing of the meteorological situation on behalf of snow cover and air temperature. More on the climate can be found in Chapter 5.1.

2.3 Hydrological system

The hydrology of the Klausen Pass and Urnerboden region is influenced by the Clariden-N Glacier and its proglacial lake. The lake, naturally dammed by a moraine deposited approximately 170 years ago (Hauser, 2024), acts as a temporary water reservoir for the valley. Water is discharged via an above-ground stream and subsurface drainage through the karstic bedrock. The subsurface drainage system has been mapped in more detail by Hauser (2024). Tracer experiments have revealed infiltration of stream water into the karstic subsurface, with resurgences several kilometres away (Hauser, 2024). However, the precise origin of some of the groundwater in this system remains unresolved. The water leaving the Griessseeli is shortly afterward retained and partly redirected through a 4.6 km tunnel to Obersand and ultimately reaches the Limmernsee reservoir after 14 km of artificial channelling.

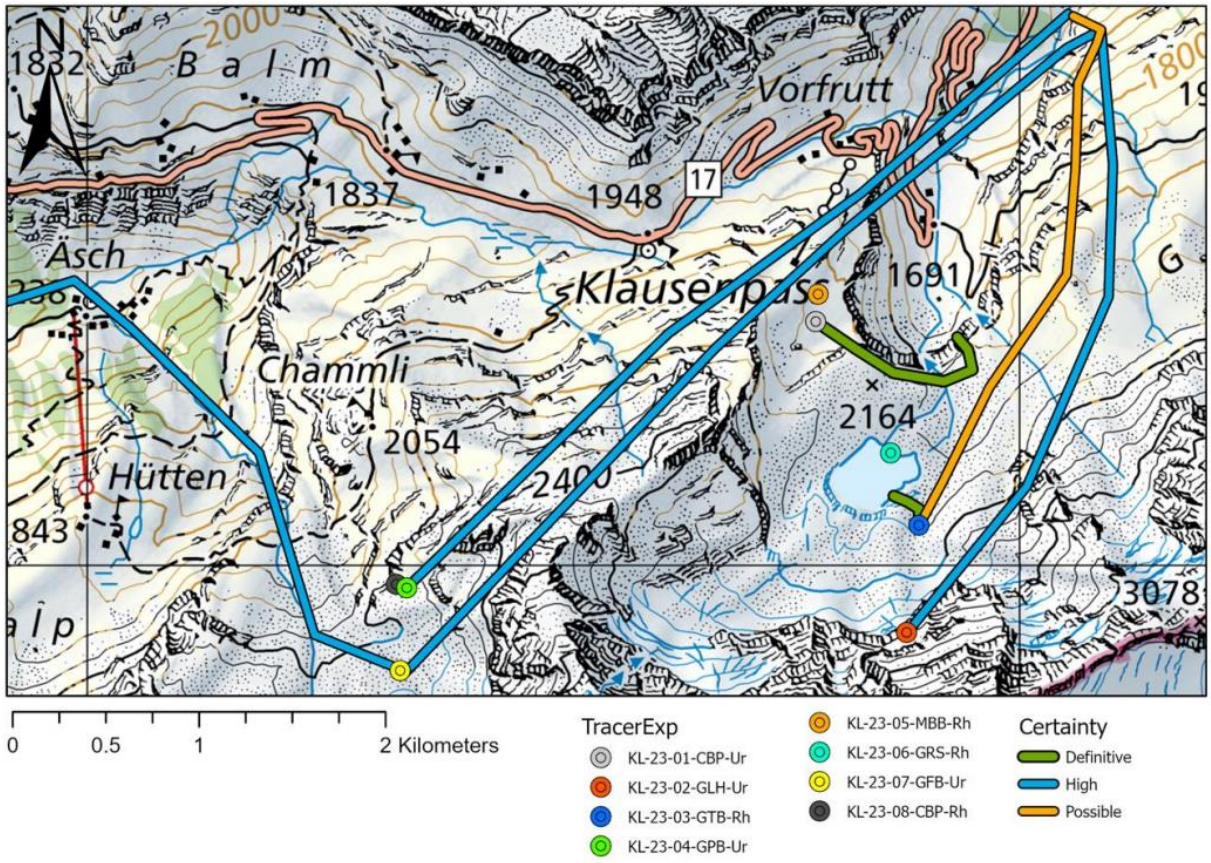

Figure 3: Subterranean karst drainage system discovered during Hauser's field study (Figure 62 in Hauser, 2024)

2.4 Geological setting

The study area lies within the main thrust zone of the Helvetic Nappes. At the base, crystalline basement rocks of the Aar Massif – comprising granites and gneisses – are overlain by autochthonous sediments and the North Helvetic Flysch. The Flysch, which is rich in clay, acts as an aquiclude, obstructing vertical water flow (Hauser, 2024). Above this, two smaller-scale nappes are present: the Griessstock and Chammlistock nappes (Figure 4). The Griessstock nappe consists predominantly of Quinten Limestone with extensive underground drainage networks, where numerous springs emerge along the thrust contact with the impermeable Flysch, reflecting the karst hydrology (Hauser, 2024). Overlying the Griessstock nappe is the Axen nappe, composed of Triassic to Cretaceous sediments. LIA and LGM Moraines can be found in the study area (see Figure 5).

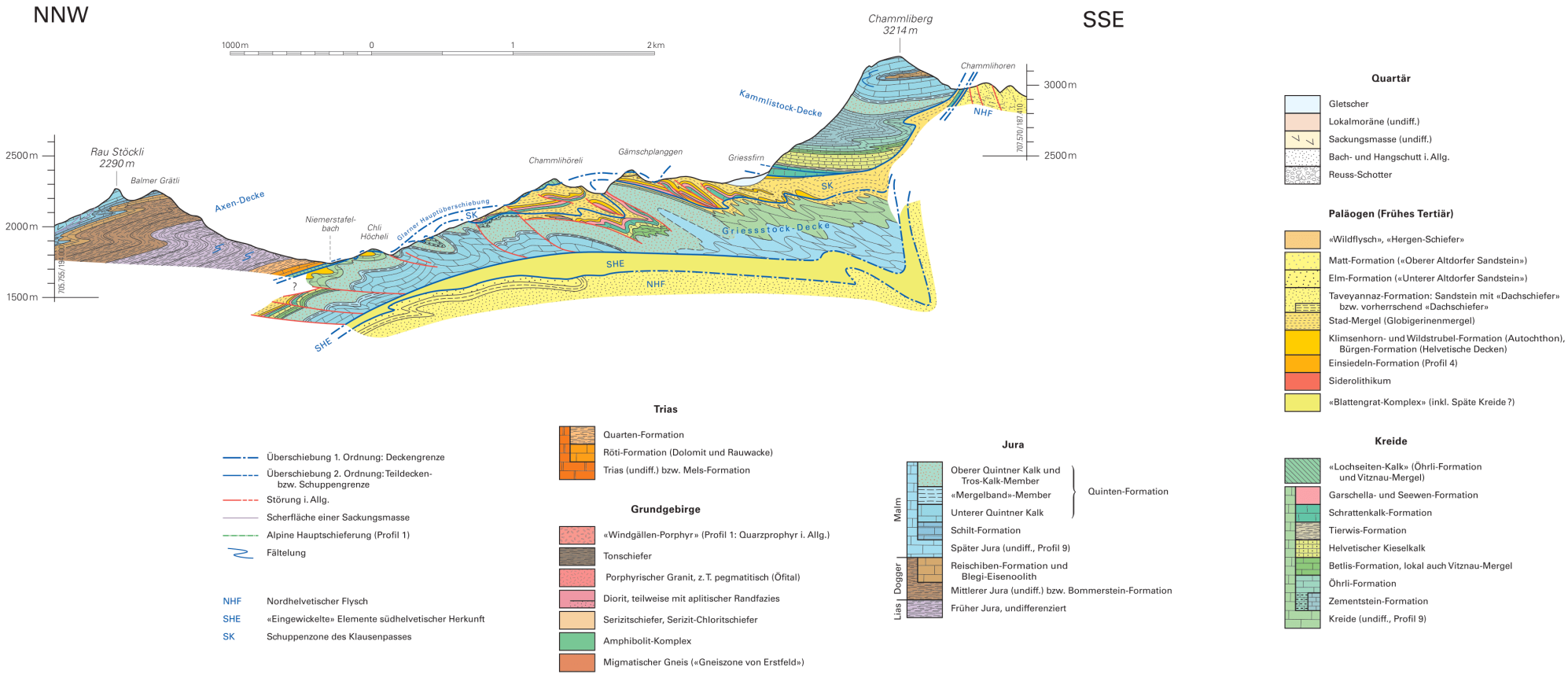

Figure 4: Geological Profile of Schächental, Klausenpass (GA25_083_Plate_II_Section_9): Map created by Hantke, R. and described by Hantke, R. & Brückner, W. both published in 2011. The Tödi area, the map division where the study area is part of, has not been published yet and this is the closest to it and probably very similar.

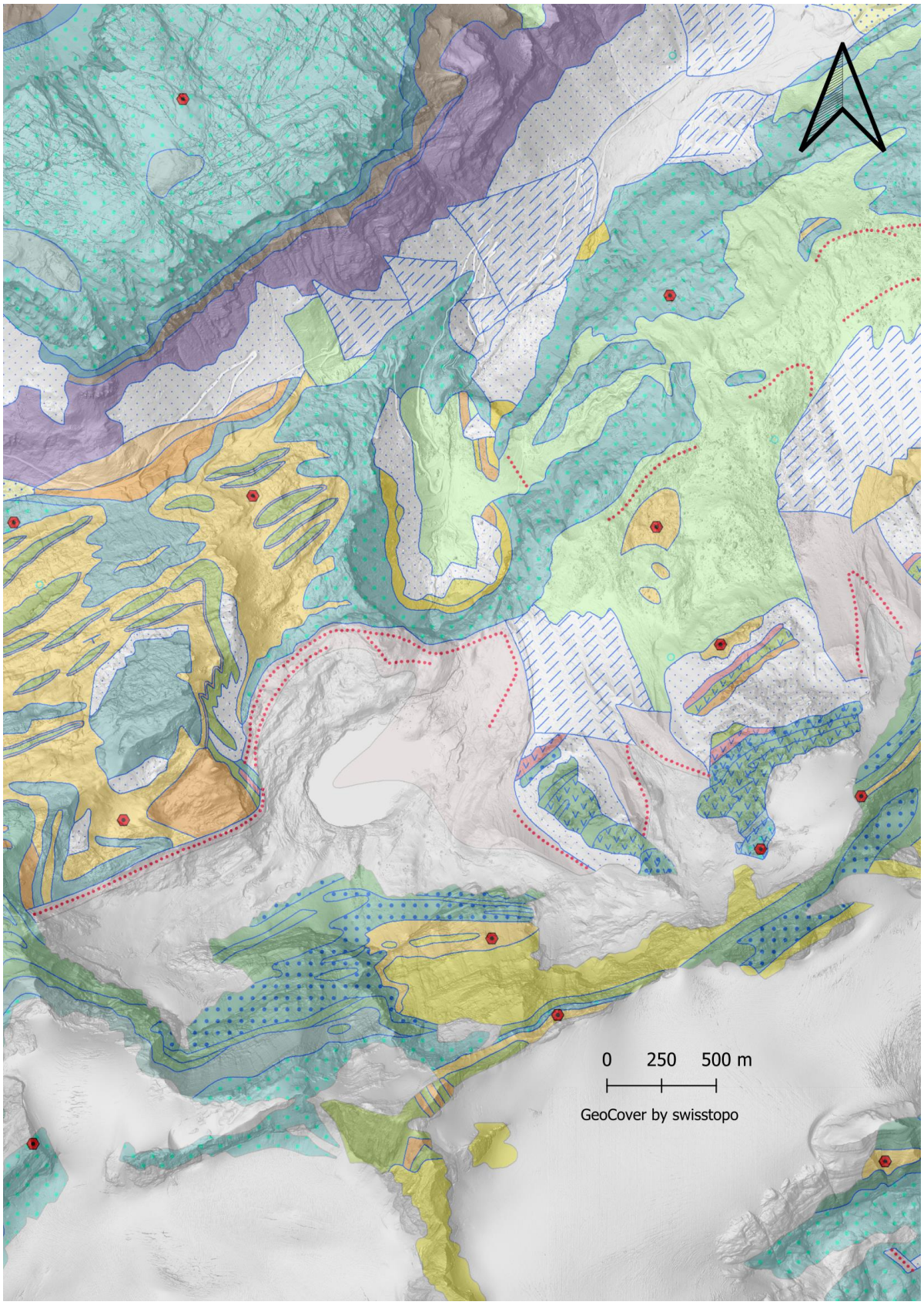

Figure 5: GeoCover of study area: The GeoCover by swisstopo depicts the near-surface area of the geological ground. The red dotted lines on grey ground show LIA moraines (undated) and on green ground LGM retreat moraines (undated). Accordingly, are grey and green areas indicating till from that time and young. Limestone is coloured in cyan and the Quinten Limestone has additional green dots. The yellow area next to the Quinten Limestone is Flysch.

3 Literature review

The literature reviewed in this chapter is primarily based on scientific publications from peer-reviewed journals, ensuring the inclusion of high-quality and reliable research findings. In addition, sources such as reports, field observations, unpublished information, and other relevant materials have been consulted to provide context and support where peer-reviewed literature is limited. The main tool for identifying and retrieving publications was Google Scholar.

The definitions and terminology used in glaciology regarding glacier mass balance are described in Section 3.1. How glaciers can be modelled, why it makes sense to do so, and what challenges need to be overcome at different scales is presented in Section 3.2. The current state of scientific knowledge regarding the related processes, namely avalanche feeding, topographic shading and debris cover, is summarised in the following three sections 3.3-.5.

3.1 Glacier mass balance

The terminology applied in this study is based on the recommendations of Cogley at al. (2011). Capital variables generally refer to glacier-wide quantities and lower case to quantities at a point. Whenever a variable is accompanied by an overdot (e.g. $\dot{b}$), a rate is expressed. Cogley et al. (2011) define *mass balance* as: "the change of mass of the glacier, or part of the glacier, over a stated span of time". When looking at an ice column with base area ds and mass m, the addition (accumulation, *c*) or removal (ablation, *a*) of mass can either be at the surface (*surface accumulation* $\dot{c}_{sfc}$/*ablation* $\dot{a}_{sfc}$), within the glacier (*internal accumulation* $\dot{c}_i$/*ablation* $\dot{a}_i$) or beneath the ice at the glacier bed (*basal accumulation* $\dot{c}_b$/*ablation* $\dot{a}_b$). Through the *flow* of ice into q_{in} or out q_{out} of the column, mass can be added or removed. Joining all this together, the *conservation of mass* can be expressed as the *mass balance rate* $\dot{m}$ of a column is:

$$\dot{m} = \dot{c}_{sfc} + \dot{a}_{sfc} + \dot{c}_i + \dot{a}_i + \dot{c}_b + \dot{a}_b + (q_{in} + q_{out})/ds \tag{3.1}$$

If the average ice density of the column $\overline{\rho}$ is constant in time, a special case of Equation 1 emerges – the continuity equation:

$$\dot{h} = \dot{b} - \nabla \cdot \vec{q} \tag{3.2}$$

With $\dot{b} = \frac{\dot{c}_{sfc}+\dot{a}_{sfc}+\dot{c}_i+\dot{a}_i+\dot{c}_b+\dot{a}_b}{\bar{\rho}}$ and the flux divergence $\nabla \cdot \vec{q}$ replacing the net horizontal fluxes per unit horizontal area from equation 1. Resulting from this, changes in glacier thickness h are only related to changes in mass. For clarity, Cogley et al. (2011) suggest the term *climatic-basal mass balance* for $\dot{b}$ which represents changes at (or near) the surface, mainly caused by climate, and those at the glacier bed, but not changes in the interior due to flow dynamics. If basal changes can be disregarded as well, the term *surface mass balance* is valid according to Cogley et al. (2011). *Surface mass balance* is the actual term used in modelling context of this study.

Since the *surface mass balance* is assumed to be equal to the *climatic-basal balance*, the *glacier wide mass balance* follows to be the sum of surface ablation and accumulation over the entire glacier surface $B = B_{sfc} = C_{sfc} + A_{sfc}$. The *glacier-wide surface mass balance rate* $\dot{B}$ is then a combination of multiple columns over the area S:

$$\dot{B} = \dot{B}_{sfc} = \int \dot{b}\, ds \tag{3.3}$$

Frontal ablation processes such as calving, frontal melting and sublimation above and melting below the waterline are not included in this formulation.

3.2 Glacier mass balance modelling

There is considerable scientific interest in better understanding and simulating the temporal evolution of glaciers, both in the past and in the future (Zekollari et al., 2022). Scientific interest sources from multifaceted topics and ranges from glaciers relation to natural hazards, over tourism, to the contribution to sea level rise (Zekollari et al., 2022). There exists a wide range of approaches to glacier evolution modelling. With respect to the temporal dimension, models can be designed to simulate past glacier states or to generate projections into the future (e.g. Schmidt et al., 2019; Zekollari et al., 2024). The temporal scale can vary substantially, encompassing annual to decadal or centennial timescales with time steps ranging from .001 to 1 year (cf. Zekollari et al., 2022). The horizontal resolution is commonly in the range 25-500 m, with exceptions exceeding this (e.g. Aðalgeirsdóttir et al., 2006).

The review by Zekollari et al. (2022) shows, using a SIA to calculate ice flow is much more common for 1D and less for 3D modelling. The application in terms of stresses, basal sliding, cross-sectional shape, and more can be very different. Full-Stokes ice flow models such as the Elmer/Ice and other sophisticated approaches are more commonly applied in 3D modelling (cf. Zekollari et al., 2022). 1D flowline models calculate mass balance by using a temperature index

(e.g. Huss et al., 2007), energy balance (e.g. Oerlemans, 1997) or degree-day model (e.g. Anderson et al., 2008), or as a function of elevation (e.g. Sugiyama et al., 2007). The evolution of glacier geometry can be either modelled using an explicit or implicit scheme, with the latter being more demanding.

In order to accurately perform large-scale regional or global glacier evolution modelling, certain simplifications are unavoidable (Zekollari et al., 2022). It is therefore of great importance to conduct detailed ice-dynamic glacier evolution studies at the scale of individual glaciers, which help to refine and validate such simplifications (Zekollari et al., 2022). These detailed studies typically address changes in surface mass balance, in combination with ice flow, the processes governing the mass transport of glacier ice (e.g. Huss et al., 2007). Modelling individual glaciers is also essential for improving the understanding of specific physical processes (e.g. Kneib et al., 2024), in the case of this study: debris cover, topographic shading, or avalanche contribution.

3.3 Low-altitude glacier

Glaciers at low mean altitude compared to the regional mean are often topographically constrained (Florentine et al., 2018). Many of them are located in cirques, where topographic effects – such as enhanced snow accumulation by snow drift or reduced surface melt through topographic shading – cause an increase in winter mass gains or a decrease in summer mass loss (Laha et al., 2017). These topographic effects not only allow the persistence of glacier ice at an incredibly low altitude, but also complicate the relationship between regional climate and topographically constrained glacier mass balance (Florentine et al., 2018).

Low-altitude glaciers are often also small in size, because the topographic favourable locations are usually small. In a study on more than 1500 glaciers in the southern Canadian Cordillera (DeBeer & Sharp, 2007) and an analysis of very small glaciers (<0.4 km^2) in the Monashee Mountains (DeBeer & Sharp, 2009), it was found that many small glaciers showed a regionally unusual stagnation in net change. This exceptionality has been related to the favourable local topographic setting of very small glaciers (DeBeer & Sharp, 2009). Small glaciers (<0.5 km^2) account for approximately 13% of the global glacierized area and store about 5% of the total ice volume (Huss & Fischer, 2016). Despite their limited size and volume, they are omnipresent, making up 80-90% of all glaciers in mid- to low-latitude mountain ranges (Huss & Fischer, 2016).

It has been suggested that, as valley glaciers retreat toward cirque-like headwalls, the influence of regional climate on their mass balance diminishes (Florentine et al., 2018). This assumption is supported by observations of decreasing thinning rates in glaciers situated within such

settings (cf. Haugen et al., 2010). However, as demonstrated by Hoffman et al. (2007), small glaciers in strongly topographically constrained environments, where processes such as avalanching and wind drift occur, can still be primarily governed by regional climatic conditions. Therefore, no trivial direct causal relationship can be inferred between topographic configuration and the dominance of specific mass balance processes.

3.4 Avalanche-fed glaciers

While all mountain glaciers receive some level of redistributed snow, avalanche-fed glaciers rely heavily on repeated avalanche deposits for their accumulation (cf. Kneib et al., 2024; Laha et al., 2017). This setup implies that the local topography exerts a decisive influence on glacier development.

> *Glaciers are termed **avalanche-fed** when a substantial fraction of mass input arises from avalanches originating in adjacent headwalls and steep valley sides (Scherler et al., 2011).*

Avalanche-fed glaciers are typically found where steep headwalls frequently shed snow and ice onto the glacier surface (Laha et al., 2017; Scherler et al., 2011). In such a setting, mass input from avalanches can represent a significant component of the glacier's mass balance (Kneib et al., 2024). This creates spatially complex patterns of snow accumulation and complicates efforts to measure or model glacier mass balance (Hewitt et al., 2011). Although such glaciers are present in many high-relief mountainous regions worldwide, they have traditionally received less systematic attention than glaciers nourished predominantly by direct precipitation (Hewitt et al., 2011). However, recent advances in observational techniques and modelling frameworks have highlighted the need for a better understanding of avalanche-fed systems (Kneib et al., 2024).

Characteristics

Avalanche-fed glaciers display several distinctive features that set them apart from precipitation-fed systems. These are the features that make avalanche-fed glaciers recognisable and distinguishable.

Low accumulation area ratio (AAR): A practical diagnostic criterion for avalanche feeding is a notably low AAR without a quick retreat or high thinning rates (D. I. Benn & Lehmkuhl, 2000; Scherler et al., 2011). The typical accumulation zone, where the glacier grows by accumulating snowfall that then compacts into ice, can be partly or entirely missing for avalanche-fed glaciers because avalanche cones and redistributed snow compensate for the missing mass (Laha et al., 2017). This is why these glaciers can maintain a viable mass balance despite having a low AAR. In some Himalayan cases, the AAR can drop below 0.2, yet the

glacier persists or even remains near equilibrium (Hynek et al., 2024; Laha et al., 2017). This apparent mismatch between a small accumulation area and the glacier's persistence indicates that mass inputs from avalanches might be bridging the gap.

Debris coverage: Due to the combined movement of snow, ice, and rock from towering headwalls, avalanche-fed glaciers often accumulate thick debris mantles in their ablation zones (Laha et al., 2017). The debris layer can have important thermodynamic consequences, including localised insulation that reduces melt rates (Banerjee & Shankar, 2014). Glacier tongues with extensive debris cover frequently stagnate rather than retreat up-valley. Still, they lose mass by thinning, which complicates direct terminus-based assessments of mass balance for debris-covered glaciers (Banerjee & Shankar, 2013).

Spatial variability of accumulation: In avalanche-fed systems, the highest accumulation rates are not necessarily near the topographic ridge but at the base of steep headwalls (cf. Kneib et al., 2024). These inputs create heterogeneous snow distributions and can lead to unexpectedly thick accumulations in certain glacier sectors (Kneib et al., 2024). This contrasts with the simplest precipitation-based models of glacier accumulation, which assume gradients related solely to elevation (e.g. Oerlemans, 1986).

Steep slopes in the surrounding terrain: Steep headwalls are fundamental for initiating both snow and ice avalanches that feed these glaciers (Scherler et al. 2011). For example, Laha et al. (2017) described several Himalayan glaciers where the slope angles in the headwall zones exceeded 30° or 35°, making them highly efficient in funnelling avalanches to the glacier surface. Scherler et al. (2011) identify a large proportion of steep, ice-free catchment above the snowline as an indicator for avalanche-fed glaciers.

Occurrence

There is currently no study available that has mapped avalanche-fed glaciers on a global scale. However, avalanche-fed glaciers are common in high-relief, steep mountains where topography amplifies gravitational snow redistribution (De Marco et al., 2022). High Mountain Asia hosts numerous glaciers that show avalanche-fed characteristics (Laha et al., 2017; Scherler et al., 2011). Their presence is also noted in parts of the European Alps (De Marco et al., 2022; Kneib et al., 2024), Greenland (Hynek et al., 2024) and New Zealand (Purdie et al., 2015).

Within the Alps, avalanche-fed glaciers tend to be found in zones with tall and steep headwalls, where rockfall and avalanche processes are dominant (e.g. Kneib et al., 2024). Likewise, in High Mountain Asia, glaciers with steep, avalanche-prone headwalls show mass-balance and thickness patterns that are only explainable by avalanche-derived accumulation exceeding direct snowfall (Laha et al., 2017). Globally, as warming raises snow lines, avalanche-fed

systems may remain more resilient in some settings because avalanche mass inputs offset the loss of direct snowfall at lower glacier elevations (Hynek et al., 2024; Laha et al., 2017).

Challenges and research gaps

Accurate mass-balance estimation is one of the central challenges concerning avalanche-fed glaciers (cf. Kneib et al., 2024). The avalanche cones and uneven snow distribution make glaciological mass-balance measurements extremely challenging (Hynek et al., 2024). Traditional stake networks or snow-pit surveys cannot easily capture avalanche-driven gains, especially if deposits form in hard-to-access, crevassed, or avalanche-prone areas (Kneib et al., 2024; Laha et al., 2017). As a result, glaciological methods often miss a large fraction of net accumulation in these environments, resulting in an underestimation of total accumulation (Laha et al., 2017). The discrepancy can be large enough to explain apparent anomalies, such as glaciers with apparently negative glaciological balances that maintain stable terminus positions (Hewitt et al., 2011).

Geodetic methods can partially correct for this gap because they measure integrated glacier-wide volume changes using repeat digital elevation models or photogrammetry (Kneib et al., 2024; Zemp et al., 2013). Thus, the difference between conventional glaciological balances and independent geodetic has provided strong evidence for the importance of avalanche-fed processes (Hewitt er al., 2011; Kneib et al., 2024). However, linking these integrated changes back to specific accumulation and ablation processes remains challenging (Kneib et al., 2024).

The future evolution of avalanche-fed glaciers likely depends on the balance of higher melt rates at low elevation and any additional avalanche accumulation and debris-induced insulation from destabilized rock walls (Kneib et al., 2024; Hynek et al., 2024). As climate warming continues, it remains uncertain whether avalanche-fed glaciers will face a slower retreat, due to continuous mass input from avalanches, or a faster, due to an increased net ablation because of higher melt rates at lower elevations (Kneib et al., 2024). However, avalanche-fed glaciers are probably the most resilient type of low-elevation glaciers und might survive even substantial atmospheric warming as pointed out by Huss & Fischer (2016).

Moving forward, open questions include how to better incorporate avalanche processes in standard glacier modelling and how ongoing warming may alter the dynamics of these unique mountain systems. Both open questions will be touched upon in this thesis by exemplary assessing the Clariden-N Glacier.

3.5 Debris-covered glaciers

In many glaciated regions worldwide, particularly in geologically young and actively uplifting mountain ranges, debris cover is commonly found on the surface of glaciers (Foster et al., 2012; Herreid & Pellicciotti, 2020; Rounce et al., 2021). In a warming climate, debris cover and thickness are expected to increase (Herreid & Pellicciotti, 2020; Scherler et al., 2011). The debris, originating from headwalls, valley slopes, glacier beds, and lateral moraines, accumulates on the glacier surface through direct deposition and melting processes (D. Benn & Evans, 2010). The thickness of the debris cover can range from millimetre to several metres, varying both within individual glaciers and between different glaciers (Rounce et al., 2021). A thin debris layer enhances melting by reducing the glacier's albedo, while a thick debris layer inhibits melt due to its insulating properties (Evatt et al., 2015; Østrem, 1959). Consequently, debris thickness is a crucial factor in modelling glacier change.

Various methods have been applied to assess supraglacial debris cover, including in-situ measurements (Mihalcea et al., 2006), terrestrial tachymetry and photogrammetry (Nicholson & Benn, 2013), and ground-penetrating radar (McCarthy et al., 2017). Several remote sensing studies have also linked supraglacial debris thickness to debris surface temperature or surface elevation changes through physical and empirical relationships (Foster et al., 2012; Juen et al., 2014; Messmer & Groos, 2024). A method employed by Messmer & Groos (2024) combines UAV thermography with a surface energy balance model and has proven to generate highly resolved debris thickness measurements. However, this and other similar studies (e.g. Bisset et al., 2023; Gök et al., 2023) face issues of scalability and uncertainty, which currently limit their effortless application at a glacier-wide scale.

Huss et al. (2007) found that debris cover on the glacier tongue reduces retreat rate by a factor of three. Although debris cover substantially affects glacier melt, other studies have shown that debris-covered and clean-ice glaciers often display surprisingly similar thinning rates (Gardelle et al., 2013; Kääb et al., 2012). This counterintuitive observation may be partially attributed to the presence of exposed ice cliffs and supraglacial melt ponds, which locally enhance melt despite the insulating debris layer (Buri et al., 2021; Miles et al., 2021; Sakai et al., 1998). Nevertheless, these thinning rates underscore the difficulty of attribution glacier mass balance to debris cover. Thus, modelling debris-covered glaciers remains challenging (Rounce et al., 2021).

4 Methods

To answer the research questions, this study is conducting a case study on the Clariden-N Glacier. The data used are described in Section 4.1. The methods used to collect this data or to derive information from said data are grouped into glaciological (Section 4.2), geodetic (Section 4.3), process-based (Section 4.4), modelling (Section 4.5).

The main use of the glaciological and geodetic methods is to capture the detailed nature of the glacier and its surrounding environment. This includes, for instance the glacier bed profile, the maximum surface melt rate or the surface geometry. The glaciological method applies in-situ measurements of ablation stakes for point measurements, but the geodetic methods are centred around the use of remote sensing data to gather glacier-wide measurements. The processes that arise from the glacier's characteristics and its environment and which are thought to influence the glacier mass balance are studied. These are avalanches (Section 4.4.1), topographic shading (Section 4.4.2) and debris cover (Section 4.4.3). Present and past glacier extents are reconstructed, and the future evolution is simulated through a SMB modelling approach described in detail in Section 4.5. It describes the inputs and outputs, the governing equations and how the model is assessed.

A potentially supporting methods which includes a photogrammetric survey of a glacier cave, as a hybrid method of glaciological and geodetic glacier mass balance measurement, is not part of this thesis but still described and documented in the Appendix B.

4.1 Data

Geodetic data

Geodetic data are entirely sourced from swisstopo and covers 16 topographic maps from 1859 until 2022 (cf. Table 2). The scale for maps published before 1963 is 1:50'000 whereas all maps from 1963 onwards are scaled 1:25'000. Since 1951 the contour line equidistance is 20 m, before that it used to be 30 m. The year of publication and acquisition is not always the same, especially for the topographic maps.

Table 2: Maps and DEM available since 1859 for the Clariden-N Glacier. The year is either the year of publication (for maps) or the year of acquisition (for DEMs).

Year	Name	Scale	Equidistance / resolution [m]
1859	Dufour map	1:50'000	30
1876	Siegfried map	1:50'000	30
1900	Siegfried map	1:50'000	30
1917	Siegfried map	1:50'000	30
1930	Siegfried map	1:50'000	30
1951	Old national map	1:50'000	20
1963	National map	1:25'000	20
1973	National map	1:25'000	20
1979	National map	1:25'000	20
1985	National map	1:25'000	20
1990	National map	1:25'000	20
1997	National map	1:25'000	20
2003	National map	1:25'000	20
2007	National map	1:25'000	20
2011	swissALTI3D DEM	-	0.5 – 3
2013	swissALTI3D DEM	-	0.5 – 3
2016	National map	1:25'000	20
2022	National map	1:25'000	20
2022	swissALTI3D DEM	-	0,5

The swissALTI3D – a DEM – from 2022 was used, which has a height accuracy (resolution) of 0.5 m. The latest version of the swissALTI3D is always available free of charge from swisstopo. Additionally, swissALTI3D versions from 2011 and 2013 were made available by the GIUZ with a height accuracy of 0.5-3 m. However, as it can be seen in Figure 6, the 2011 version is of much lower resolution above 2000 m a.s.l. compared to the 2013 version. Thus, the DEM from 2011 has not been used for this thesis.

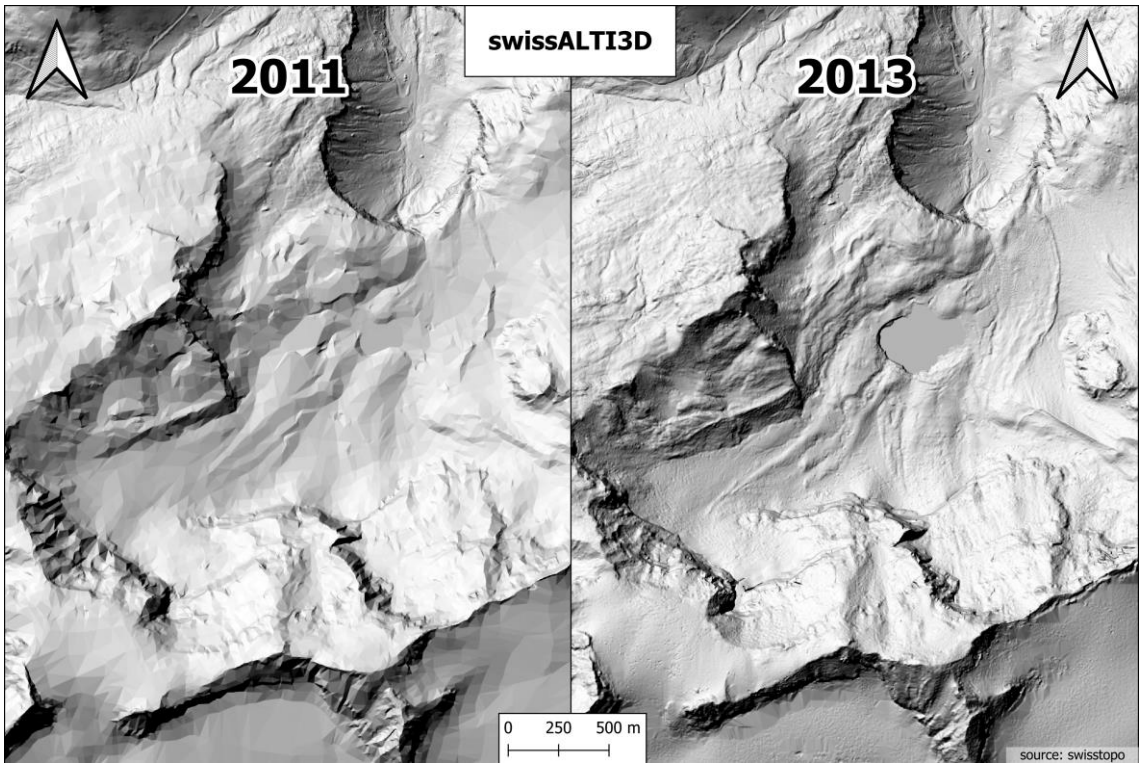

Figure 6: DEM resolution comparison: swissALTI3D 2011 versus 2013.

Glaciological data

Glaciological measurements of four ablation stakes are available since 2023 until summer 2025, with a discontinuity in summer 2023. Eight ablation stakes were measured by Andrin Hauser from 27 July 2023, until 1 October 2023 and four continued by Mattia Salvi from 18 July 2024 until 22 July 2025.

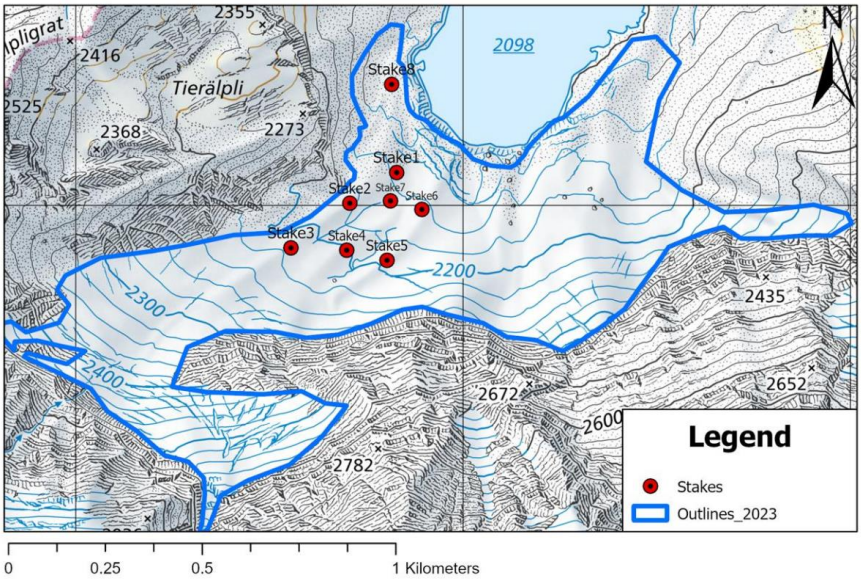

Figure 7: Ablation stake measurement locations (Appendix 15 in Hauser, 2024). Stakes 1, 5, 6 and 8 were continues until 2025.

Process-based data

Process-based information was retrieved from several sources. For avalanche frequency and type a series of ~7000 hourly photographs from 1 January 2023 until 10 Oktober 2024 was used. They were taken automatically by an installed field camera, which was set up by the Canton of Uri and has an image resolution of 640x480 pixels. For the assessment of topographic shading simulated shadows were sampled using the web application ShadeMap, which "simulates shadows taking terrain, building and canopy heights into account." (www.shademap.app). 100 samples were taken, spread out over the 1951 glacier extent. The debris cover thickness estimate stems from Andrin Hauser's work and the same goes for the PDDF.

Meteorological data

Meteorological data mainly consist of data retrieved from IMIS-Snowstations by the SLF Stations. There has never been a supraglacial meteorological measurement station installed, thus there is no site-specific climate data available. The closest approximation to site-specific precipitation measurements is from a pluviometer (named KLUS), which was analysed by Hauser (2024). Climate change data for future scenarios were retrieved from the CH2018 Swiss Climate Change Scenarios Product Browser (www.service.meteoswiss.ch/productbrowser).

4.2 Glaciological method

Overview

The glaciological (observation) method is a point-based measurement of ablation and accumulation. The in-situ measurements are interpolated between the measurement points and extrapolated over the unsurveyed parts of the glacier (Zemp et al., 2013). Ablation is measured from ablation stakes, which are poles drilled into the glacier ice surface. Accumulation is measured by digging snow pits. Measurements are often carried out annually at the end of each hydrological year. A seasonal or even shorter time interval of observation is less common for monitoring glacier surface mass balance due to labour intensity but can be very reasonable depending on the aim of study. The glaciological method uses well-established techniques and tools, but its precise execution, for instance number and density of measurement locations, depends on glacier characteristics, site accessibility, aim of the study, and resources.

The spatial interpolation is traditionally performed using the contour line method proposed by Østrem & Brugman (1991). However, there are other options that are often utilised such as statistical analysis (Lliboutry, 1974) or the application of an observed mass balance gradient on the glacier hypsometry. The extrapolation on unsurveyed regions is not trivial and requires

expert knowledge. The spatial inter- and extrapolation results in a glacier-wide surface mass balance, which is most commonly converted and expressed as in metres water equivalent (m w.e.) or metres water equivalent per year (m w.e. a^{-1}).

> *"ELA, AAR, and mass balance-gradients are usually calculated from mass balance distribution with elevation (ranges)." (Zemp et al., 2013)*

The surface mass balance is either referenced to a floating-date, fixed-date or stratigraphic time system. Fixed-date means, that each field survey is conducted at a fixed calendar date, where a floating-date time system allows for a certain range of dates around a certain point for the field survey. The stratigraphic system conducts field surveys at a subsequent annual minimum in surface mass balance.

According to (Zemp et al., 2013), the glaciological method is subject to random and systematic error that can source from (i) field measurements on the point locations, (ii) spatial averaging (or extrapolation), and (iii) changes in glacier area and elevation.

Application in this Study

In 2023 on behalf of his master's thesis, Andrin Hauser made ablation stakes measurements with the aim of obtaining summer ablation. He started the measurement series on 27 July 2023, and ended on 1 October 2023, when he removed four of the eight initially drilled stakes. The remaining stakes were then continuously measured until summer 2025 by the author of this thesis. However, due to an unexpectedly high melt rate, the measurement series during summer 2023 is discontinuous. Only one stake remained drilled over the whole summer period, thus only the minimum melt could be deduced for summer 2023. Nevertheless, all stakes were reintroduced into the ice in September 2023 and thereafter no measurement gaps are apparent for the four remaining stakes. The four ablation stakes are installed near the glacier terminus in a rather flat and debris-covered part of the glacier. For the conversion of volume loss into water equivalent (m w.e.) an ice density of 900 kg/m³ is assumed.

As seen in the overview a glacier-wide mass balance can be inter- and extrapolated from a set of glaciological point balance observations. This often results in significant deviations from the geodetic mass change, which generally can be accounted to limited observation points and the thereof inadequate estimate of unmeasured areas (Sold et al., 2016). In this study the topographic constraint is a major limitation, leading to limited observation points. Due to the steep and high rock walls with regularly occurring gravitational mass movement, it is not sensible to maintain measuring points in the directly affected areas. This is why the measuring stakes were only installed in the glacier tongue area near the lake, where the risk of avalanches, rockfalls and similar hazards is significantly reduced. Additionally, the stakes were drilled at

diverse locations to account for topographic differences and debris thickness variations (Hauser, 2024).

*The **rockfall** from 21 June 2025 showed that the risk assessment is indeed valid and that a misjudgment could have had fatal consequences.*

Thus, a dense network of snow pits and ablation stakes was not possible to operate and therefore no glacier-wide mass balance assessment possible. Snow-pit measurements were not reasonable as the glacier has no true accumulation zone (AAR ≈ 0), where snow turns into firn and ice. However, what can be measured is the maximum ablation, which is expected at the glacier tongue, where the ablation stakes are installed.

Expectations

The **maximum ablation** resulting from the glaciological observation are expected to be truthful with little uncertainties. However, due to the short series of measurements, it is to be expected that the long-term average will deviate from this. As it is carried out over a short period of time, the summation of errors is less of a problem. The glaciological method applied in study this thought to introduce possible errors only through field measurement (cf. Figure 8). This is because the maximum ablation at the glacier terminus is the only surface mass balance value of interest, thus no spatial inter- or extrapolation is needed. Area and elevation changes are so small for the Clariden-N Glacier, they can be ignored. Regarding errors resulting from field measurements, the most meaningful introduction could have resulted from the height determination. The uncertainties from height determination could stem from: Measurements by different people, the one-month measurement gap or the artificial debris reassemble at the drilling hole.

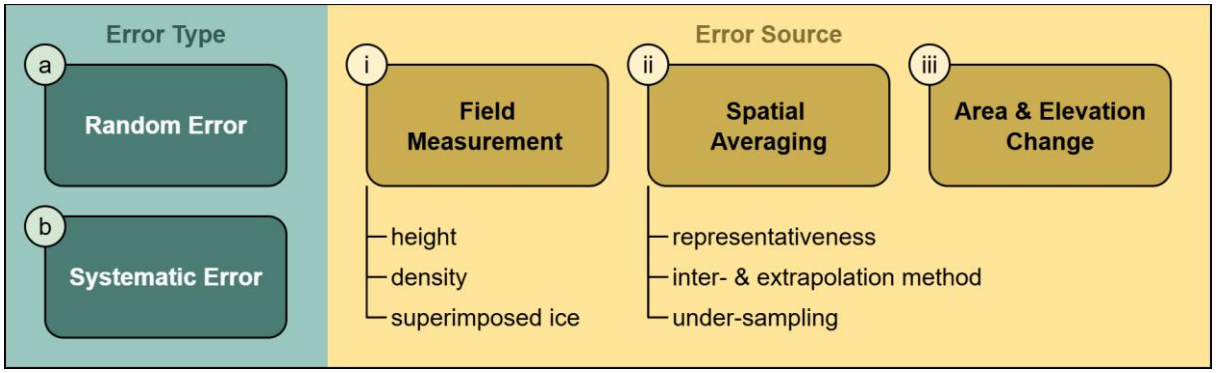

Figure 8: Sources and type of glaciological errors.

4.3 Geodetic method

Overview

The geodetic method quantifies glacier mass balance by repeatedly mapping surface elevations to derive changes in glacier volume (Zemp et al., 2013). This is typically done by differencing DEMs from two points in time and calculating elevation changes (Joerg & Zemp, 2014). Surface elevation data can be obtained using various techniques, including ground-based surveys, aerial photogrammetry, satellite-based InSAR, or laser altimetry (Zemp et al., 2013). Ideally, geodetic surveys are carried out at the end of the ablation season, just before the first significant snowfall, to minimize seasonal snow effects. The resulting volume change is expressed in cubic metres, requiring either the measurement or assumption of ice/firn density to convert volume to mass. Because changes in the bedrock elevation are neglectable on decadal timescales, the geodetic method captures the full glacier mass balance, including surface, internal, and basal components (Zemp et al., 2013).

Application in this study

Here, the most recent swissALTI3D DEM from 2022 was compared to the swissALTI3D from 2013, providing a glacier-wide mass balance estimate over a nine-year interval.

If no or only one DEM would be available, a less accurate geodetic mass balance estimate can still be made by comparing it to contour lines from topographic maps. In a rudimentary way the contour lines of the topographic maps can be used to reconstruct the glacier surface and thus serve as a replacement for the DEM. This approach is far less accurate than the comparison of two high resolution DEMs.

Expectations:

It is expected to derive an accurate **geodetic mass balance** with little uncertainties. Nevertheless, the geodetic method is subject to systematic and random errors (Zemp et al., 2013). Systematic error is expected to be small because both DEMs should be co-registered by swisstopo. Density assumption will probably be the biggest source of random error and overall uncertainty.

4.4 Process-based methods

The process-based methods deal with three of the possibly relevant processes for additional accumulation of the Clariden-N Glacier: Avalanches, topographic shading and debris cover. By applying these methods, it is anticipated to get an insight into the contributions of the different processes to the glacier mass balance (attribution).

4.4.1 Avalanches

To estimate the contribution of avalanches to the glacier's surface mass balance, information on frequency, magnitude, and properties of potential avalanche events is essential. Luckily, a camera situated north of Griessseeli proved particularly well suited for this task. The camera is permanently installed and oriented toward the lake, whose observation had been the main reason for its installation. Nonetheless, a larger area of the glacier (~50%) is visible in the background (cf. Figure 9). Between January 2023 and October 2024, more than 7000 images were captured at hourly intervals between 6 am and 6 pm and manually reviewed, allowing consistent visual monitoring of avalanche activity.

Based on this image series, avalanche events were identified, and their deposition zones were manually mapped in QGIS. The avalanche depositions were grouped both spatially and temporally. Four spatial zones were defined where avalanche depositions created on the same day were aggregated and threated as one event. Figure 9 presents the four deposition zones with the number of distinct avalanche events. Each event was classified by type (snow, debris, snow and debris, ice and indefinable) with the intention to refine the attribution of avalanches to surface mass balance. The frequency of events was determined by recording the number days of avalanche activity observed over the monitoring period. This mapping served as the basis for quantifying patterns of avalanche activity and assessing their potential relevance for localized mass gain on the glacier.

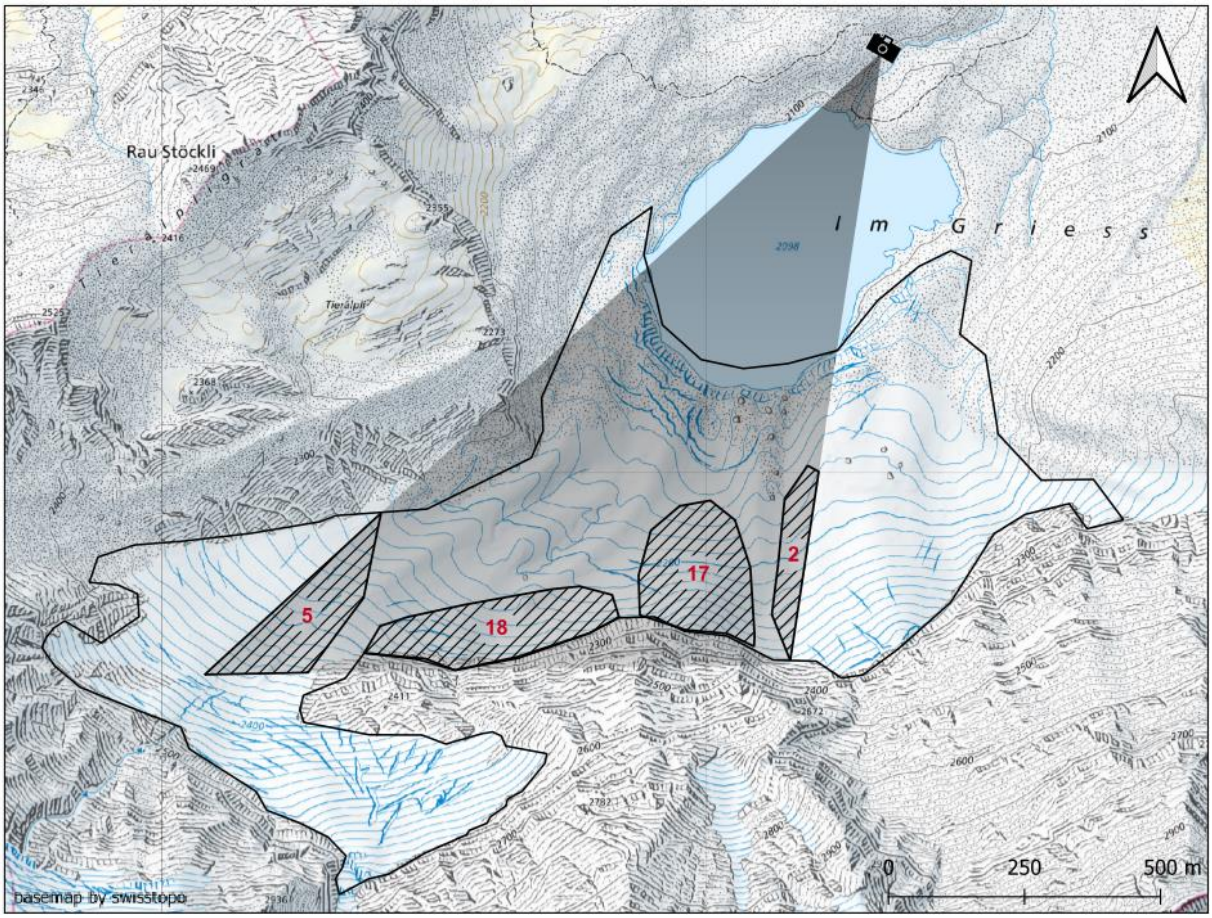

Figure 9: The location, direction and coverage of the field camera is indicated by the camera symbol and the black triangle. The camera covers approximately 50% of the entire 2022 glacier area. Avalanche events recorded between January 2023 and October 2024 are grouped and the sum is depicted as red numbers.

4.4.2 Topographic shading

Topographic shading plays an important role in determining direct solar radiation on a glacier and includes shaded relief (self-shadowing) and cast shadowing. For this study this distinction is not made, and the entire shading is accounted to cast shadowing. This is the shadow casted by the Clariden headwall, which reduces incoming solar radiation reaching the glacier surface. To quantify this reduction, the duration of sunlight and energy received by it over a flat surface (reference), unaffected by topographical shading, are compared with simulated values over the actual glacier surface. For this purpose, annual sunshine duration (hours/a) and total incoming shortwave radiation SW (kWh/m²/a) are determined at 100 sample points on and near the glacier and subsequently interpolated across the entire glacier surface. These sample points are calculated using the ShadeMap web application. ShadeMap computes the sun's position based on a given map location and time of year, tracing a path from each pixel on the map towards the sun. If this path intersects with terrain features the pixel is classified as shaded; otherwise,

it is classified as sunlit (ShadeMap, 2024). By summing up the sunlit timestamps over a year, the annual sunshine duration is calculated for a respective point on the glacier.

The duration of sunlight exposure alone does not directly correlate with ice melt rates, rather, it is the total incoming shortwave radiation $SW\downarrow$ that is crucial (Arnold et al., 2006). $SW\downarrow$ is influenced by the zenith angle, because as the zenith angle increases, the air mass – the distance solar radiation travels through the atmosphere – also increases, resulting in greater atmospheric absorption and reflection of incoming solar radiation (Olson & Rupper, 2019). SW further increases with the height above sea level, as the air mass decreases (Olson & Rupper, 2019). Other factors influencing $SW\downarrow$ like cloud cover, atmospheric composition, and local atmospheric conditions such as humidity and temperature, are not included in the assessment of topographic shading, because they are hardly quantifiable and assumed to have little effect overall.

4.4.3 Debris cover

The debris cover was determined by Hauser (2024) at the ablation stakes and other points on the glacier and then inter- and extrapolated to the glacier area of 2023. These measurements were integrated into a PDD model to assess their influence on ablation. No reassessment of the debris cover was carried out in the present study, as debris cover measurements taken at the four remaining measurement stakes from 2024 until 2025 resulted in corresponded to those of Hauser (2024). The agreement strengthens the confidence in correctness of this data. Consequently, the spatial distribution of debris thickness is not reanalysed here, but the effects of debris cover are taken into account in the interpretation and discussion of the results.

4.5 Glacier model

The one-dimensional glacier model used in this study is based on a shallow ice approximation (SIA). The model connects glacier ice dynamics implemented in *glaciermodel.py* with SMB climate forcing from *climates.py*. This setup enables experimentation with different climate scenarios and bed geometries, while maintaining a clear link to the governing equations of glacier evolution. The necessary inputs and resulting outputs are described in Section 4.5.1. The governing equations that form the basis for the calculation of all relevant processes are described in 4.5.2. Verification of the model was omitted, as it is already frequently used and was not developed as part of this thesis. It is therefore directly proceeded to calibration, where the individual input parameters are tuned to produce numerically stable, reliable and accurate results. The validity of the model simulations is tested in the following by validating it against the glacier length change of a 71-year period.

4.5.1 Model input and output

Table 3: Model inputs and outputs.

Input		
Numerical parameter	**Model parameter**	**Geometry**
grid size, Δx [m]	Glen flow-law rate factor, A_{Glen} [MPa]	bed topography
time step, Δt [a]	Glen's law exponent, n_{Glen}	reference width, W_0
run time, t_{max} [a]	ice density, ρ_{ice} [kg m^{-3}]	reference height, H_0
x-direction extent, x_{max} [a]	gravity acceleration, g [m s^{-2}]	ice surface, z_0
storing interval, Δt_store [a]	mass balance gradient, ġ [m w.e. a^{-1} m^{-1}]	
Climate forcing	z_{ELA}	
Output		
ice thickness, H_s [m]	volume, V_s [m]	
glacier width, W_s [m]	glacier length, L_s [m]	
surface elevation, z_s [m a.s.l.]	ELA, z_{ELA} [m a.s.l.]	
surface mass balance, b_s [m w.e. a^{-1}]		

In order to run, the model requires three types of inputs: numerical parameters, model parameters and geometry. The **numerical parameters** control the discretisation and set up the simulations. These include the grid spacing parameter Δx defining the spatial resolution of the flowline grid, the integration time step Δt, the total run time t_{max}, the horizontal length x_{max}, and the interval at which results are stored Δt_store. **Model parameters** specify the physical dynamic and flow properties of ice. The Glen flow-law rate factor A_{Glen} and the exponent n_{Glen} define the creep relation between stress and strain. Ice density ρ_{ice} and gravitational acceleration g determine the driving stress, while the mass balance gradient $\dot{g}$ controls how the surface mass balance changes with elevation. **Geometry** demands the bedrock topography along the flowline, alongside reference width W_0 and height H_0, which define the valley shape. The initial ice surface elevation z_0 is the last component relevant for the geometric input. The

climatic forcing is incorporated into the model with z_{ELA}, which can be specified as a constant or a historical time series.

The model produces a series of variables describing the glacier. Outputs include ice thickness along the flowline, which is a result of the solved continuity equation. The related glacier width W_s and surface elevation z_s define the ice volume V_s, which is the integrated cross-section along the flowline. The glacier length corresponds to the glacier terminus position, where surface and bedrock elevation are equal.

4.5.2 Governing equations

Continuity equation

How ice thickness $H(x,t)$ evolves over time is defined by the continuity equation.

$$\frac{\partial H(x,t)}{\partial t} = \dot{b}(x,t) - \frac{1}{W(x)}\frac{\partial}{\partial x}[Q(x,t) \times W(x,t)] \tag{4}$$

The SMB at a given time t at point x is given as $\dot{b}(x,t)$, $Q(x,t)$ is the respective ice flux and $W(x,t)$ the width of the glacier at that point in time and space. This means, that H changes as a combination of climate forcing and the divergence of ice flux.

Surface mass balance

Equation (5) describes the SMB as a linear function of surface elevation in relation to ELA.

$$\dot{b}(x,t) = \dot{g} \times (z_s(x,t) - z_{ELA}(t)) \tag{5}$$

The mass balance gradient $\dot{g}$ defines the rate at which a point above or below the ELA gain or lose mass. With a steeper gradient, less elevation difference is needed for the same accumulation or ablation.

Stress and deformation

Gen's flow law (6) describes how ice is deformed and connects strain rate $\dot{\varepsilon}$ to basal shear stress τ. A is the rate factor and n the flow exponent.

$$\dot{\varepsilon} = A\tau^n \tag{6}$$

The basal shear stress τ is increasing with steepness and ice thickness as follows:

$$\tau = \rho g H \frac{\partial z_s}{\partial x} \tag{7}$$

Ice flux

How ice moves along the flowline is defined by the volumetric ice flux.

$$Q = \frac{2A \cdot W}{n+2}\left(\rho g \frac{\partial z_s}{\partial x}\right)^n H^{n+2} \tag{8}$$

With n = 3 ice flux scales with the cube of surface slope and with the fifth power of ice thickness, making glacier flow highly sensitive to geometry.

Diffusion

Flux divergence is expressed as diffusion for numerically implementing it into the model.

$$\frac{\partial Q}{\partial x} \propto D \frac{\partial^2 z_s}{\partial x^2} \tag{9}$$

The effective diffusivity is then defined as:

$$D = \frac{2A \cdot W}{n+2}\left(\rho g \frac{\partial z_s}{\partial x}\right)^{n-1} H^{n+2} \tag{10}$$

Semi-implicit

This glacier model is a semi-implicit scheme because ice flow is solved implicitly through the tridiagonal matrix which solves the diffusion equation, but the SMB is explicit, as it is simply added to the updated solution. The difference is that the explicit part makes the glacier in the next step dependent only on the current glacier, whereas in the implicit part, the glacier in the next step is additionally dependent on itself.

4.5.3 Model assessment

Verification – the first step of model assessment – checks if the glacier model itself has been implemented correctly and ensures that equations are solved correctly. Verification is not carried out in this study, as this model is one that is already frequently used and was not developed as part of this thesis.

Calibration builds the second part of model assessment and tries to find an optimal set of parameters that introduces as little uncertainty as possible. Model calibration or parameter optimization is a procedure to systematically find a good set of parameters to produce accurate and reliable results. In glacier mass balance modelling, this process is essential for refining the representation of mass balance components, thereby improving the model's ability to simulate glacier evolution under varying climatic conditions (Zekollari et al., 2022). The primary

objective of calibration is to minimize discrepancies between observations and simulations by systematically adjusting key parameters within plausible ranges. This ensures that the model can adequately reproduce past glacier behaviour and provide reliable projections for future changes (Zekollari et al., 2022). Several parameters are poorly constrained and thus need to be adjusted, to have results fitting the observations. For calibration the glacier length (terminus position) from 2022 is being used as the observational measurement to be reproduced. As part of the calibration a sensitivity analysis was conducted to examine the influence of different parameters on the model results. This intensive procedure is described in depth in the following section.

Validation is the last step which evaluates if the calibrated model results sufficiently represent the observed reality, which is done by comparing simulated and observed values that have not been used during the calibration. While the calibration was based on the 2022 glacier length, the validation is done by comparing against historic length changes (1951-2022) and surface height changes (1963-2022).

4.5.4 Model calibration and sensitivity analysis

The *sensitivity analysis* is part of the model calibration and evaluates the effect of specific parameters on the model output. *Mitigation strategies* describe ways to alter this effect. It is divided into two parts based on the type of parameter: *numerical* and *physical*. The *numerical sensitivity analysis* examines the impact of numerical (runtime) parameters varying within reasonable ranges. Ideally, these should have minimal influence, as they do not represent glacier physics. The *physical sensitivity analysis* assesses the influence of physical parameters on the model output. The model should respond sensibly to changes in these parameters; or its proper functioning is questionable. Mitigation strategies for numerical parameters try to minimize the sensitivity; for physical parameter, optimization strategies try to increase the functioning and robustness of the model simulations.

Under consistent conditions, only the values of the respective parameter are changed, and it is checked whether a difference is visible. The conditions are then adjusted, and the same process is repeated until an acceptable amount of data has been collected. This process is the same for all parameters analysed. To keep the computations limited, initial testing was conducted by adjusting values by hand. These tests revealed significant variations in the results by adjusting the grid spacing parameter dx and glacier bed properties. Other variations remained in expected ranges. Thus, the numerical sensitivity analysis concerns only dx and the physical sensitivity analysis is concerned with bed topography, W_0 and H_0.

Numerical sensitivity analysis – Δx mitigation strategies

The running parameter *dx* should preferably have no influence on the simulation outcome but rather be chosen on behalf of the required or preferred resolution. Therefore, three different methods to decrease the influence of *dx* are presented, all targeting the elevation profile of the glacier bed.

Flattened bed: The easiest way to achieve this is to flatten, smooth, or simplify the topography, which is akin to approximating the uniform bed topography (where *dx* has very little influence). This solution benefits from a simple implementation, a low risk of overcomplication, and no need for an individually constructed mass balance. Moreover, it has been successfully applied in other studies (cf. Laha et al., 2017). However, simplification can obscure the true nature of flow properties, making interpretation difficult. It also makes comparison with the control points for checking the geometry more difficult.

Adjusted bed: Another way to deal with the very steep cliff above the glacier is by aligning the top edge of the cliff to a multiple of dx. This way, at least the start of the cliff is equal among the different dx simulations. It is expected that this solution will retain the specific steep topography and its influence on the flow properties, while minimising the influence of dx. Whether this reduces the influence of dx is nevertheless questionable and must therefore be evaluated.

Shortened bed: A more elaborate approach excludes the steep cliff above the glacier completely and concentrates only on the area covered by the glacier. This means that the glacier is not fed by ice downflowing in the 'accumulation area' on the steep flank above the glacier, as is the case in the other two solutions, but by 'direct' additional accumulation in the upper area of the glacier itself. This might reduce the influence of dx. A more accurate interpretation of the simulations in comparison with the control points might be possible. However, it remains speculative to what extent this approach is advisable, as the artificially constructed mass balance is based on possibly vague assumptions. Therefore, this approach will not be part of the simulation results in this paper but will be discussed in this context.

The evaluation of the best *dx* mitigation strategy – method in minimizing the influence of the numerical parameter *dx* – is following a quantitative comparison framework. The main evaluation criterium is *dx* sensitivity, which is reflected in the standard deviation σ or the range of glacier lengths of the ten best performing simulations. The less sensitive *dx* is, the less dependent the results are on *dx* and thus the better the performance of the method. To verify the physical truthfulness and determine the simulation performance, $|\Delta L|$ is considered. The mean absolute length difference $|\Delta L|$ is the absolute difference between the simulated glacier termini and the geodetically derived glacier terminus position. For calibration only results for the year

2022 are of concern and the compared dx values are 30, 35, 40, 45 and 50. The improvement is quantified as follows:

$$Improvement\ [\%] = \left(1 - \frac{\sigma_{new}}{\sigma_{ref}}\right) \times 100 \tag{10}$$

Physical sensitivity analysis – W/h optimization strategies

The glacier bed might not be the typical physical parameter, it can (when modelling) be a tuneable input. Depending on the glacier bed properties, which in the case of Clariden-N Glacier is based on several assumptions, different results can be expected. Thus, the sensitivity of the glacier mass balance simulations to changes in the glacier bed profile and cross-sectional shape is assessed and optimized.

"W/h" optimization strategies

The cross-sectional shape of the glacier bed influences the results of the simulation, and is based on the reference width W_0 and height H_0 as follows:

$$W(x) = W_0(x) \times \sqrt{\frac{H(x)}{H_0(x)}} + \varepsilon \tag{10}$$

The two reference parameters height and width define the parabolic valley shape and should thus be chosen deliberately so resulting parabola approximates the dimensions of the real glacier bed. A parabola is often a good approximation to the cross-sectional valley shape of a typical valley glacier. However, due to the very different topography of the Clariden-N glacier bed and its surroundings, finding a representative parabola to represent this is prone to be challenging. For this reason, various approaches for the reconstruction of the glacier bed shape are proposed, tested and evaluated for their accuracy and usefulness. These approaches, compared to the dx mitigation strategies, do not try to eliminate sensitivity on simulation results, but rather try to find a realistic solution where simulations run consistently error-free.

The Clariden-N Glacier is wider than long, and thus opposite of a typical valley glacier which is longer than wide. This leads the initial question regarding the glacier bed shape, namely the **scope**. The scope decides whether the glacier is modelled over the full extension ("full width" approach) or only a part of it ("partial width" approach). Generally, it is preferable to model the whole glacier at once because ice volume, ice flow and the glacier's geometry can be compared better to geodetic or glaciological observations. However, due to the high complexity of the Clariden-N Glacier and lacking observational data, it is easier and possibly more purposeful to

only look at a certain part of the glacier. In the case of a partial width approach, the parabola can represent besides bedrock also glacier ice itself. This means that the existing glacier ice which borders the area of interest is treated as bedrock. The “full” and “partial width” approaches are generally both compatible with all types of glacier beds (realistic, flattened, shortened & adjusted).

Having selected the scope of interest, the **form** (width along the flowline) can adopt different dimensions. Either the parabola has the same shape along the whole profile (“uniform”) or it does not (“narrow” or “wide accumulation”). The **transitions** in form are implemented as step or linear changes.

There are of course many more possible strategies that could be tested, but these suggested seemed to be the reasonable options for the Clariden-N Glacier specifically. The different approaches are described below with an emphasis on possible outcomes. This should help to understand the interpretation of the results.

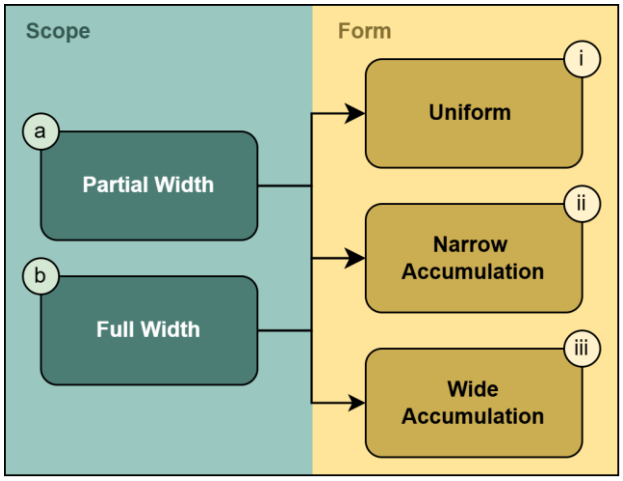

Figure 10: The cross-sectional shape of the glacier bed varies depending on assumptions and purpose of usage. The scope defines the extent of interest of the glacier. A partial width (a) focuses on a specific flow region whereas the full width (b) targets the entire glacier. The form defines the cross-sectional shape profile along the flowline. A uniform (i) shape profile is indifferent in form along the whole profile, the narrow accumulation (ii) is characterized by a tighter form on the headwalls and the wide accumulation (iii) the opposite of that.

Scope

Full width: To reach the full width of the glacier is the goal of this method. It does not model a part of the glacier but tries to do the full glacier at once which follows the normal approach for a valley glacier. Thus, the shape needs to be very flat and wide, so the ice can be built up over the entire width. Due to the very complex topography the interpretability of this approach might be useless in this regard. For the reconstruction of climatic conditions, it could prove valuable.

Partial width: Only a part of the glacier is modelled. The bed width is limited to a section which is assumed to be somewhat self-contained. This method might be more precise in producing simulations that represent the true geometry. However, it might lack in accuracy when it comes to the representation of climatic conditions.

Form

Uniform width: A uniform or constant width along the flowline is the simplest form and most often the first choice when assessing the glacier mass balance through a 1D flowline modelling approach. It is easily interpretable and does not require detailed knowledge of the topographic restrictions.

Narrow accumulation width: A narrow width in the accumulation area is an uncommon phenomenon. Usually, the accumulation area is much wider to be able to balance the mass loss in the ablation area. However, for the Clariden-N glacier we know from the hypsometry, that the shape of the glacier is far different with the major glacier area at low elevation and small amounts in higher elevations.

Wide accumulation width: Under the reasonable assumption that snow drift originating from the Claridenfirn majorly influences the Clariden-N glacier's mass balance, the wide accumulation width approach comes into play. Due to this additional accumulation the headwall is widened to account for this.

Transition

Apart from Scope and Form the *transition* type can be chosen. Here ***step*** and ***linear*** transition are used to shape the cross-sectional shape transitions of non-uniform glacier beds.

5 Results

5.1 Glacier development from 1859 until 2025

The Dufour map is the oldest map that shows the extent of the Clariden Glacier around 1859. The accuracy of the data collection is far from what we have today, which is why we can only get a rough impression. What can certainly be said is that the glacier extended to the edge of the Klus cliff, where vast amounts of till can be found today (cf. Figure 11). This is also in line with moraines drawn on the GeoVector map (Figure 5) and geomorphological observations in the field. The Siegfried map, which replaced the Dufour map, shows the Clariden-N Glacier in varying sizes, but generally decreasing, on four topographic maps from 1876 to 1930. It was only with the introduction of the Old National Map, the predecessor of the National Map, that the map resolution was considered sufficient to collect quantitative spatial data.

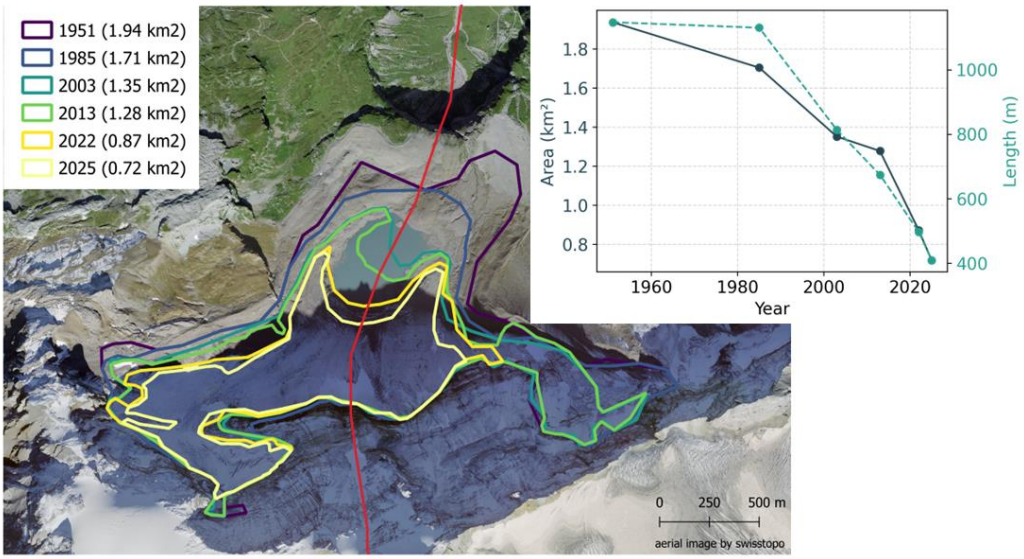

Figure 11: Glacier area and length development: The outlines show the Clariden-N Glacier area development from 1951 until 2025. The change in area and length over time are presented in the graph.

The hand-drawn glacier outlines (Figure 11) show a rapid decline in glacier area since 1951. The nearly 2 km^2 of glacier area present in 1951, has shrunk to approximately 37% in 2015. The decline has been particularly pronounced since 2013, with the glacier losing an average of 46,577 m^2, or 6.5 football fields, of glacier surface annually. This strong decrease in glacier

area might be partly explained due to a possible overestimation of glacier area in the east of the 2013 outline (cf. Figure 18). If this rate of area loss remains constant, all the ice on the Clariden-N Glacier will have melted by 2040. The glacier length along the flowline has experienced similar changes, ending up in 2025 with only 35% of the length the glacier had in 1951. This is a total retreat of 738 m or 10 m per year. Since 1985, the length retreat is much more pronounced. If the retreat rate since 2013 continues into the future, there will not be any glacier ice in the path of the flowline in 2045.

The hypsometry of the Clariden-N Glacier (Figure 12) shows that the largest proportion of its surface area is located at lower elevations and generally decreases as elevation increases. A comparison between 1951 and 2022 shows that ice surface area has been lost at all altitudes. The greatest loss of area occurred at lower altitudes. Ice above 2600 m a.s.l. is practically non-existent in 2022, whereas 71 years ago it still reached up to 2700 m a.s.l. Similarly, ice at proglacial lake level (~2100 m a.s.l.) has vanished. The average altitude has fallen by 40 m during this period.

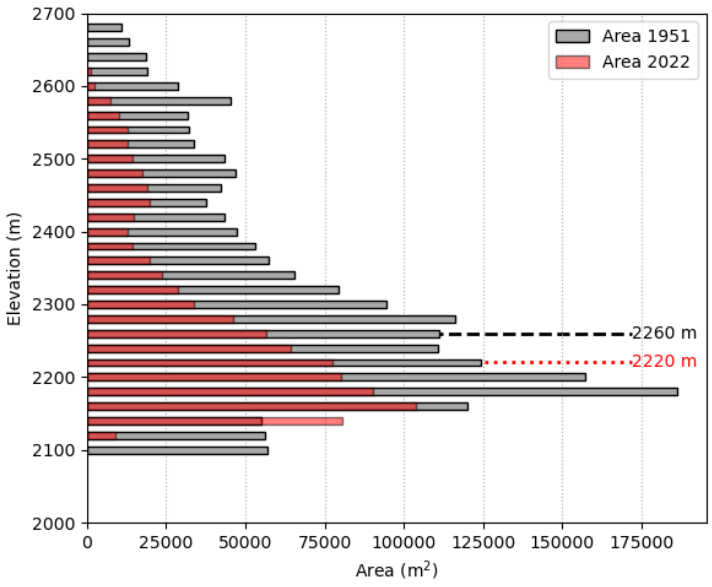

Figure 12: Hypsometry of Clariden-N Glacier in 1951 and 2022 with marked mean elevation.

The elevation changes at the control points are intentionally controlling parameters for the simulations but they themselves offer interesting insights into the glacier evolution (Figure 13). The control points are derived from topographic maps starting in 1963 a DEM from 2022. Overall, the annual elevation changes increase with time. From 1963 to 1990, the glacier surface changed the least, whereas from 2016-2022 the glacier surface changed the most (except E and F). The largest annual elevation changes are observable at control point D during the 2016-2022 period. The second-highest change observed is at control point C (the one just above D)

also during the same period. The points E and F have not experienced any elevation change during this period, as they are located over the proglacial lake.

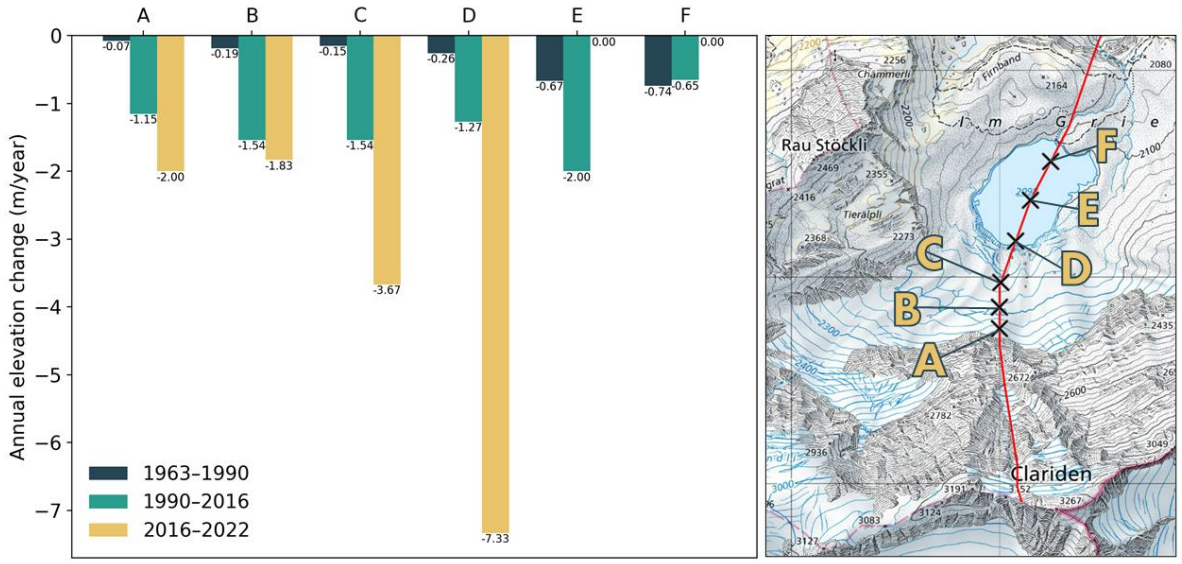

Figure 13: Glacier elevation changes - (1963-2022): Changes in elevation for control points A-F observed on topographic maps and a DEM are presented as annual elevation changes and divided into the three periods

If the cartographers at swisstopo for the National Map can be trusted, it can be concluded that the glacial lake first appeared supraglacially at the tongue in 1990 as two small ponds. In the next map edition from 1997, it is already mapped as one proglacial lake, and the tongue appears to have receded significantly (Figure 14). Latest in 2003, the glacier ice was in contact with the lake and forming a steep edge. The glacier lake has never stopped growing in area since. Hauser (2024) recorded several calving processes in the summer of 2023. A bathymetric survey planned in November 2024 failed on site because the water presented itself in a solid aggregate state, while researchers and equipment were expecting a liquid. Thus, the bathymetry of the glacier lake remains unknown. However, a lesson was learned: A boat can be carried more easily by two people than alone.

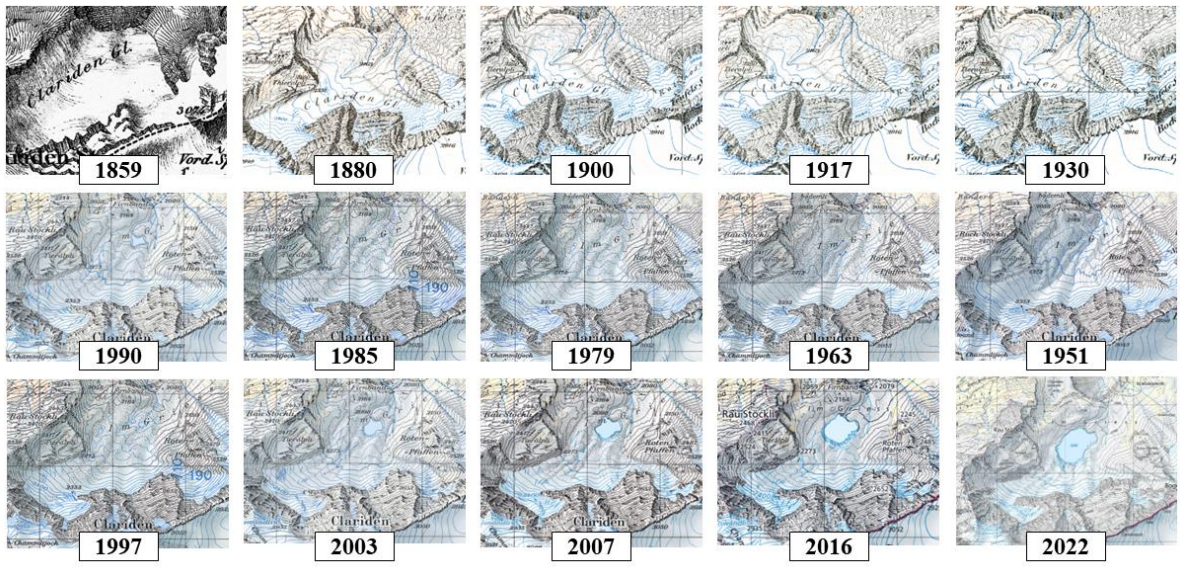

Figure 14: Series of topographic maps of the study area by swisstopo.

The meteorological data from the IMIS stations provide information about snow depth and air temperature for the entire 21st century. It shows that air temperature depends on altitude – a station at a lower altitude measures higher air temperatures. The average lapse rate over the entire period is -6.8K/km (cf. Chapter 5.5). However, snow depth does not show this dependence. The lowest IMIS station, Ortstock Matt (1824 m a.s.l.), measures a thicker snow cover on average than the Seewli station, which is more than 200 m higher. There are no statistically significant trends observable. However, the regression line shows a small decrease in snow height and an even smaller increase in air temperature.

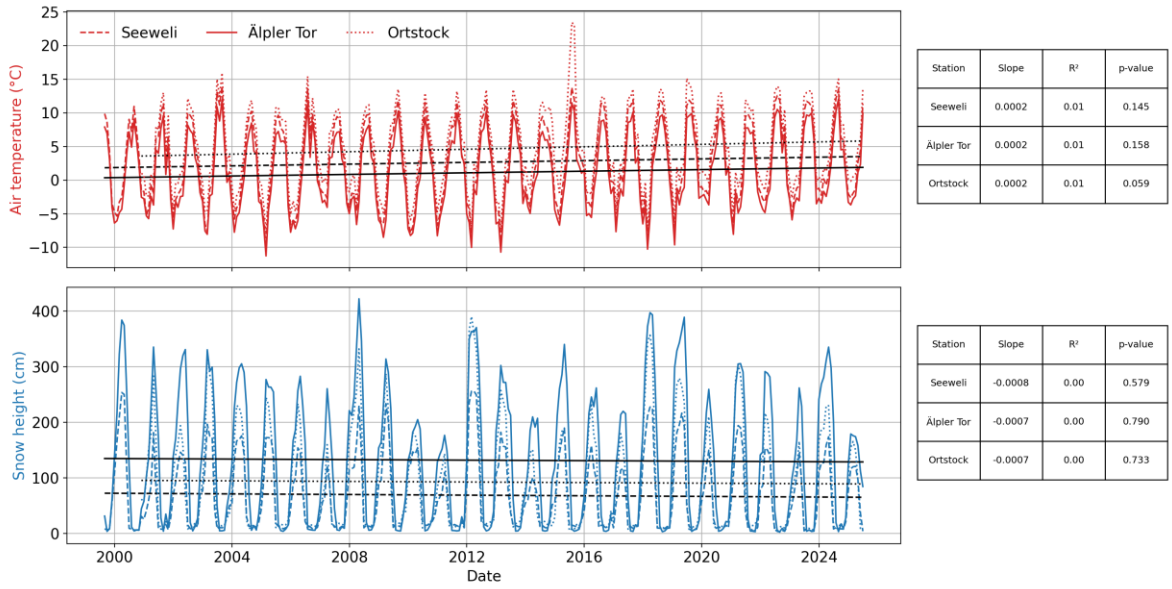

Station	Slope	R^2	p-value
Seewli	0.0002	0.01	0.145
Älpler Tor	0.0002	0.01	0.158
Ortstock	0.0002	0.01	0.059

Station	Slope	R^2	p-value
Seewli	-0.0008	0.00	0.579
Älpler Tor	-0.0007	0.00	0.790
Ortstock	-0.0007	0.00	0.733

Figure 15: Air temperature and snow height for the entire measurement period of the three IMIS stations Seewli, Älpler Tor and Ortstock Matt are presented as monthly means. The tables on the right show slope, R2 and p-value of the linear regression.

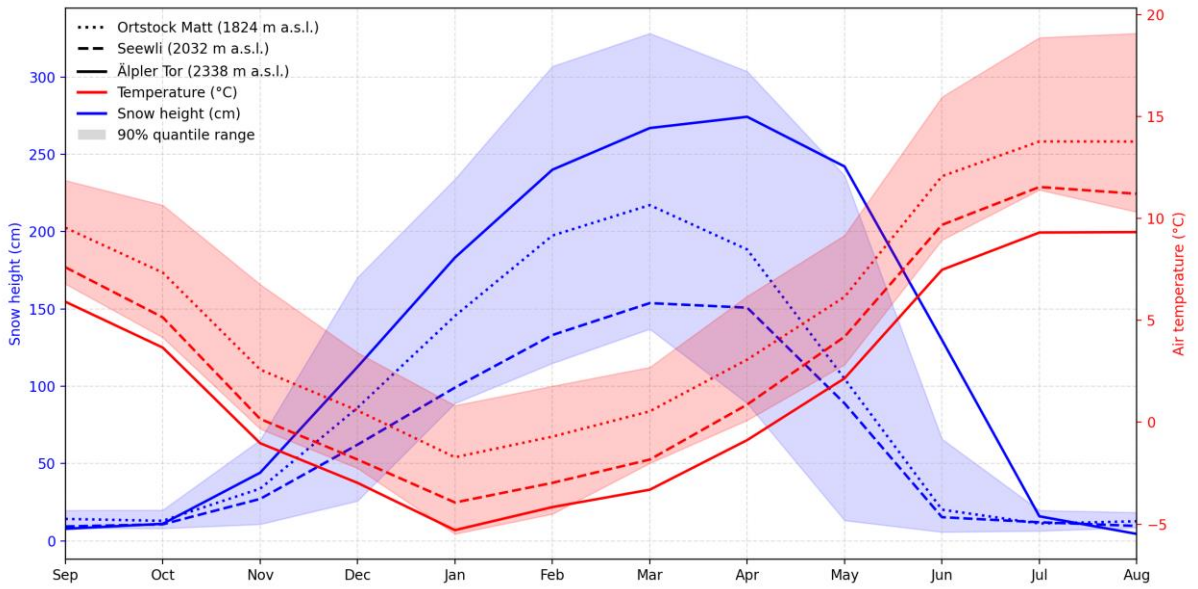

Figure 16: Annual air temperature and snow height: Monthly means for each station are averaged over the entire measurement period. The 90% quantile range for the Ortstock Matt station is depicted ad the blue and red colored plane.

The snow period in Figure 17 indicates the duration of continues winter snow height above 15 cm at the IMIS stations. This threshold is included, because the stations also measure a snow height of a few centimetres during summer which might has to do with vegetation. The short snow-covered period in Winter 07-08 is most probably a result of unusually high fall temperatures (cf. Figure 15). There is no value for 2025 at Älpler Tor station because snow cover of 80 cm was still measured at the cut of date at end of June. The linear regression lines in Figure 17 show a clear decrease in snow cover period for all stations. The least pronounced reduction can be observed for the highest elevated station Älpler Tor.

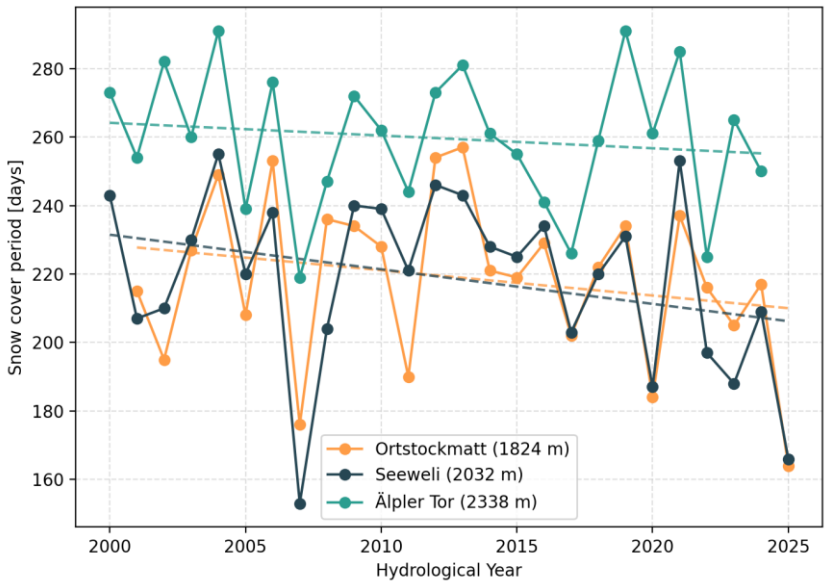

Figure 17: Duration of snow-covered period in days calculated from snow height measurements of three IMIS snow stations with linear regression slopes: -0.74 (Ortstock Matt), -1.01 (Seewli), -0.37 d a^{-1} (Älpler Tor).

5.2 Geodetic and glaciological mass balance

Here, the geodetic and glaciological results are presented. First, the glacier-wide geodetic balance, then the glaciological and finishing with the correction for uncertainties.

5.2.1 Geodetic mass balance

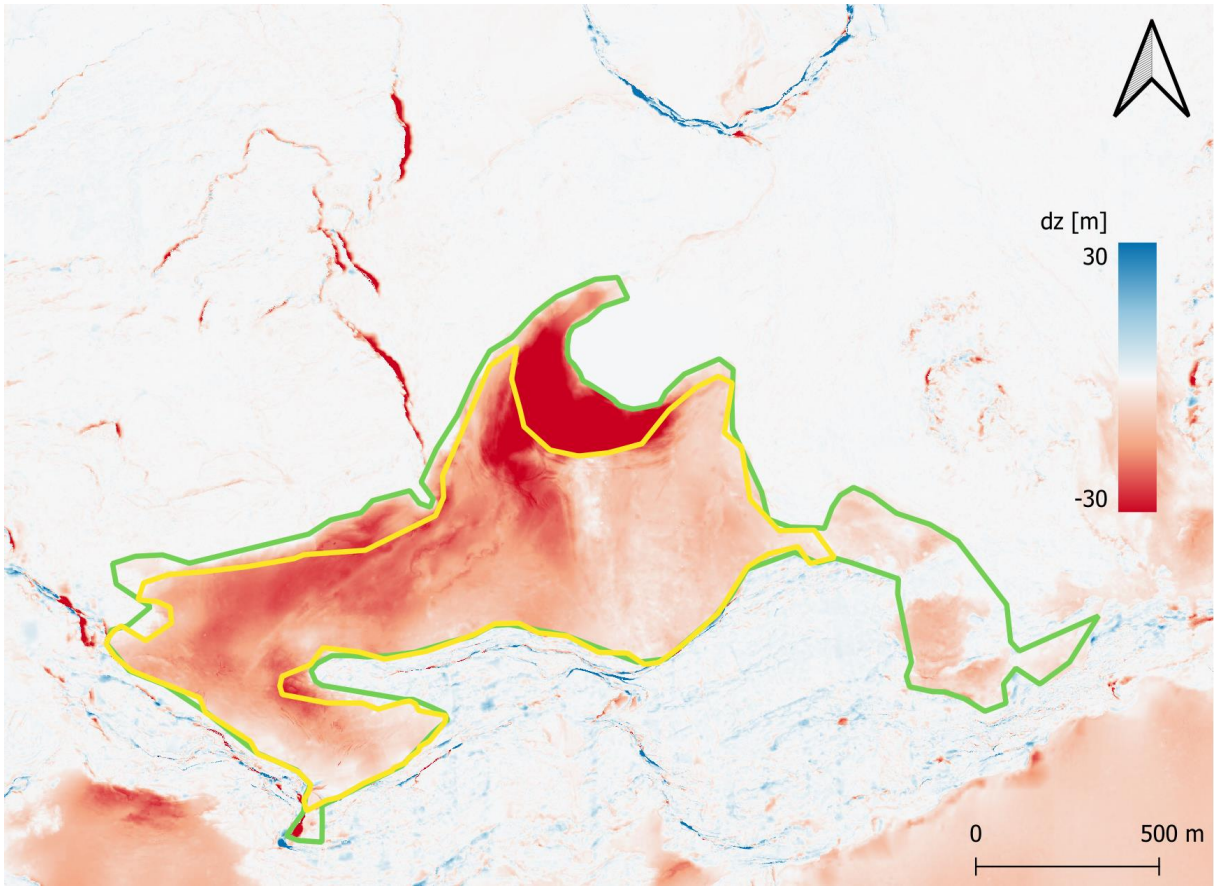

Figure 18: DEM-Differencing between 2013 and 2022 with marked glacier outlines (green 2013; yellow 2022).

The geodetic observation indicates a decrease of glacier area of approximately 0.4 km^2 (45'011 m^2 a^{-1}) over the nine-year period from 2013 to 2022. The differencing of the two DEMs over the 2013 glacier outlines resulted in a volume change ΔV of nearly 8'000'000 m^3. The mean thickness change $\overline{\Delta h}$ over the mean glacier area $\bar{S}$ ($\frac{Area_{2013}+Area_{2022}}{2}$) is calculated to be -7.39 m. The biggest changes are observable at the lake front, whereas areas in the central and eastern part of the glacier showed very little change in elevation.

Table 4: Statistics of DEM differencing 2013-2022.

Mean thickness change $\overline{\Delta h}$	-7.39 m
Area change ΔS	-405'099 m^2
Volume change ΔV	-7'953'348 m^3

The geodetic mass balance B_{geod} is presented as mass change in metre water equivalent (m w.e.) and calculated as follows by assuming an ice density ρ_{ice} of 900 kg/m^3.

$$B_{geod} = \frac{\Delta V}{S} \times \frac{\rho_{ice}}{\rho_{water}}$$

The geodetic mass balance over the 9 years comes out to **-6.65 m w.e.** or **-0.74 m w.e. a^{-1}**.
The

The resampling of the higher resolved DEM from 2022 (0.5 m) to the lower resolution of the 2013 DEM (2 m) before the DEM-Differencing leads to a slightly lower geodetic mass balance of -4.9 mm (-0.66 %) in comparison to no resampling.

Table 5: Parameters, values and units used for geodetic survey.

Symbol	Parameter		Value	Unit
a	years		9	
p	pixel size		2	m
ρ_w	density water		1000	kg m^{-3}
ρ_i	density ice		900	kg m^{-3}
S_0	area 2013		1’279’015	m^2
S_1	area 2022		873’916	m^2
S	area mean		1’076’466	m^2
ΔS	area change	$= S_0 - S_1$	-405’099	m^2
Δz	surface height change	$= \sum DEM_1(x,y) - DEM_0(x,y)$	-3’976’674	m
Δh	mean thickness change over S	$= \Delta z / S$	-7.39	m
Δh_{2013}	mean thickness change over S_0	$= \Delta z / S_0$	-6.22	m
Δh_{2022}	mean thickness change over S_1	$= \Delta z / S_1$	-9.10	m
ΔV	volume change over S_0	$= \Delta z \times p$	-7’953’348	m^3
B_{geod}	geodetic mass balance	$= (\Delta V / S) \times (\rho_i / \rho_w)$	-6.65	m w.e.
$B_{geod,a}$	annual geodetic mass balance	$= B_{geod} / a$	-0.74	m w.e. a^{-1}

5.2.2 Glaciological mass balance

Due to the complete melting of many ablation stakes, none of the measurement series is continuous or complete. Consequently, several temporal gaps exist in the dataset, either because no replacement stakes were installed or because the original stakes had fully ablated prior to subsequent measurements. For this reason, it was decided not to present the individual measurement series of the ablation stakes or their respective locations. Instead, the analysis focuses on the cumulative mean, maximum and minimum derived from the values of each measurement period. Ablation stake number 8 was excluded from the calculation, as it was installed in a location that exhibited minimal surface change and experienced very limited melt. As such, it does not appear to be representative of the maximum ablation typically observed at the glacier terminus. The mean melt rates for each period were successively summed to obtain the average cumulative melt, which is depicted as a dashed black line in Figure 19. The same figure also displays the range of values in grey, representing the cumulative minimum and maximum melt across all stakes. To convert thickness change into ablation a_{glac} and ablation rate $\dot{a}_{glac}$ the same densities are used as for the geodetic mass balance $A_{glac} = \Delta h \times \frac{\rho_{ice}}{\rho_{water}}$.

Table 6: Statistics of ablation stakes measurements 2023-2025 showing ice loss.

	Δh [m]	a_{glac} [m w.e.]	$\Delta \dot{h}$ [m a^{-1}]	$\dot{a}_{glac}$ [m w.e. a^{-1}]
Minimum	-3.53	-3.18	-1.71	-1.54
Mean	-4.28	-3.85	-2.07	-1.86
Maximum	-5.02	-4.52	-2.43	-2.19

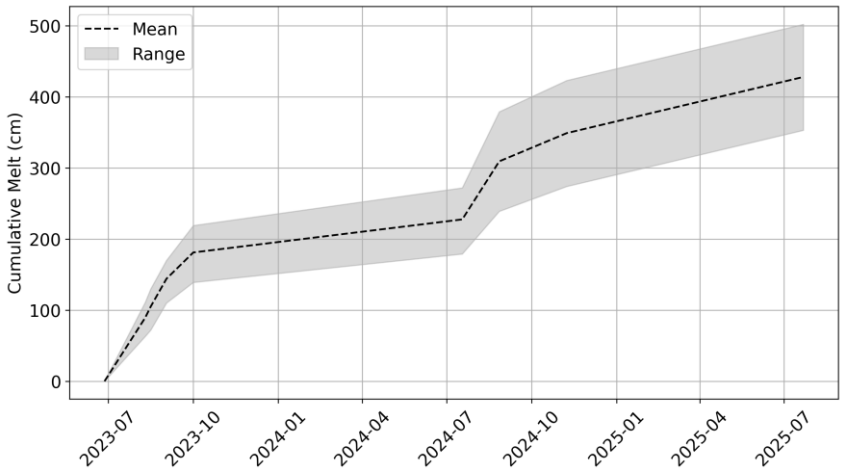

Figure 19: Cumulative melt (ice loss) in centimetre over the entire glaciological measurement period (27.06.2023 - 22.07.2025). The summation of the mean ice loss per measurement window is shown as the dashed black line. The grey area shows the range between the summation of the minimum and maximum ice loss per measurement window.

5.2.3 Corrected glaciological and geodetic mass balance

Comparing the two mass balance estimates is difficult, because two different elements where measured. The geodetic mass balance measured the glacier-wide balance over a nine-year period. The glaciological method measured maximum ablation over a two-year period. Thus, a comprehensive uncertainty assessment as described by Zemp et al. (2013) is neither possible nor needed. However, possible sources of error – random or systematic – are still addressed to keep in mind when working or interpreting the data.

To check whether the two DEMs were co-registered the horizontal and vertical alignment of DEMs was executed using the co-registration algorithm "dem_align.py" from the "demcoreg" python script. As expected, the results (Appendix 1) showed no improvement; thus, the co-registration was already properly done.

The systematic error (+0.002 m w.e.) of the geodetic method arises from co-registration and is directly added to the balance and was determined using a stable, ice-free area. Since no elevation change is to be expected in stable areas, the standard deviation over the square root of the number of independent pixels is the remaining systematic error of the DEM difference. The glaciological method is regarded as free from systematic error, as it relies on direct and well-established field measurements which, when conducted rigorously, do not inherently introduce consistent bias.

Random errors, on the other hand, essentially define the error bars. For the geodetic method, random error sources mainly from the density assumption:

$$\sigma_{geod,\rho} = \overline{\Delta h} \cdot \frac{\sigma_\rho}{\rho_{water}} = \pm 0.443\ m\ w.e.\ \ or \pm 0.049\ \text{m w. e. a}^{-1}\ , \tag{4}$$

with $\sigma_\rho = 60\ kg\ m^{-3}$. For the glaciological method, random error was estimated from two contributions: ±0.04 m w.e. due to field measurement variability of two people and ±0.3 m w.e. from uncertainty due to interrupted measurement series. Over the two years of glaciological measurement, this results in a random error of ±0.34 m w.e. or ±0.17 m w.e. a^{-1}. The corrected geodetic mass balance and glaciological ablation are presented in Table 7.

Table 7: Corrected glaciological ablation (2 years) and geodetic mass balance (9 years) and their annual rates.

geodetic mass balance, B_{geod}	**-6.65** ±0.44 m w.e.
glaciological ablation, a_{glac}	**-4.52** ±0.34 m w.e.
geodetic mass balance rate, $\dot{B}_{geod}$	**-0.74** ±0.05 m w.e. a^{-1}
glaciological ablation rate, $\dot{a}_{glac}$	**-2.19** ±0.17 m w.e. a^{-1}

5.3 Avalanche feeding

The photo analysis of the hourly in-situ camera from January 1st, 2023, until Oktober 9th, 2024, (648 days) resulted in 28 days of newly observed avalanche deposits over the observed glacier surface 0.43 km^2 (~50% of total glacial area). On 40% of the observed glacier surface at least once avalanche deposits were detected. The summed area of yearly avalanche deposits comes up to 60% (0.253 km^2) of the total observed glacier area. Given the results from this two-year photo analysis, it is predicted that up to 65% of the entire glacier surface area can be affected by avalanches in a 10-year return period (Figure 22). By affected it is meant that it is either part of the release area, the flow path or the deposition area.

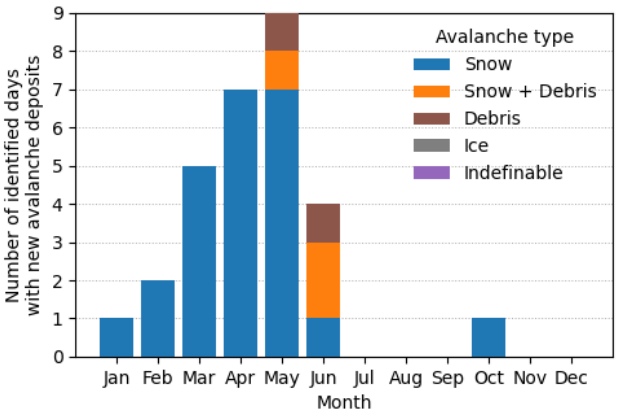

Figure 20: Annual distribution of avalanche events: Each day where an avalanche deposit on the glacier was recognised counts as an avalanche event. It is categorized by type and summed per

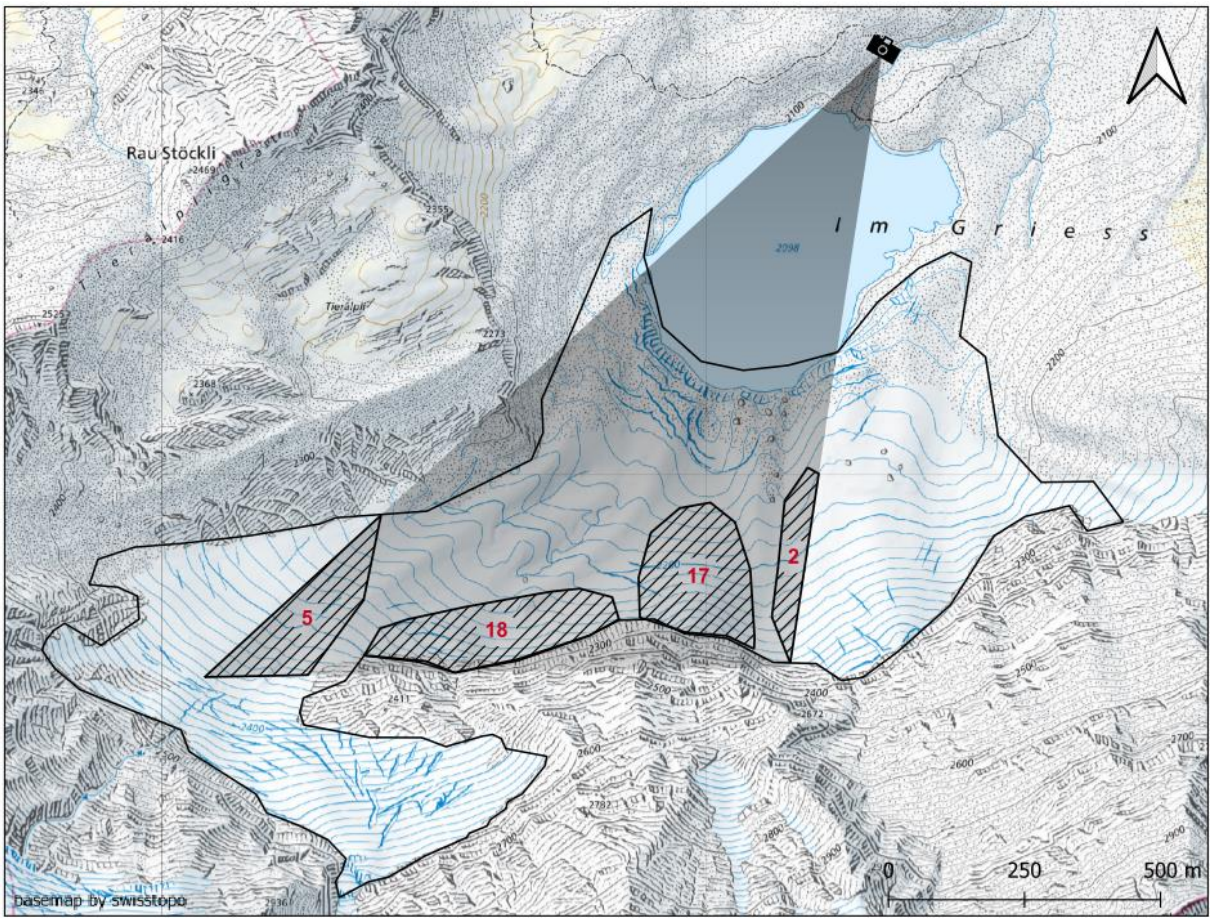

Figure 21: The number of detected avalanches by photoanalysis grouped per area on the glacier are displayed in red. The camera angle and its focal length determine the cone-shaped coverage.

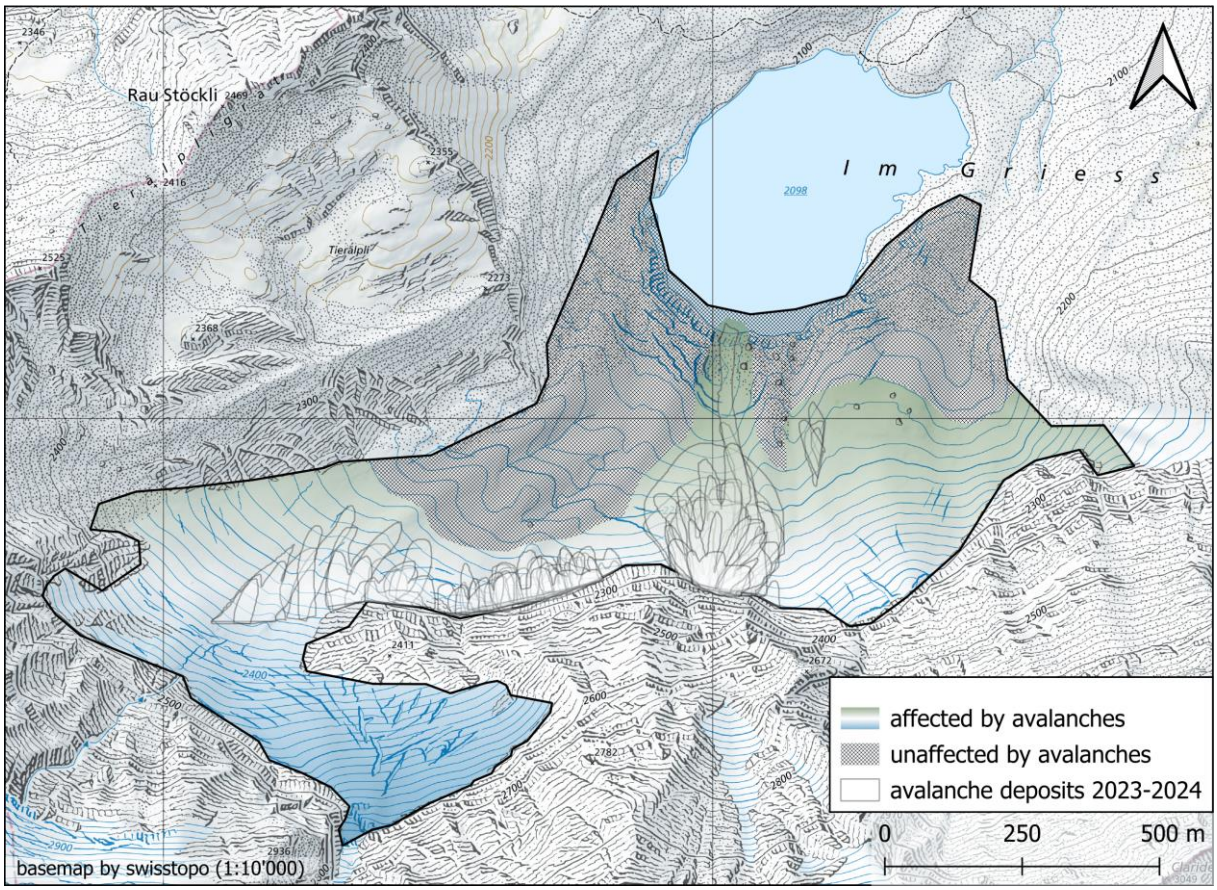

Figure 22: Area which are expected to experience avalanche impact of 10-year return period are coloured in blue, white and green. Blue areas are expected to be more likely avalanche release areas, white represent the increased probability of the area being a flow path and green are areas where depositions are most likely. Additionally, areas which are expected to be unaffected by any kind of direct avalanche activity are marked as well.

5.4 Topographic shading

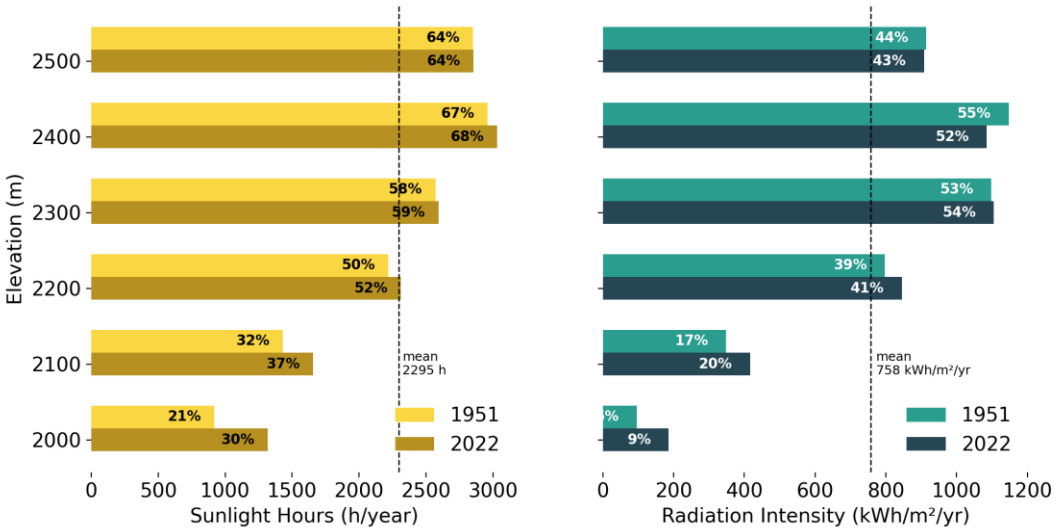

Figure 23: Topographic shading effect per elevation band: The reduced annual sunlight hours and reduced shortwave energy flux (radiation intensity) is grouped by altitude and categorized into 100-metre altitude bands for the glacier extent of 1951

As Figure 24 shows, the topography majorly influences the distribution of incoming shortwave radiation on the glacier surface. The topographic shading effect is smallest in the north, where the glacier tongue and proglacial lake are. The greatest effect can be seen in the highest, most southern part of the glacier and beneath the steepest headwalls. The topographic shading effect, as the reduction in sunlight hours, results in a different distribution pattern than as the reduction in shortwave energy flux. This complements the expectation that sunlight hours alone do not paint the whole picture of shortwave radiation induced melt. Broken down by altitude and categorized into 100-metre altitude bands, a clear difference over time can be seen in the lower-elevated parts of the glacier, which received more sunlight in 1951 than in 2022 (Figure 23). This can be explained by the larger area that still existed in the lower part of the glacier in 1951. The 2400 m altitude band shows an interesting anomaly, where the reduced sunshine duration was less in the preceding year, but the reduced shortwave energy flux was not. The overall mean reduction in sunlight and shortwave energy flux over the glacier surface in 2022 was 751 kWh m^{-2} a^{-1} and a minimum 2295 hour less sunlight per year.

Table 8: Glacier-wide shortwave radiation and melt potential for reference and simulated values on the 2022 glacier surface.

Variable	Value	Unit	Meaning
Glacier area	873 916	m^2	Glacier surface area in 2022
Mean sim *SW* ↓	1295.3	kWh m^{-2} a^{-1}	Mean simulated incoming shortwave radiation over the glacier
Mean ref *SW* ↓	2046.6	kWh m^{-2} a^{-1}	Mean reference (flat, no topography) incoming shortwave radiation
Mean *SW* ↓ reduction	751.3	kWh m^{-2} a^{-1}	Mean reduction per m^2 due to shading
Total sim *SW* ↓	1.13×10^9	kWh a^{-1}	Glacier-integrated incoming shortwave (simulated)
Total *SW* ↓ reduction	6.57×10^8	kWh a^{-1}	Glacier-integrated energy loss compared to flat reference
Mean sim melt potential	13.96	m w.e. a^{-1}	Mean annual melt potential per m^2 (simulated incoming)
Mean reduced melt potential	8.10	m w.e. a^{-1}	Mean reduced melt potential per m^2 due to shading/topography
Total sim melt potential	1.22×10^7	m^3 w.e. a^{-1}	Glacier-integrated melt potential volume (simulated)
Total reduced melt potential	7.08×10^6	m^3 w.e. a^{-1}	Glacier-integrated melt potential volume not realized because of shading
Relative reduction	≈ 37 %		Fraction of potential incoming radiation (and melt) lost due to shading/topography

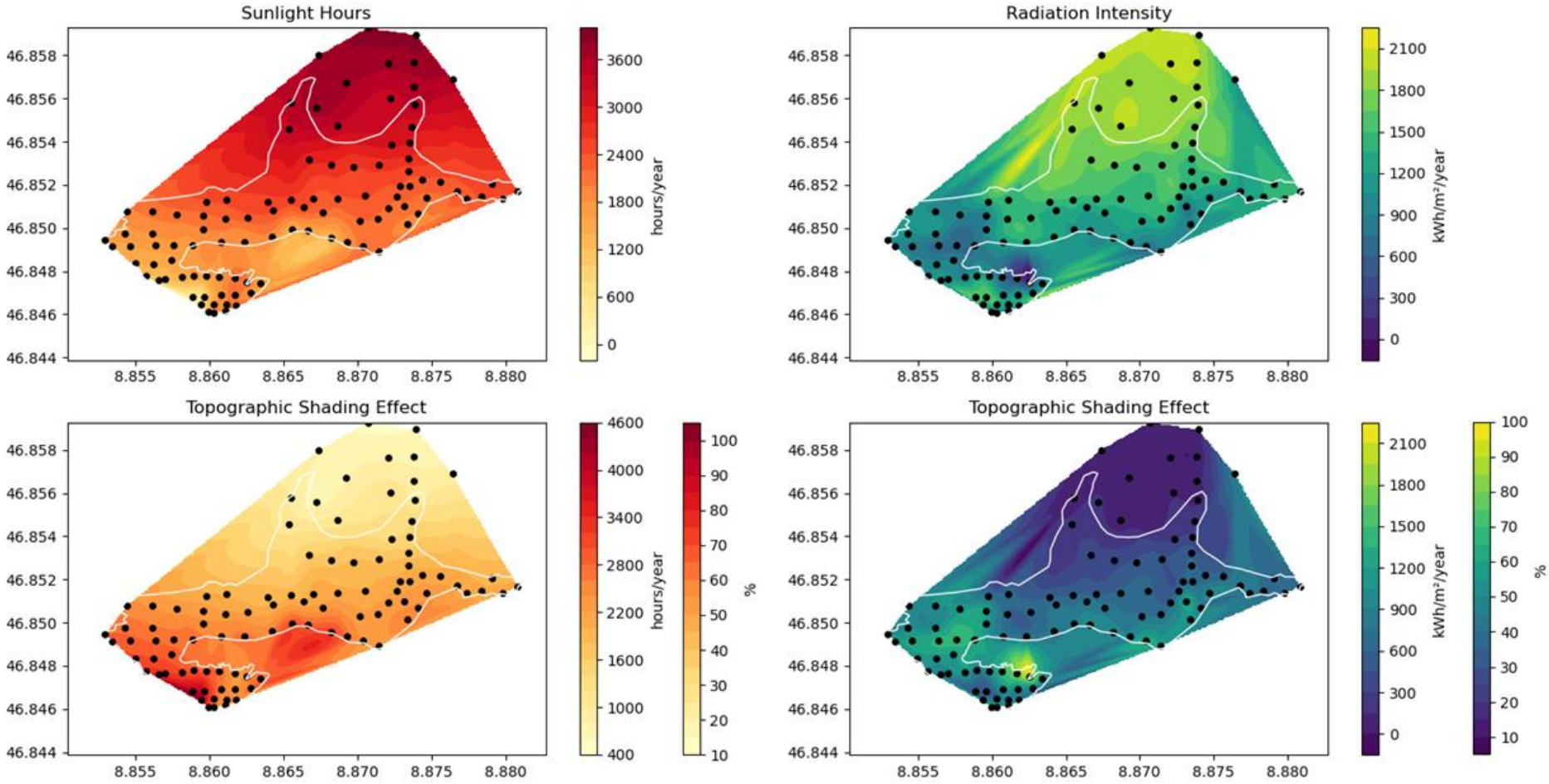

Figure 24: Topographic shading effect: At the sample points (black) annual sunlight hours and total incoming shortwave radiation (radiation intensity) was simulated and interpolated (cubic). The glacier outline of 2022 is shown in white. The topographic shading effect – the difference from the simulated value to the reference on a point on a flat surface of equal altitude and latitude – is shown in the lower plots as absolute (reduced hours per year and reduced incoming shortwave radiation per square metre per year) and relative values.

5.5 Near-surface temperature lapse rate

As an addition to the commonly used literature lapse rate value of 6.5 K/km, a region-specific estimate has been done using the three automatic SLF snow stations Ortstock Matt (ORT2, 1824 m a.s.l.), Seewli (SCA2, 2032 m a.s.l.), and Älpler Tor (SCA3, 2338 m a.s.l.). For each station, the 30-minute air temperature measurements were used. The mean temperature $\overline{T_s}$ over the entire measurement period was then calculated for each station so that each station contributed one mean value.

$$\overline{T_s} = \frac{1}{n_s} \sum_{k=0}^{n_s} T_{s,k}$$

These station-mean temperatures $\overline{T_s}$ are 4.7 °C (ORT2), 2.69 °C (SCA2) and 1.13 °C (SCA3). Paired with the corresponding station elevations (in metres above sea level), an ordinary least-squares (OLS) linear model was then fitted across the three stations.

$$\overline{T_s} = \alpha + \beta z_s + \varepsilon_s$$

The fitted slope β represents the change in mean near-surface air temperature per metre of elevation. By convention, the lapse rate Γ is reported as a positive number describing the magnitude of cooling with height and was therefore obtained as the negative of the slope. A negative β thus corresponds to a positive lapse rate. The intercept α represents the extrapolated mean temperature at sea level. The resulting lapse rate is-**6.8 K km^{-1}** (-0.68 K hm^{-1}) or 147 m K^{-1}. A simpler method of averaging the station means without a regression comes out at -7.2K/km.

Because each station contributes a single mean value, differences in data availability within the period do not bias the regression, as each station has equal weight. To reduce seasonal sampling effects, monthly means can be calculated first and subsequently averaged. However, this was not considered necessary, nor to estimate the uncertainty the lapse rate Γ as with only three stations the confidence interval remains relatively wide.

5.6 Modelling results

5.6.1 Model input

Table 9: Model inputs for calibration and validation.

	input	value	unit
numerical parameter	grid size, *dx*	30, 35, 40, 45 and 50	metre
	time step, *dt*	0.25	year
	run time, *tmax*	2022	year
	x-direction extent, *xmax*	3000	metre
	storing interval, *dt_store*	1	year
model parameter	Glen flow-law rate factor, A_{Glen}	**75**	MPa
	Glen's law exponent, n_{Glen}	3	
	Ice density, ρ_{ice}	917	kg m^{-3}
	Gravity acceleration, *g*	9.81	m s^{-2}
	Mass balance gradient, ġ	0.007	m w.e. a^{-1} m^{-1}
	bed topography	reference, flattened, adjusted, shortened	
Geometry	reference width, W_0	100, 300 or 500	m
	reference height, H_0	30	m
	ice surface, z_0	0	m
	Climate forcing, z_{ELA}	2200–2600	m a.s.l.

The model is initialized without any glacier ice in the year 0 and it needs about 100 years to build up the ice build-up time leading to the year itself. For all model simulations where a climate forcing was applied using the historic ELA series, the climate forcing was applied at the very start of the build-up.

The numerical (running) parameters dx, dt, tmax, xmax, and dt_store can be chosen freely but should be treated with care. If values exceed reasonable ranges, the model can become

numerically unstable or inaccurate. After initial testing the values depicted in Table 9 were found to be optimal for the Clariden-N Glacier and the goal of this thesis. Where more than one value is noted, the parameter needed to be calibrated.

5.6.2 Calibration

"dx" problem solved

To minimize the influence of dx, three *different mitigation* strategies were tested but only the *flattened bed* approach proved successful. The *flattened bed* is an approach in which the glacier bed profile above the glacier is a straight line with uniform slope, that prevents disruption of glacier formation on behalf of the additional accumulation. This simplification does not result in a significant loss of realism, as the focus lies solely on the additional accumulation, not on the glacier bed itself (except for one bump, see Figure 25) which starts at $x \geq 800$. The flattened bed method performed excellently well and reduces the influence of *dx* by approximately 98% (see Table 11). The remaining difference in simulated and observed glacier length ΔL now falls within the range of variation caused by the choice of *dx*, which cannot be entirely avoided.

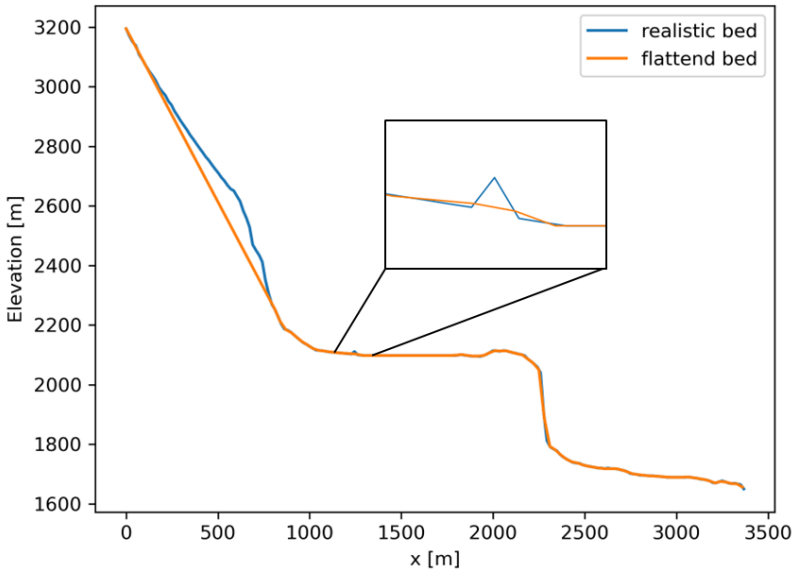

Figure 25: Realistic vs. flattened glacier bed.

For the *shortened bed* an ELA climate forcing does work, even if the surface area above the ELA is limited for mass to accumulate. However, in a changing climate the performance and dx sensitivity is not good.

The results show that the reconstruction of glacier length under constant climate is possible with great accuracy. The gap between the elevation control point A and the glacier surface

presents a missing mass comparable, though not useful, to the Dark Matter Problem revealed by Vera Rubin & Kent Ford (1970). The gap between control point B and the ice surface, presents an overestimation of ice thickness. The glacier terminus in Figure 31 is modelled as levelling off instead of a steep front. In conclusion, the *shortened bed* model in a constant and changing climate fails to accurately simulate accumulation (missing mass), ablation (overestimated thickness) and terminus geometry.

The *adjusted bed* method proved unsuccessful, as the upper edge of the cliff happened to coincide with a multiple of three out of the five selected *dx* values. Thus, the method was already applied unintentionally. For the remaining two *dx* values, the adjustment introduced a difference of only 5 and 15 metres, respectively. Even so, this modification showed no noticeable effect on the *dx* sensitivity. Thus, the adjusted beds, or the alignment of the top edge of the steep cliff, does not provide an improvement to the model results. This is also because by aligning only the most prominent edge, a lot of other terrain specific elevation differences remain. By interpolating the glacier bed to dx these elevation differences can be exemplified.

"W/h" problem solved

The "W/h" problem describes the various possibilities for modelling the width and height (cross-sectional shape) of the glacier bed along and across the flowline. As always in modelling, the general aim is to represent reality as accurately as possible. However, as the "dx" problem has already shown, realism is not always the best approach. Therefore, attempts were made to implement the three factors scope, form and transition in the most sensible and effective way possible while keeping dx sensitivity as low as possible.

The **scope** chosen for all simulations was partial width. This means that the focus is only on a specific part of the glacier and not the entirety of it (full width). Due to the difficulty in identifying the flow dynamics, it is assumed that today's glacier functions more like an interaction between several individual areas and that there are few interactions or dependencies between these areas. For this reason, a prominent part of the glacier with a visible avalanche cone was selected to be reconstructed. A *full width* was not part of the evaluation due to high complexity and insufficient expectations on interpretability and comparison of results.

The best type of **form** depends on the modelling goal. All form profiles performed nearly equally well and had very similar dx dependencies. Therefore, it is solely a question of what one wants to achieve. If the goal is to simulate additional accumulation, choose wide accumulation. If the goal is to simulate low accumulation, choose narrow accumulation. If you want neither, choose uniform. For the narrow accumulation, a linear **transition** is recommended; however, the transition type can be chosen deliberately, and good results are possible. For a wide accumulation a step change can reduces instability issues related to dx sensitivity. The reduced instability effects only simulations which are far off from the 2022 terminus, thus the effect is not relevant for the goal of recreating the 2022 glacier extent. Step change is thus slightly more advisable when it comes to recreating older or greater glacier extents.

In conclusion, the glacier bed geometry is best kept simple; complex topography does not improve the reproduction of reality but increases model instability.

Table 10: Results of dx sensitivity mitigation and optimization strategie: The Top 1 shows the best simulation result, which is the combined mean of 5 simuations run with the specified ELA and dx values 30,35,40,45 and 50. The measure defining the goodness is the length differnce between observed and simulated glacier length $|\Delta L|$. $|\Delta L|_{1951\text{-}2022}$ presents the ELA which caused the best representation of length evolution over the period 1951-2022 with the least mean absolute length deviation. The top 10 averages the ten best simulation results. Simulations are always calculated in an ELA intervall of 10m. The "dx" sensitivity is expressed as the mean range and standard deviation of the top 10 simulations. Since each simulation result consists of 5 simulations with different dx, each result is the mean with an assiciated range and standard deviation. The Improvement is the procentage of dx sensitivity reduction from reference.

Mitigation Method	**Optimization Strategy**	**Top 1**		**Top 10**		**dx sensitivity**	**Improvement**
		$\|\Delta L\|_{2022}$ [m] / **ELA**	$\|\Delta L\|_{1951\text{-}2022}$ [m] / ELA	$\|\Delta L\|_{2022}$ [m]	$\|\Delta L\|_{1951\text{-}2022}$ [m]	range (std) [m]	
Flattened bed	ai	17 / **2400**	207 / 2390	127	325	40.5 (σ = 15.1)	**98.06 %**
Flattened bed	aii1	9 / **2340**	208 / 2320	173	354	20 (σ = 8.9)	**98.86 %**
Flattened bed	aii2	27 / **2310**	188 / 2300	179	391	45 (σ = 18.8)	**97.59%**
Flattened bed	aiii1+2	23 / **2450**	193 / 2450	162	391	41 (σ = 14.7)	**98.12 %**
Adjusted bed		≈ reference		≈ reference		≈ reference	~ 0 %
Reference		576 / **2550**	709 / 2550	688	799	1889 (σ = 780.4)	

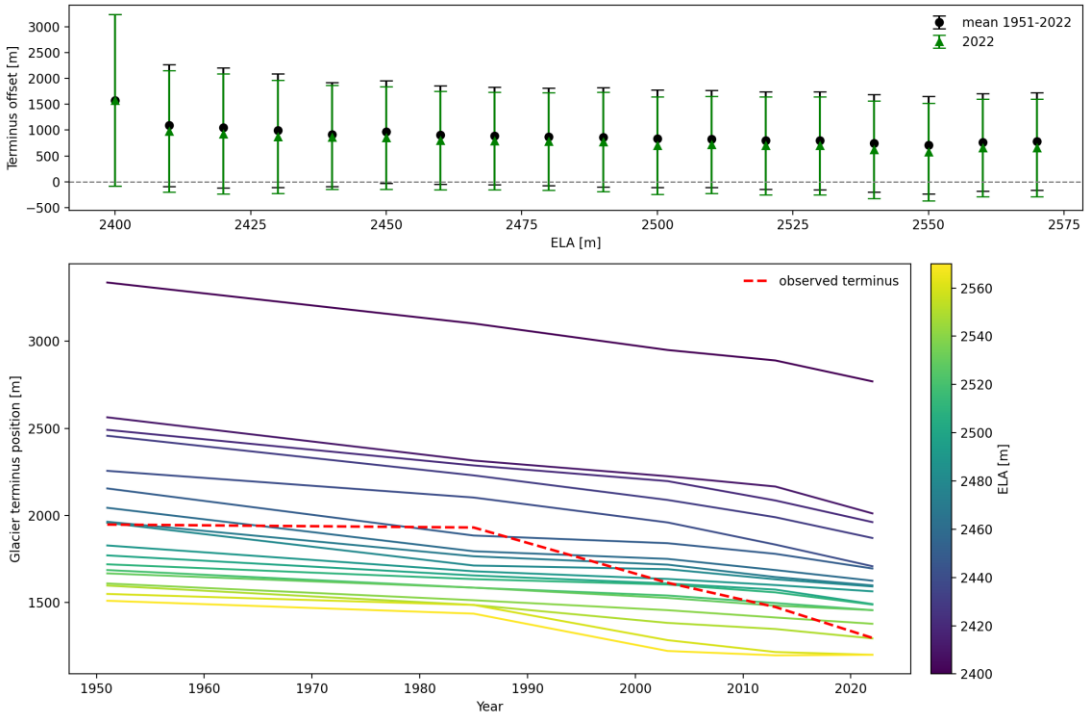

Figure 26: Simulation results – reference: Model simulations for every 10th m ELA between 2400 and 2580 m a.s.l. The upper plot shows the mean absolute terminus offset (|observed -simulated glacier length|) as a black dot or green triangle. The black dot represents the mean difference from the glacier terminus positions at the years 1951, 1985, 2003, 2013 and 2022. The error bar indicates the range of results with varying dx between (30-50 m), thus the sensitivity. The lower plot shows the development of simulated glacier terminus positions for ELA model runs, as the mean of results with different dx, in comparison to the observed terminus position from 1951 to 2022.

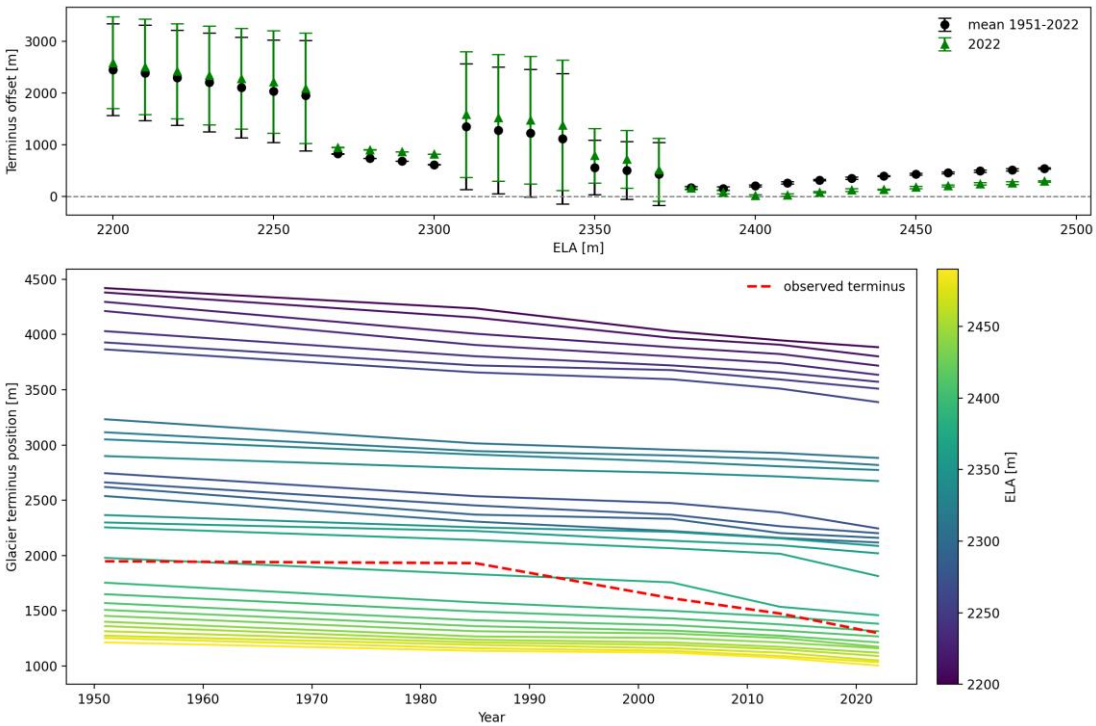

Figure 27: Simulation results – flattened bed optimization ai: uniform; best ELA 2400 (to reconstruct 2022 length) or 2390 (to reconstruct 1951-2022 lengths).

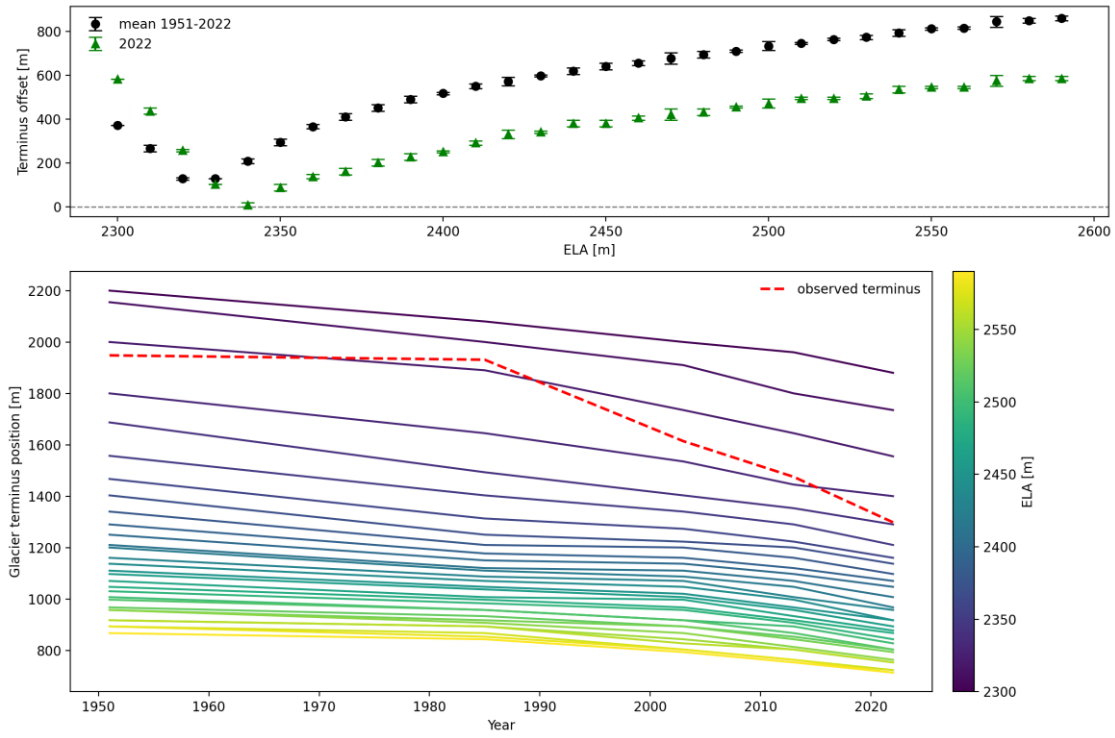

Figure 28: Simulation results – flattened bed optimization aii.1: Model simulations for every 10 m ELA between 2300 and 2600 m a.s.l. Scope: Partial width, Form: Narrow accumulation, Transition: Step (x > 800 m: W = 300 m, h = 30 m; x > 725: W = 100 m, h = 30 m); best ELA 2340 (to reconstruct 2022 length) or 2320 (to reconstruct 1951-2022 lengths).

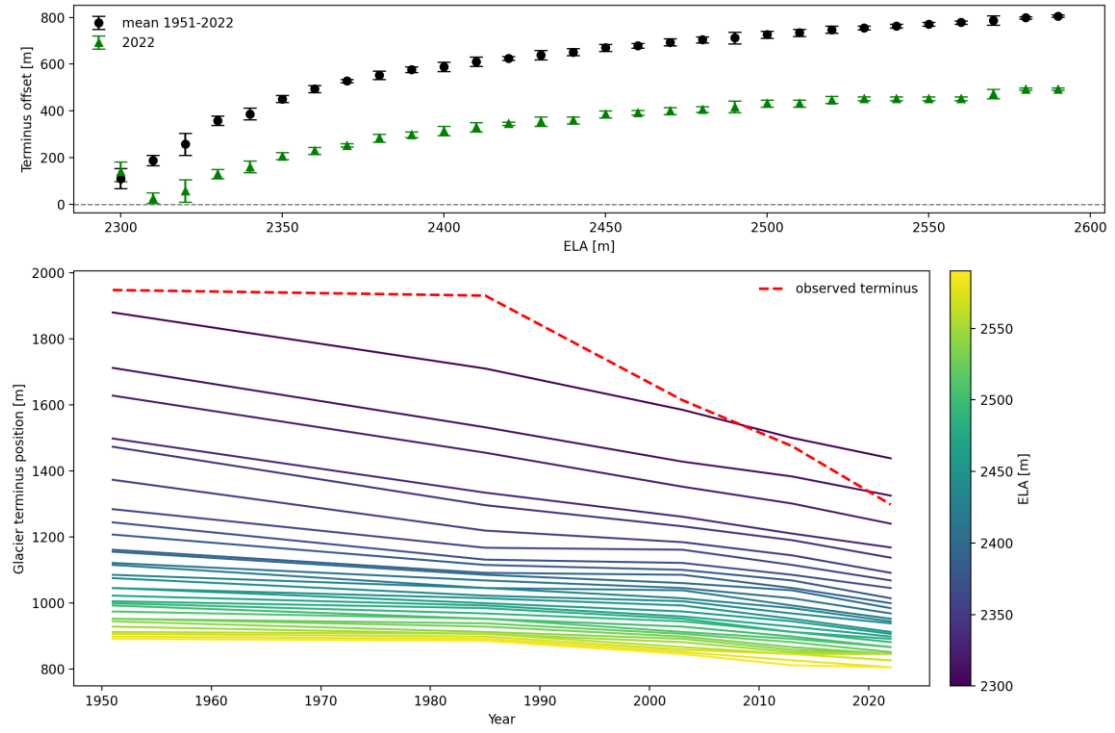

Figure 29: Simulation results – flattened bed optimization aii.2: Same as aii.1 but with linear transition from x = 0 to x = 800; best ELA 2310 (to reconstruct 2022 length) or 2300 (to reconstruct 1951-2022 lengths).

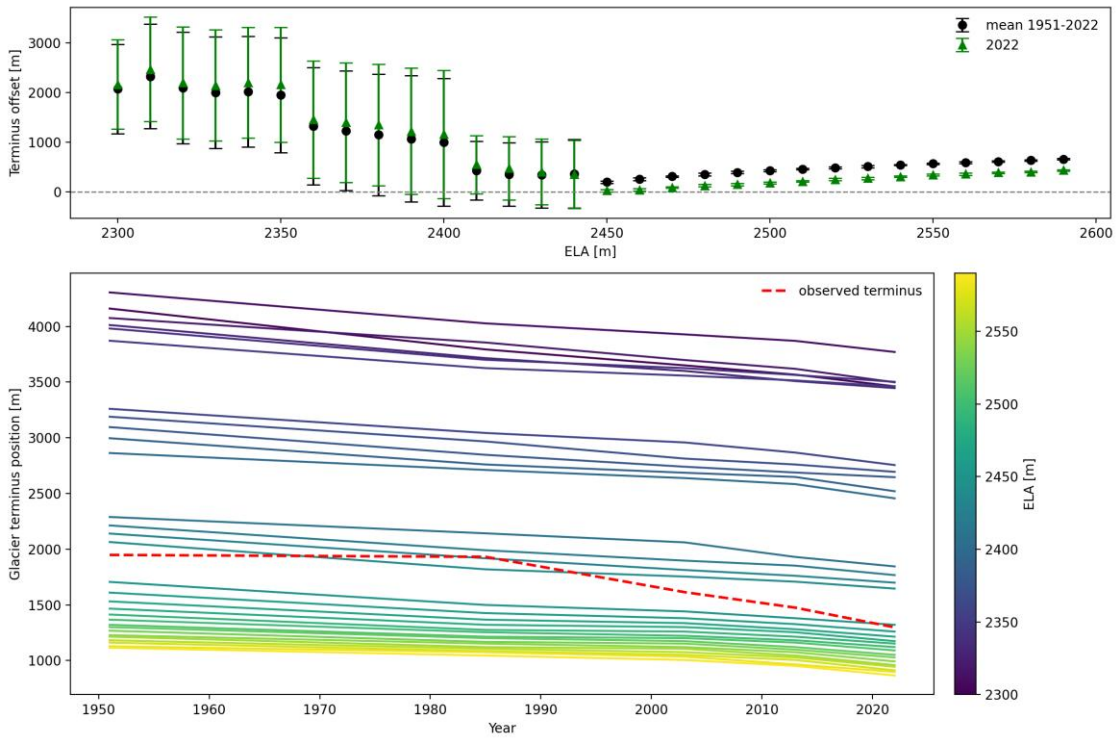

Figure 30: Simulation results – flattened bed optimization aiii.1+2: Model simulations for every 10 m ELA between 2300 and 2600 m a.s.l. *Scope*: Partial width, *Form*: Wide accumulation, *Transition*: Linear (x > 800 m: W = 300 m, h = 30 m; x = 0: W = 500 m, h = 30 m); best ELA 2450 (to reconstruct all glacier lengths between 1951-2022).

5.6.3 Glacier reconstruction through climate forcing

The *top 10* simulations are the ones that most accurately reconstruct the 2022 glacier length (see Table 10). A simulation is always to be understood as the average of five simulations with the same ELA but different *dx* values. The best simulation for each optimization strategies is between 9 and 27 m for $|\Delta L|_{2022}$. Thus, it is concluded that calibration went well.

The same simulations struggle to simulate the observed glacier retreat. It becomes evident through the averaged length differences of the years 1951, 1985, 2003, 2013 and 2022 presented as $|\Delta L|_{1951\text{-}2022}$ in Table 10. This discrepancy suggests recalibration.

The optimal ELA to recreate glacier length depends on the optimization strategy. A uniform cross-sectional shape along the whole flowline (ai) models the 2022 length best with an ELA of 2400 the period 1951-2022 with an ELA of 2390 m a.s.l. A narrow accumulation area (aii) causes the ELA to drop to 2310 (step) or 2340 m a.s.l. (linear) for the 2022 length, and to 2300 or 2320 m a.s.l. for the period 1951-2022 lengths. With a wide accumulation area, the same glacier length can be modelled with a higher ELA of 2450 m a.s.l. Interestingly, step or linear transition does not affect the simulation when applying a wide accumulation area. In

conclusion, the ELA to reproduce the glacier as of 2022 is modelled to be somewhere between 2310 and 2450 depending on assumptions.

5.6.4 Glacier reconstruction with a shortened bed

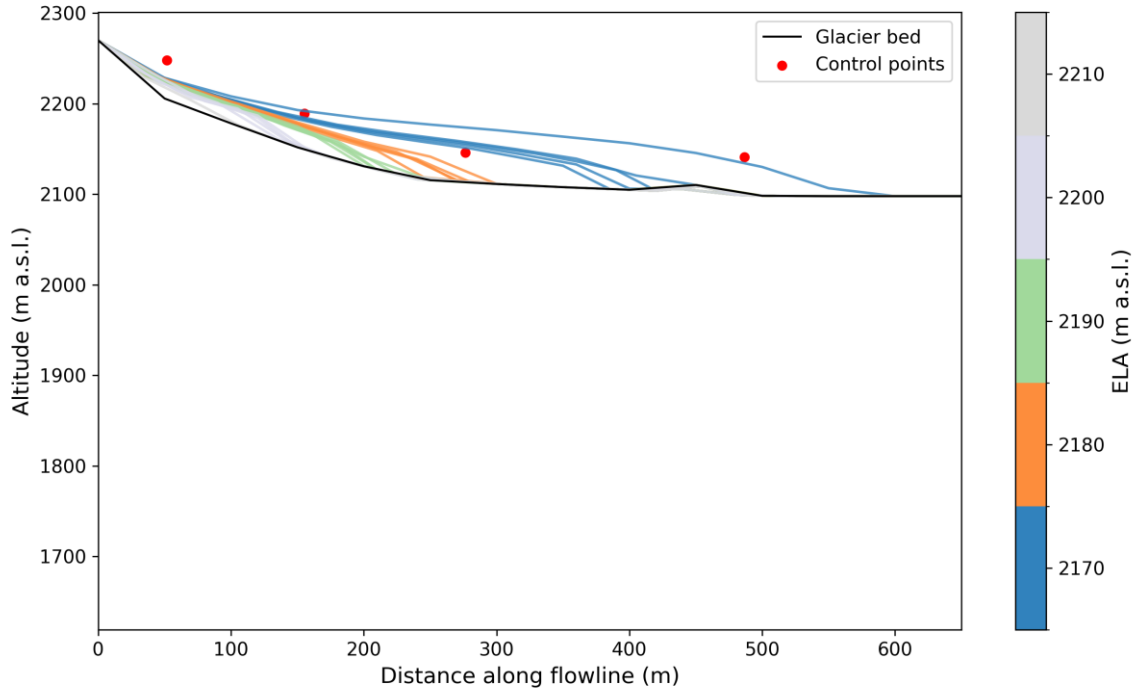

Figure 31: Shortened bed glacier reconstruction of 2022 glacier surface.

For the *shortened bed* a constant ELA does work, even if the surface area above the ELA is limited for mass to accumulate. However, in with a historical climate forcing the performance and dx sensitivity is not good.

The results show that the reconstruction of glacier length under constant climate is possible with great accuracy. The gap between the elevation control point A and the glacier surface presents a missing mass comparable, though not useful, to the Dark Matter Problem revealed by Vera Rubin & Kent Ford (1970). The gap between control point B and the ice surface, presents an overestimation of ice thickness. The glacier terminus in Figure 31 is modelled as levelling off instead of a steep front, which is related to the non-inclusion of frontal ablation in the model.

In conclusion, the *shortened bed* model in a constant and changing climate fails to accurately simulate accumulation (missing mass), ablation (overestimated thickness) and terminus geometry.

5.6.5 Slope and surface roughness increase model inaccuracy

Initial simulation tests with different dx and ELA combinations, under a realistically reconstructed glacier bed profile, revealed a significant influence of the grid spacing parameter dx on the glacier mass balance results. The influence of *dx* resulted insignificant for test simulations with uniform bed types regardless of their steepness. This leads to the assumption, that the high influence of dx is a result of the linear interpolation in constructing the glacier bed profile when dealing with non-uniform profiles. This may explain the difficulties encountered when modelling complex and steep bed topography, such as the cliff just above the glacier. This assumption is highlighted by the significant improvement in accuracy when flattening the glacier bed. To support this hypothesis, the slope was analysed in terms of angle and surface roughness/complexity. The results show that with both increasing steepness and complexity a greater difference between the interpolated and the reference bed is generated. In conclusion, greater complexity and steepness of the glacier bed profile along the flowline leads to an increased sensitivity of the model results to the grid size.

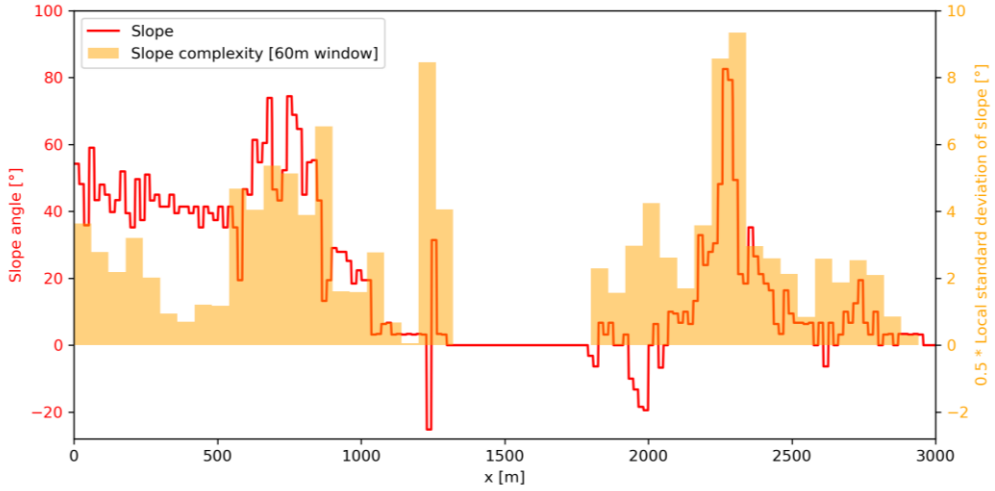

Figure 32: Slope and slope complexity: The red line shows the slope along the flowline; in other words, it shows the angle or steepness of the bedrock. In orange is shown the surface complexity or roughness.

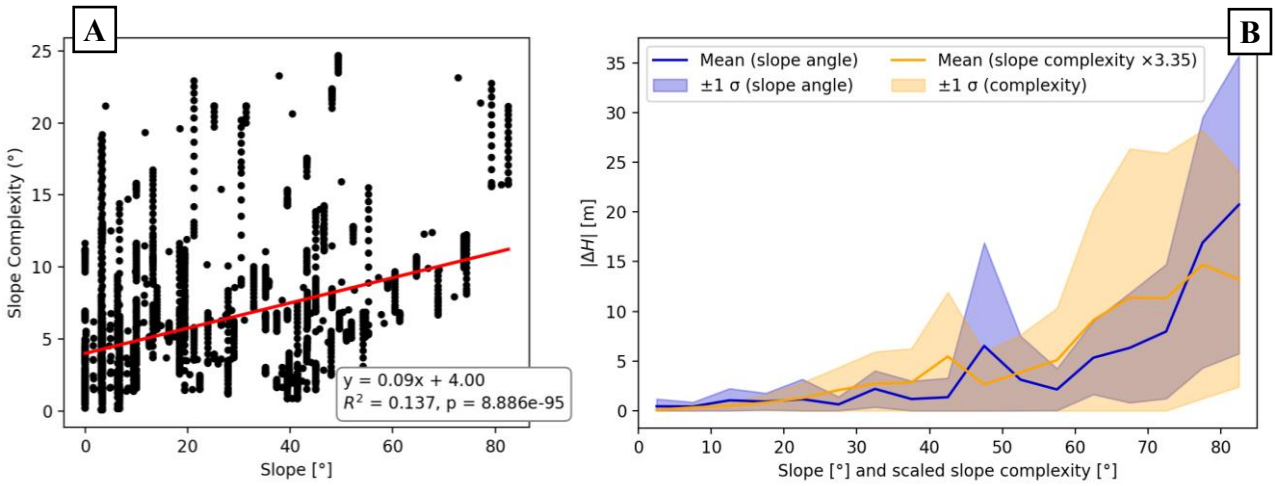

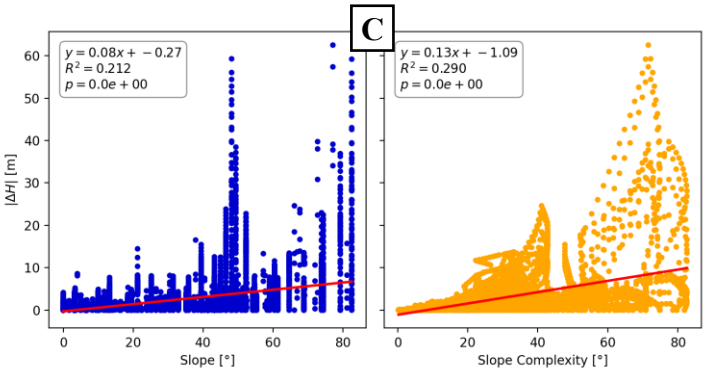

Figure 33: Slope and slope complexity: [A] shows slope vs slope complexity (unscaled) as a scatter plot with a linear regression line (red) indicating a statistically significant but weak linear relationship between slope and slope complexity. [B] shows slope (blue) and complexity (yellow) grouped in 5° bins with their standard deviation in relation to $|\Delta H|$, the absolute height difference of the interpolated in respect to the original glacier bed. Slope complexity was scaled by *3.55 in order to have comparable graphs. [C] presents scatter plots of slope and slope complexity against $|\Delta H|$ with linear regression lines indicating a statistically significant but weak to moderate relationship.

5.6.6 Future glacier simulation

Table 11: Summer surface temperature change expected compared to 1981-2010. Values are based on the CH2018 Swiss Climate Change Scenarios for the canton of Uri. Respectively ELA adaptions to the same period for simulating glacier evolution are shown.

Emission scenarios	2035		2060		2085	
	[+°C]	[+m]	[+°C]	[+m]	[+°C]	[+m]
RCP 2.6	1.4	210	1.7	255	1.6	240
RCP 4.5	1.7	255	2.6	390	2.9	435
RCP 8.5	1.9	285	3.1	465	4.9	735

As demonstrated in previous studies, variations in the equilibrium line altitude (ELA) are primarily governed by changes in summer temperature. For modelling, the ELA increase is chosen to be 150 metres for every one Kelvin rise in summer temperature. A study by Larocca et al. (2024), which uses snowline altitude as a proxy for the ELA arrives at comparable magnitudes, reporting a shift of approximately 127 ± 5 m per degree summer temperature change. This is also in accordance with the derived lapse rate for near surface temperature for the study area in Chapter 5.5 The CH2018 Swiss Climate Change Scenarios for the canton of Uri provide expected temperature changes compared to the 1981-2010 average. This translates into an ELA rise of about 240 m (+1.4 °C) by the end of the century under RCP 2.6, 435 m (+2.9 °C) under RCP 4.5, and 735 m (+4.9 °C) under RCP 8.5 compared to the average ELA (Temperature) between 1981 and 2010. The simulations were carried out using the aii1 approach with an ELA of 2340 m a.s.l.

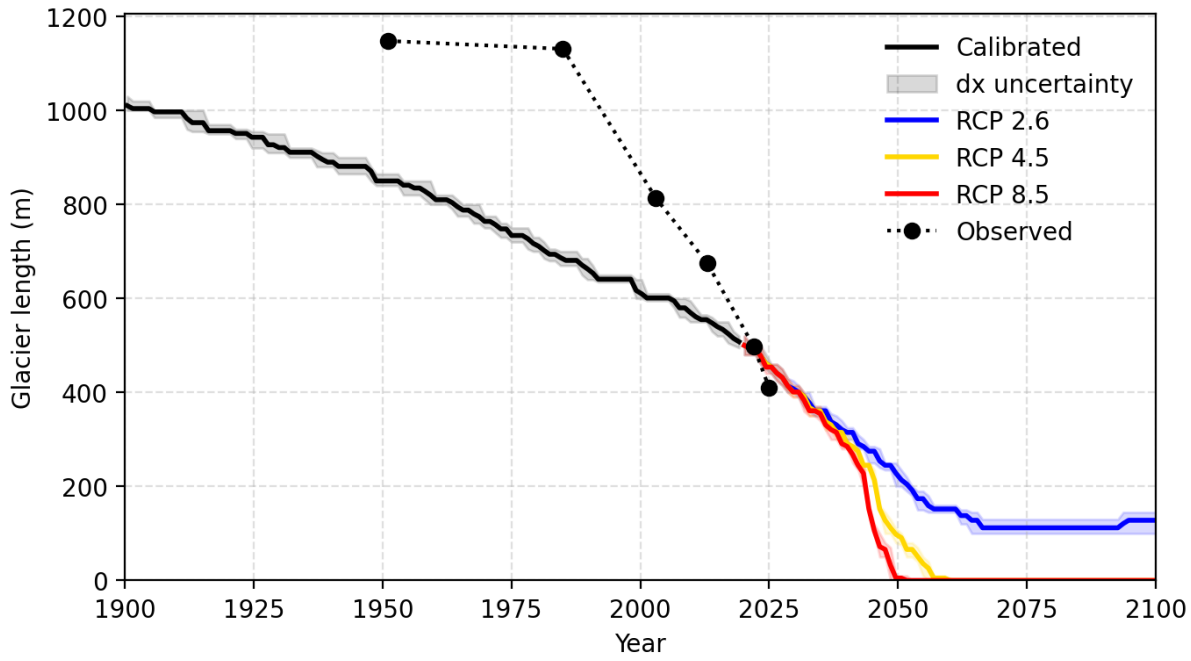

Figure 34: Glacier length evolution simulated until 2100 with different emission scenarios and observed length (1951-2025).

The results show that under the RCP 2.6 scenario, the glacier will withstand the complete melting and remain a small ice patch of 100m length from 2060 onwards with possibly even gaining mass at the end of the century. The RCP 4.5 leads the glacier ice to be completely gone by 2060 and the RCP 8.5 even earlier by 2052.

5.7 Comparison with other low altitude alpine glaciers

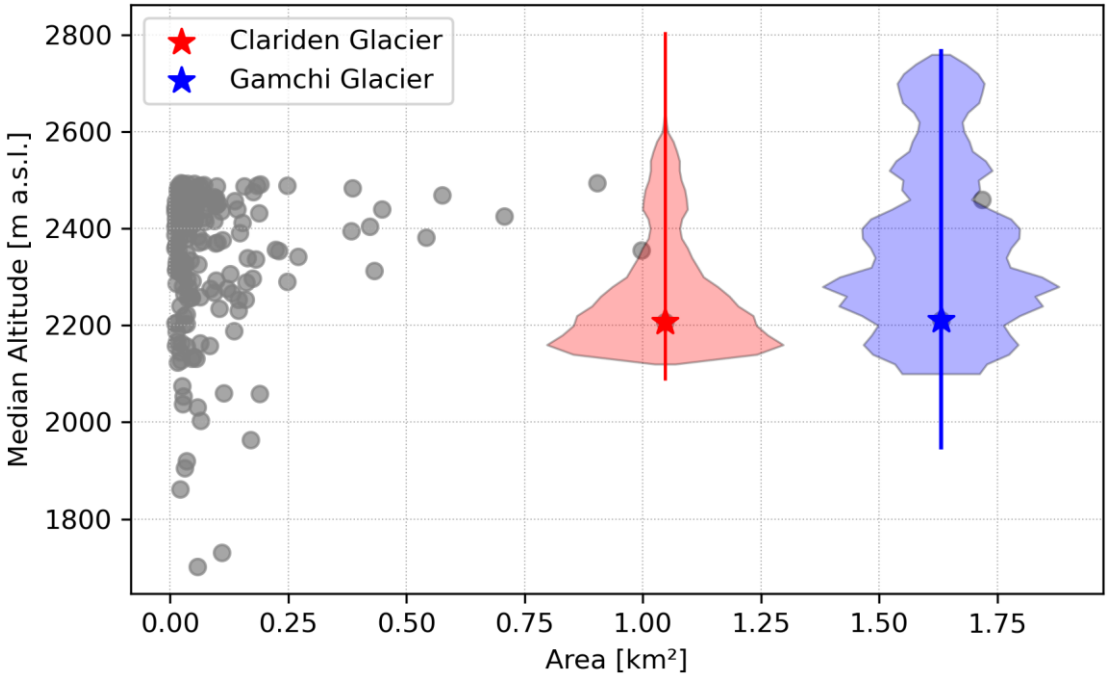

Figure 35: All glaciers within the RGI 7.0 with a median altitude <2500. Clariden-N Glacier (red) and Gamchi Glacier (blue).

In order to compare the Clariden-N Glacier with other low-altitude glaciers, the glacier outlines from RGI 7.0 were used. Figure 35 shows the ratio of area to altitude of all glaciers in the European Alps below 2500 m a.s.l. Two outliers can be identified that appear to be at a median altitude of approximately 2200 m a.s.l. and are of considerable size These are the Clariden-N Glacier and the Gamchi Glacier in the Bernese Oberland. The star symbol shows the position on the grid, and the vertical (red/blue) line shows the range of elevation as it is presented in the RGI 7.0. By self-drawing outlines and elevation contour lines for the Gamchi and Clariden-N glacier using the 2022 DEM and Swiss national topographic map, the hypsometry for 2022 were derived. It shows a very different image for the two glaciers. The derived median altitude of the Clariden-N Glacier is in line with the RGI 7.0, but very greatly underestimated for the Gamchi Glacier. Thus, the Clariden Glacier is unique in its median altitude to area ratio.

The Claridenfirn, which is just south of the headwall, has a reported ELA >2900 m a.s.l. for 2020 and und mean altitude of 2860

6 Discussion

6.1 Model performance and limitations

The model successfully reproduced the 2022 glacier length with great accuracy across different sets of input parameters. The strong influence of grid size on the simulation results was successfully mitigated using different approaches. It was found; realism is not always the optimal approach to produce realistic result. The high influence of slope and slope complexity on dx sensitivity and the simulation results, can be explained due to the high sensitivity of ice flux to surface slope[2] and ice thickness[5]. When validating the results against the glacier length change between 1951 and 2022, a significant underestimation became evident. This discrepancy can be explained by the non-inclusion of mass balance processes in the governing equations, particularly frontal ablation. A deliberate decision was made not to recalibrate to the glacier length change between 1951 and 2022 in order to avoid incorrectly incorporating frontal ablation processes. Otherwise, the calibration would only be useful until 2025, as from then on there will be no calving and increasingly fewer overall frontal ablation by the bare ice cliff.

The glacier bed profile beneath the ice was approximated by in-situ investigations following glacier caves and expert knowledge. GPR or other methods were not applicable due to the debris cover interrupting the signal. However, only slight variations from the real bed are expected, due to the small distance and good observations beneath the ice.

The proglacial lake which emerged just when the strong retreat phase started around 1990 and related ablation processes, could explain the pronounced and rapid retreat of Clariden-N Glacier. Even with a wide accumulation area, such strong retreat could not be reproduced by the model. To achieve this, the model input would need to be heavily modified – either by adjusting flow parameters to allow faster ice movement, reworking the ELA forcing to reflect a warmer and/or drier climate, or by modifying the governing equations to include a new frontal ablation scheme. Since glacier surface velocities and flow direction were hardly quantifiable and very small (see Hauser, 2024), only the latter seems plausible. Hauser (2024, Table 17) observed and documented several major frontal ablation events, including calving. A misrepresentation of the recession rate in numerical models, especially during the transition

from land-terming to lake-terminating, is found by Sutherland et al. (2020) Thus, the model performance would benefit from integrating frontal ablation processes into the model.

The model applies a uniform mass-balance gradient and thus cannot account for the spatial heterogeneity induced by debris cover, avalanche cones and topographic shading. These simplifications is a limiting factor for simulating past and future dynamics but are typical of one-dimensional SIA models, which prioritise simplicity over completeness (Zekollari et al., 2022). Nevertheless, an artificially designed mass balance gradient could simulate the implications of the results found by the process-based methods and contribute to the understanding of these interactions.

The uncertainties identified here point out promises and limitations of a simple model for an abnormal glacier. It is adequate for reconstructing broad patterns but fails to represent individual processes. This is where interpretations are important to fill gaps and explain mismatches between the observations and the simulations.

6.2 Limitations of photo analysis for avalanche detection

There are several limitations to the avalanche frequency, size and type analysis (cf. Section 4.4.1 and 5.3). The major ones are related to the photographs, their coverage and resolution. The camera only covered about 50% of the glacier, as the focus of the installed camera is on the behaviour of the glacier lake and not the glacier itself. Some avalanche events were surely missed because they were outside the frame. The rather poor image resolution (640x480 pixels) in combination with exposure problems and lack of colour depth resulted in surface roughness or colour often being the only indicator for avalanche depositions. However, it was difficult to distinguish between melt and deposition, as changes in colour or surface roughness can indicate either process. Thus, there is the possibility that some avalanche events were misinterpreted as rapid surface melting and therefore not counted towards avalanching, or that avalanche deposits were counted as such even though they were not.

Another challenge concerns the distinguishability of avalanche types. It was not possible to distinguish between ice, snow, or ice and snow avalanches because the deposition can only be interpreted by roughness and colour. Moreover, debris avalanches can only be clearly identified on snow, as the image resolution is too low to detect newly deposited debris on an already debris-covered surface. In comparison, to snow avalanches on snow, debris avalanches on debris do not significantly change the surface roughness, which is why the possibility exists that debris avalanche deposits on debris have been missed.

To estimate the size of an avalanche not only is the area of need but also volume and density. However, the only approximation that seemed sensible is the area, which is done by visual approximation and drawn in a GIS program to measure the area. By additionally estimating the depth and density on even less data, the uncertainty would be increased even more, which seems to be useless. The resulting area of deposition should only serve to provide a general idea of size. Moreover, as half of the glacial area is not covered by the camera, the total avalanche frequency is underestimated. Field observations in summer 2024 and spring 2025 revealed many avalanche deposits that lie outside the camera coverage but are nevertheless on the glacier. The actual number of annual avalanche events will therefore be higher. How much the ratio of avalanche affected and unaffected glacial surface area will differ remains debatable but is expected to be similar. Same can be expected by the summed area of avalanche deposits.

The photo series does not cover the entire second year as it ends in October. This implies that some avalanche events might be missing. However, as there was only one avalanche event observed from July until December it is most likely not the case. A longer photo series over more than two years would surely increase the robustness of the analysis, and can allow for more profound conclusions about annual, seasonal variabilities.

Under the given circumstances, photo analysis of snow avalanche deposits worked well for most cases on snow-covered surfaces. Future analyses would benefit from higher resolved images and improved camera positioning to improve the detection and classification of avalanche depositions on all surfaces. However, the differentiation between snow and ice avalanches is hardly conceivable even with improved image quality.

6.3 Topographic shading effect

The results on topographic shading show a ~37% reduction of incoming shortwave radiation due to cast shadowing from the Clariden north face. The shading effect is different depending on elevation due to the complex topography. It is especially hard to quantify in higher elevated parts, which might also be related to a lower sample size. The assumption of cast shadowing exerting the major influence on topographic shading, and neglecting the distinction of casted and self-shading, is in line with the findings of Olson & Rupper (2019). They found that cast shadowing is especially for lower elevations the dominant mechanism in determining total shading of glaciers in HMA. Olson & Rupper (2019) also suggest that topographic shading influences glacier response and mass balance estimate. This is also expected from the modelling results. A reduced overall reduction in potential melt consequently leads to less simulated ablation, meaning that ablation is overestimated in the model, thus suggesting a higher ELA, thus a warmer climate.

The topographic shading effect is especially important for north and south-facing glaciers (Olson & Rupper, 2019). Since the north facing Clariden-N Glacier receives a lot less solar radiation the opposite is true for the south facing Claridenfirn and Hüfifirn. The shading effect can therefore explain at least part of the difference in mean altitude and ELA. Significant topographic shading on the Hüfifirn is only expected along the south side of the Hüfifirn below the ridge from Piz Cazaraul to Heimstock and Piz Val Pintga. There is no significant topographic shading expected over the entirety of Claridenfirn.

Similar or even less topographic shading effect compared to the Claridenfirn is expected for ice caps and plateau ice fields. Ice caps are a type of glaciers which can be completely unaffected by cast shadowing. Plateau ice fields are unlike ice caps topographically constrained thus the amount of cast shadowing is potentially larger. Consequently, glaciers with less cast-shadowing are more exposed and influenced by atmospheric factors such as atmospheric transmission or cloud cover. This can also have potential consequences on glaciers sensitivity to large volcanic eruptions with aerosol injections like the 1991 CE Pinatubo or 1831 CE Zavaritskii eruption (Hutchison et al., 2025). Decisive is not the climate cooling effect, which is significant for such large events (~1 °C for Zavaritskii, Hutchison et al., 2025) but affects glaciers on a regional scale equal. It is the atmospheric transmission influence by the increase of stratospheric aerosol content, which is thought to reduce incoming solar radiation, thus having a smaller effect on glaciers with a significant amount of topographic shading.

6.4 The future of Clariden-N Glacier

A (false) spark of hope

A slower retreat should become apparent in the upcoming years, as the glacier ice is no longer in contact with the lake probably since 2024 and certainly since 2025. The steep, mostly clear-ice glacier front will therefore flatten over time and debris will cover the bare ice. By then at latest, the insulating effect of the debris should reduce the ablation rate.

In addition, the topographic shading effect decreases ablation rates further as the retreated glacier then experiences less incoming shortwave radiation, because most of the glacier ice is now close to the Clariden headwall.

If current temperature and precipitation trends (since 2000) continue, no big surprises are to be expected. The slight increase in near surface air temperature and very small decrease in precipitation are probably not effectively influencing the evolution of Clariden-N Glacier. However, ablation will be further intensified if the snow-free periods continue to be as long as for example in 2025. By mid-July 2025, last year's firn (an avalanche cone in the modelled flow

path) was already exposed and melting, which means that already at this point in the year, the mass balance was lower than at the end of the previous hydrological year.

For arctic mountains in similar settings as the Clariden-N Glacier it is expected that under the assumption of a higher likelihood of strong winter precipitation events accumulation by avalanches can become more important (Hynek et al., 2024). Since heavy winter and spring precipitation events are expected to increase under all emission scenarios for the Swiss Alps (Appendix 3), the same conclusion can be drawn for Clariden-N Glacier, where avalanching can become an even more important part of accumulation. However, the decreasing annual snow-covered period, might counteract this effect. This means that even if the frequency or size of avalanche deposits increases the total time where these events can happen will be shorter. Thus, snow avalanches depositing on the Clariden-N Glacier are not expected to significantly change anytime soon.

The last ice standing

The extinction of Clariden-N Glacier is to be expected within the next 20-30 years, depending on how a glacier is defined. The last ice standing is thought to be avalanche fed cones in very close proximity to the Clariden headwall. They could survive even longer as avalanching is not expected to decrease in the near future.

The different climate scenarios most probably have very little effect on the evolution. Even though the RCP 2.6 scenario did simulate a stagnation in retreat at where the glacier remains with a length of approximately 100m, it is interpreted as an underestimation of retreat, especially of the current retreat rate, as discussed beforehand. For this study RCPs are being used instead of SSPs because they have at the time of writing this thesis not been developed or published for Switzerland.

The great divide

The glacier is soon going to divide itself into an upper and lower glacier. During the glacier inspection in July 2025 the passage (2’708’190, 1’189’580) between the upper and lower part of the glacier was small (<100m) and thin (~10m). A cave at the edge of the passage, where a small stream was flowing, led about five metres beneath the ice to bedrock. Neither part has a true accumulation zone thus, redistributed snow and avalanching will continue to be the driving process for potential accumulation.

Low is not small

The area-altitude comparison of the lowest elevated glaciers in the European Alps showed that the Clariden-N Glacier is in fact a huge outlier. No other glacier of similar size is nearly as low

in elevation as the Clariden-N Glacier. The general observation that low-altitude glaciers are very small (<0.5 km^2) due to a limited area of sheltered and topographically constrained cirques (De Beer & Sharp, 2009, Huss & Fischer, 2016), is not supported by the Clariden-N Glacier just yet. However, it will be in a few years (~2030, if current area loss rate continues) when Clariden-N Glacier has fallen below the 0.5 km^2 mark.

It's there until it's gone

The proglacial lake is expected to remain of similar extent for the following years and maybe decades. Since the lake drains and freezes during winter, causing the water level to lower, the refilling of the lake is expected to be earlier with an earlier end to the snow-covered period. Once the glacier is extinct and the ice has mostly melted the total volume of water received by the lake, the water intake of the KLL and the Fätschbach will be less. Since the karst causes a chaotic underground water flow network, it could well be that the size or form of the lake changes more quickly than anticipated.

7 Conclusion

This thesis set out to understand why the Clariden-N Glacier, despite its exceptionally low mean altitude and climatically adverse setting, still exists today. By combining geodetic and glaciological observations, process-based analyses (avalanches, topographic shading, debris cover), and a calibrated 1-D SIA flowline model, it provides an integrated picture of the glacier's present state, recent evolution, and likely future.

[R1] What climatic conditions are required to reproduce the current extent of the Clariden-N Glacier in a mass-balance model?

Calibration experiments indicate that the present (2022) glacier length can be reproduced for equilibrium-line altitudes (ELAs) in the range ~2310–2450 m a.s.l., depending on assumptions about glacier-bed properties. best The -performing configurations match the 2022 length within 9-30 m; however, all runs underestimate the retreat rate, pointing to missing processes of frontal ablation at the proglacial lake and spatial heterogeneity (debris cover, avalanche feeding and topographic shading) not resolved by a uniform mass-balance gradient.

[R2] Which specific processes and environmental characteristics contribute to the persistence of Clariden-N Glacier under climatically unfavourable conditions?

All three observed processes contribute to the persistence of the Clariden-N Glacier. Avalanche feeding, is derived from an hourly photo analysis (2023–2024), which shows deposits on ~60% of the imaged area, which is translated to a decadal impact of up to ~65% when extrapolated over the full glacier. This is evidence that frequent avalanche inputs structurally support the mass balance, especially in close proximity just below the steep headwall. The topographic shading effect on the Clariden-N Glacier, in form of shadows casted from the Clariden north wall, reduces incoming shortwave by ~751 kWh m^{-2} a^{-1} on average (~37% of potential direct SW). The effect is more dependent on the proximity to steep headwalls than to elevation. Thus, near headwalls, where most of the remaining ice is now concentrated, substantially less melt energy is available. Debris cover thickness and glacier wide extrapolation from Hauser (2024) are consistent with stake-site checks in this study.

Together with redistributed snow, due to the glacier's north-facing orientation and constrained topography, these processes explain how Clariden-N can persist at a median altitude of only ~2220 m a.s.l. This very special setting and interplay of processes also illustrates why the Clariden N-Glacier is a true exceptionality among Alpine glaciers.

[R3] To what extent do avalanche deposition, debris cover, and topographic shading contribute to the mass balance?

The attribution is difficult and mostly qualitative, because the methods are not standardised and results are not unified. What is certain, is that avalanche depositions on the glacier originating from the headwall's are frequent and cover a large area of the glacier surface. Mass flux itself is however not yet quantified due to unknown thickness and density of the depostions. Topographic shading is affecting the whole glacier with an energy reduction of ~751 kWh m^{-2} a^{-1} (~37%). Even if not all of the energy would be accountable to melt, a significant melt suppression is still evident. The debris cover is exerting a positive influence on the mass balance by insulating ice across most parts of the glacier.

[R4] How will the Clariden-N Glacier evolve in the future?

Near term, retreat is expected to slow relative to recent years because the glacier front has lost contact with the proglacial lake (likely since 2024, certainly since 2025). The steep, clean-ice cliff will flatten, debris cover will insulate the tongue, and increasing topographic shading, as ice retreats further toward the head wall will further suppress melt. Field observations in July 2025 indicate an upcoming fragmentation into an upper and a lower glacier at a narrow, thin passage. With no true accumulation zone, the persistence of Clariden-N Glacier will continue to rely heavily on avalanche feeding and redistributed snow.

The trends for longer snow-free periods will intensify ablation despite modest trends in temperature and precipitation since 2000. Avalanche deposition will remain important and possibly increase in size and frequency, due to heavier winter and spring precipitation events, but a shortening snow-covered period limits this net benefit. Overall, avalanches, debris insulation, and shading will delay but not halt shrinkage.

At the scale of decades, Clariden-N is projected to disappear as a coherent glacier within ~20–30 years, with the "last ice" persisting as avalanche-fed cones near the headwall. Emission scenario choice changes timing not outcome. Even under optimistic forcing, apparent late-stage stagnation is interpreted as an underestimation of retreat, due to the non-inclusion of processes related to the proglacial lake and spatial heterogeneity in the model. The glacier's exceptional status as a very low-altitude glacier with significant area will eventually be lost. The lake will

probably persist, but post-glacial runoff will diminish, and karst-controlled drainage may drive quicker-than-expected changes in lake form and connectivity.

In conclusion, Clariden-N will vanish as a coherent glacier by mid-century, while small, avalanche-fed remnants near the headwall may survive for some years or decades longer.

Ultimately, this study aims to encourage future work on exceptional glaciers such as the Clariden-N Glacier. The learnings the glacier still hides on, in, below, or next to its ice is far from being revealed. So future research can quantify avalanche mass flux (multi-sensor mapping, UAV/LiDAR/snow-radar), couple debris and shading to a distributed energy-balance, survey bathymetry and implement a frontal-ablation module, further improve model sensitivity, define extinction criteria and monitor last-ice" remnants or compare with similar outliers in other mountain ranges. In the Appendix B, an exciting methodology is waiting to be put awaits you another. Alternatively, Appendix B outlines a novel methodology whose groundwork has already been completed and which now awaits application.

A
Appendix

Appendix 1: Co-registration of DEM (swissALTI3D) from 2013 (source) and 2022 (reference). Horizontal and vertical alignment of DEMs was executed using the co-registration algorithm "dem_align.py" from the "demcoreg" python script d. The histogram on the bottom left shows the distribution of elevation difference per pixel before and after the co-registration.

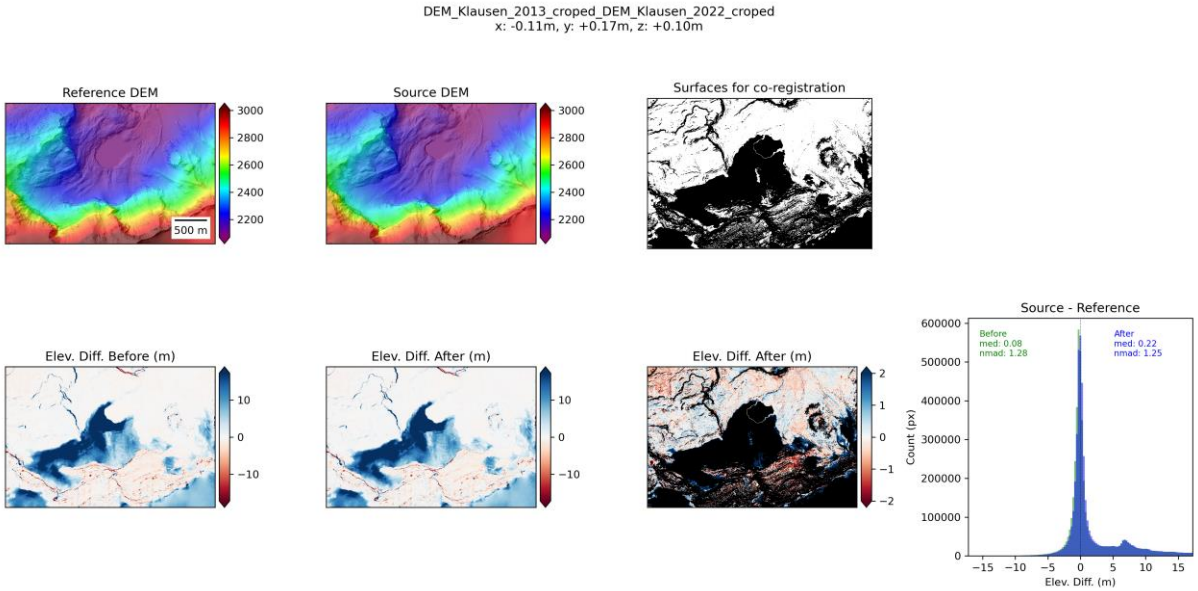

Appendix 2: The topographic shading effect and annual intensity reduction per elevation band for the glacier extent of 1951 and 2022. The topographic shading effect is expressed in hours of intercepted direct sunlight by topography per year for a point

Elevation bands	Topographic shading effect [h/y]		Annual intensity reduction [kWh/m^2]	
2000	920.08	(20.74 %)	96.55	(4.79 %)
2100	1432.38	(32.30 %)	348.91	(17.21 %)
2200	2219.52	(50.05 %)	796.67	(38.96 %)
2300	2571.86	(58.00 %)	1097.61	(53.21 %)
2400	2959.32	(66.75 %)	1147.14	(55.10 %)
2500	2852.12	(64.34 %)	914.41	(43.59 %)
Mean$_{1951}$	**1814.55**	**(40.92 %)**	**571.72**	**(27.90 %)**
2000	1319.61	(29.75 %)	186.52	(9.21 %)
2100	1656.11	(37.34 %)	415.99	(20.50 %)
2200	2313.7	(52.17 %)	845.13	(41.33 %)
2300	2594.93	(58.52 %)	1105.2	(53.58 %)
2400	3032.22	(68.39 %)	1085.04	(52.10 %)
2500	2855.04	(64.41 %)	907.64	(43.27 %)
Mean$_{2022}$	**2141.42**	**(48.29 %)**	**712.93**	**(34.76 %)**

Appendix 3: CH2018 Climate Scenarios for the Canton of Uri.

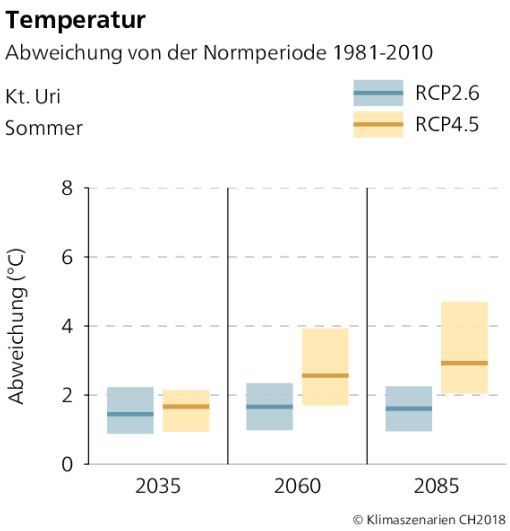

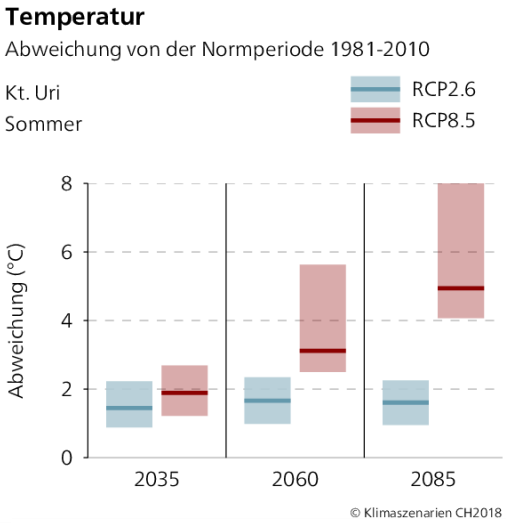

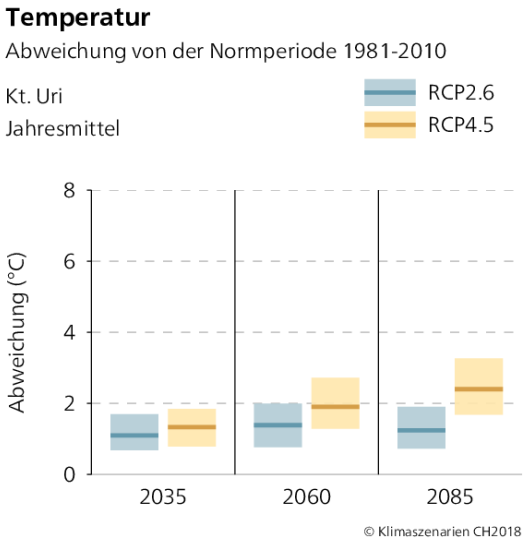

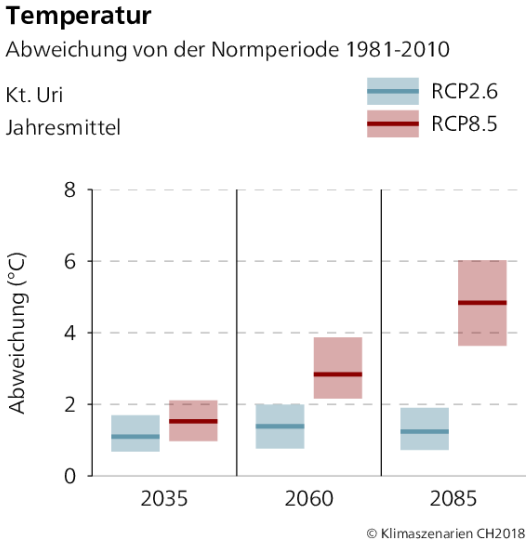

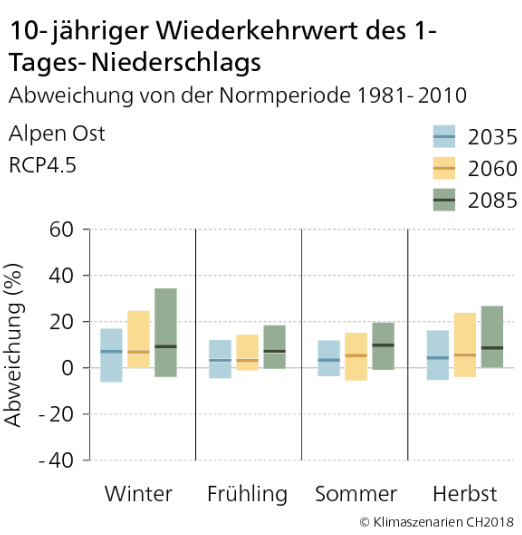

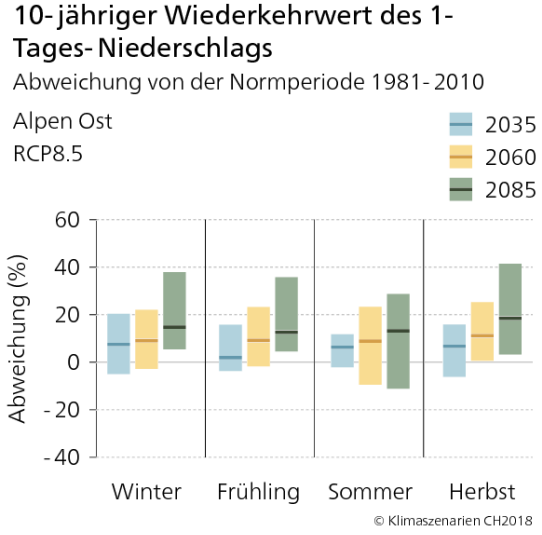

Appendix 4: Elevation difference between glacier bed (input/reference/original) and resampled with different dx.

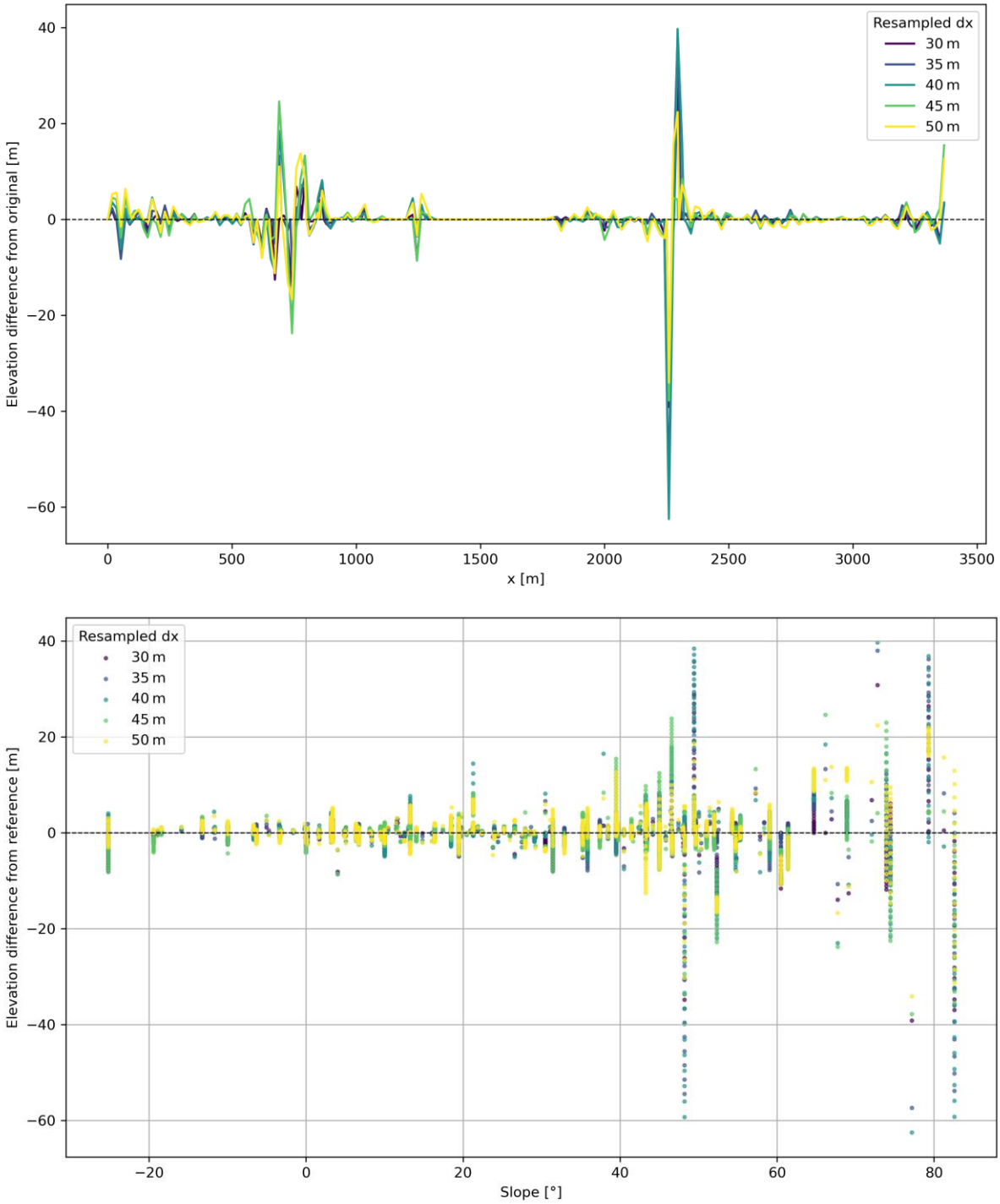

Appendix 5: Surface complexity (normalized) and slope.

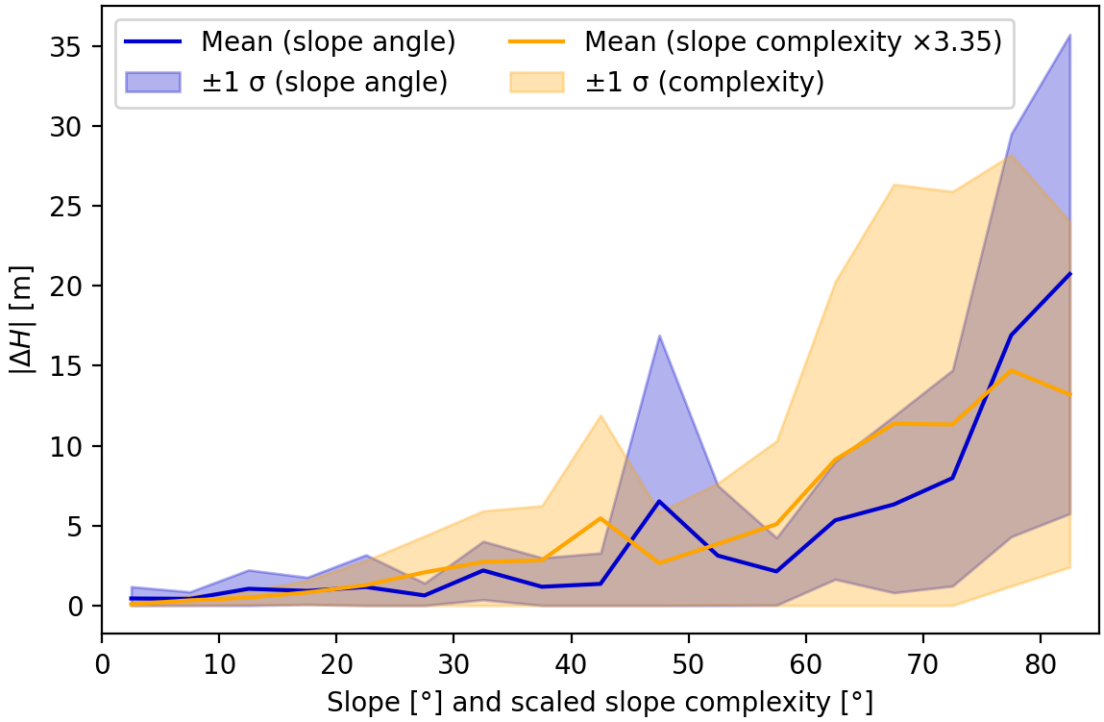

B

Photogrammetry of a glacier cave

An innovative, to my knowledge not yet documented or applied method in the literature is explored here: deriving glacier mass balance from repeated photogrammetric surveys of a glacier cave by constructing 3D models and subtracting them. The proof-of-concept was not completed for two main reasons. First, no ground control (e.g., GCPs or scale bars) was included during image acquisition, precluding calibration and validation and leaving the metric scale of the models – and thus the reported units – insufficiently constrained and potentially arbitrary. Second, the computational demand proved prohibitive for the available hardware, which made processing very time consuming (which however should not be an excuse). However, With, proper planning (referencing during acquisition) and adequate computing resources, this surely is an interesting method worth investigating.

Data availability

Nonetheless, the ~2000 images and 3D models are archived and happily made available upon request to maetti.salvi[at]gmail.com. Due to the collapse of the Klausen Grotto, the data can no longer be reproduced, which makes the further processing of the data even more desirable.

Field Work

Two photographing missions were conducted to survey the Klausen Grotto. The first took place on 26 June 2024 with approximately 500 photos taken. One the second mission on 8 November 2024 roughly three times more images were created. The larger number in November is explained by access constraints during summer: a substantial amount of snow remained inside the cave well into the summer season, making the section above the tunnel confluence inaccessible. By autumn, most of the trapped snow had melted, allowing full passage through the cave.

All images were captured with the Canon EOS 70D at a constant 18 mm focal length, which is important for image calibration and for maintaining consistent object distances. The photographs were taken in the afternoon under sunny daylight conditions. Overcast skies are generally preferred in glacier surface photogrammetry to reduce shadows and reflections, this

was of limited relevance concerning the Klausen Grotto because most images were taken inside the cave. In fact, available light was both a benefit and a limiting factor, because illumination was naturally scarcer deep inside the cave than near the entrance, making it challenging to produce uniformly high-quality images in the darker central sections. Consequently, images from the interior tend to be less sharp and exhibit lower colour depth. As a result, the colouring of the 3D model or point cloud does not fully represent reality, particularly in the cave centre.

Processing

To improve the input quality for subsequent processing, all images were reviewed individually, and those with obvious faults or insufficient quality were removed before alignment.

The processing workflow is mainly done in Agisoft Metashape. It starts with photo alignment which is performed to estimate camera locations and lens distortion parameters. Successful alignment requires sufficient image overlap and multiple viewing directions for each cave section; images that cannot be related to others will fail to align.

After alignment, a sparse point cloud consisting of tie points was generated. Tie points mark features identified in more than one image and matched across views. While this point set resembles a point cloud, it primarily serves as an aid to refine camera geometry and distortion parameters rather than a final surface. The sparse cloud typically contains inaccurate or weakly supported points that should be removed before proceeding. This cleaning was carried out using Metashape's available tools (e.g., gradual selection based on reconstruction uncertainty and reprojection error) to remove low-confidence points while retaining well-supported ones.

With a cleaned sparse cloud, a dense point cloud was then computed. To reduce noise in the dense cloud, "Filter by Confidence" was applied with a threshold of 2, which removes most noisy regions while preserving the core geometry. The dense cloud was exported to CloudCompare where additional manual cleaning of noise was done, before continuing in Agisoft with the mesh construction.

Visualisation (not done)

For visualisation, the point cloud or the mesh can be imported into Blender, to produce 3D views and renderings. Due to the aforementioned lighting limitations during acquisition, texture colours in the central cave should be interpreted with caution.

Data statement

All raw and processed, self-obtained **data** used for this thesis is available on request to maetti.salvi[at]gmail.com. All third-party data is freely (with some exceptions) available from the respective publisher.

I hereby state the use of the **ChatGPT** 4-5 for "AI assisted copy editing" and assistance in coding. "Ai assisted copy editing" is defined by Nature Editorial policies as: "AI-assisted improvements to human-generated texts for readability and style, and to ensure that the texts are free of errors in grammar, spelling, punctuation and tone. These AI-assisted improvements may include wording and formatting changes to the texts, but do not include generative editorial work and autonomous content creation." It is important to note that all content, unless otherwise stated or referenced, reflects the author's own work.

The formatting of this Thesis is based on a **template** created by Patrik Fuhrer and Pedro De Almeida (Software Engineering Group, University of Fribourg, Switzerland). The template is open source and freely available from: https://www.unifr.ch/inf/softeng/en/resources/thesis-templates.html

References

Aðalgeirsdóttir, G., Jóhannesson, T., Björnsson, H., Pálsson, F., & Sigurðsson, O. (2006). Response of Hofsjökull and southern Vatnajökull, Iceland, to climate change. *Journal of Geophysical Research: Earth Surface*, *111*(3). https://doi.org/10.1029/2005JF000388

Anderson, B., Lawson, W., & Owens, I. (2008). Response of Franz Josef Glacier Ka Roimata o Hine Hukatere to climate change. *Global and Planetary Change*, *63*(1), 23–30. https://doi.org/10.1016/j.gloplacha.2008.04.003

Arnold, N. S., Rees, W. G., Hodson, A. J., & Kohler, J. (2006). Topographic controls on the surface energy balance of a high Arctic valley glacier. *Journal of Geophysical Research: Earth Surface*, *111*(2). https://doi.org/10.1029/2005JF000426

Banerjee, A., & Shankar, R. (2013). On the response of Himalayan glaciers to climate change. *Journal of Glaciology*, *59*(215), 480–490. https://doi.org/10.3189/2013JoG12J130

Banerjee, A., & Shankar, R. (2014). *Estimating the avalanche contribution to the mass balance of debris covered glaciers*. https://doi.org/10.5194/tcd-8-641-2014

Benn, D., & Evans, D. J. (2010). Debris Entrainment and Transport. In *Glaciers and glaciation* (2nd ed., pp. 333–362). Hodder education.

Benn, D. I., & Lehmkuhl, F. (2000). Mass balance and equilibrium-line altitudes of glaciers in high-mountain environments. In *Quaternary International* (Vol. 65).

Bisset, R. R., Nienow, P. W., Goldberg, D. N., Wigmore, O., Loayza-Muro, R. A., Wadham, J. L., MacDonald, M. L., & Bingham, R. G. (2023). Using thermal UAV imagery to model distributed debris thicknesses and sub-debris melt rates on debris-covered glaciers. *Journal of Glaciology*, *69*(276), 981–996. https://doi.org/10.1017/jog.2022.116

Braithwaite, R. J. (1995). Positive degree-day factors for ablation on the Greenland ice sheet studied by energy-balance modelling. *Journal of Glaciology*, *41*(137), 153–160. https://doi.org/10.3189/s0022143000017846

De Marco, J., Carturan, L., Maset, E., Cucchiaro, S., Visintini, D., De Infanti, R., & Cazorzi, F. (2022). Century-long multi-source analyses highlight decreasing vulnerability for a small, debris-covered and avalanche-fed glacier in the eastern Italian Alps. *Journal of Hydrology*, *615*. https://doi.org/10.1016/j.jhydrol.2022.128586

DeBeer, C. M., & Sharp, M. J. (2007). Recent changes in glacier area and volume within the southern Canadian Cordillera. *Annals of Glaciology*, *46*, 215–221. https://doi.org/10.3189/172756407782871710

DeBeer, C. M., & Sharp, M. J. (2009). Topographic influences on recent changes of very small glaciers in the monashee mountains, British Columbia, Canada. *Journal of Glaciology*, *55*(192), 691–700. https://doi.org/10.3189/002214309789470851

Evatt, G. W., Abrahams, I. D., Heil, M., Mayer, C., Kingslake, J., Mitchell, S. L., Fowler, A. C., & Clark, C. D. (2015). Glacial melt under a porous debris layer. *Journal of Glaciology*, *61*(229), 825–836. https://doi.org/10.3189/2015JoG14J235

Florentine, C., Harper, J., Fagre, D., Moore, J., & Peitzsch, E. (2018). Local topography increasingly influences the mass balance of a retreating cirque glacier. *Cryosphere*, *12*(6), 2109–2122. https://doi.org/10.5194/tc-12-2109-2018

Foster, L. A., Brock, B. W., Cutler, M. E. J., & Diotri, F. (2012). A physically based method for estimating supraglacial debris thickness from thermal band remote-sensing data. *Journal of Glaciology*, *58*(210), 677–691. https://doi.org/10.3189/2012JoG11J194

Gardelle, J., Berthier, E., Arnaud, Y., & Kääb, A. (2013). Region-wide glacier mass balances over the Pamir-Karakoram-Himalaya during 1999–2011. *Cryosphere*, *7*(4), 1263–1286. https://doi.org/10.5194/tc-7-1263-2013

GLIMS. (n.d.). *GLIMS Glacier Viewer*. https://www.glims.org/maps/glims.

Gök, D. T., Scherler, D., & Anderson, L. S. (2023). High-resolution debris-cover mapping using UAV-derived thermal imagery: Limits and opportunities. *Cryosphere*, *17*(3), 1165–1184. https://doi.org/10.5194/tc-17-1165-2023

Haugen, B. D., Scambos, T. A., Pfeffer, W. T., & Anderson, R. S. (2010). Twentieth-century changes in the thickness and extent of Arapaho Glacier, Front Range, Colorado. *Arctic, Antarctic, and Alpine Research*, *42*(2), 198–209. https://doi.org/10.1657/1938-4246-42.2.198

Hauser, A. L. (2024). *Multi-Method Investigation of the Hydrological and Glaciological System of Griess Glacier on Klausenpass*.

Herreid, S., & Pellicciotti, F. (2020). The state of rock debris covering Earth's glaciers. *Nature Geoscience*, *13*(9), 621–627. https://doi.org/10.1038/s41561-020-0615-0

Hoffman, M. J., Fountain, A. G., & Achuff, J. M. (2007). 20th-century variations in area of cirque glaciers and glacierets, Rocky Mountain National Park, Rocky Mountains, Colorado, USA. *Annals of Glaciology*, *46*, 349–354. https://doi.org/10.3189/172756407782871233

Huss, M., & Fischer, M. (2016). Sensitivity of very small glaciers in the swiss alps to future climate change. *Frontiers in Earth Science*, *4*. https://doi.org/10.3389/feart.2016.00034

Huss, M., Sugiyama, S., Bauder, A., & Funk, M. (2007). Retreat scenarios of Unteraargletscher, Switzerland, using a combined ice-flow mass-balance model. *Arctic, Antarctic, and Alpine Research*, *39*(3), 422–431. https://doi.org/10.1657/1523-0430(06-036)[HUSS]2.0.CO;2

Hutchison, W., Sugden, P., Burke, A., Abbott, P., Ponomareva, V. V., Dirksen, O., Portnyagin, M. V., MacInnes, B., Bourgeois, J., Fitzhugh, B., Verkerk, M., Aubry, T. J., Engwell, S. L., Svensson, A., Chellman, N. J., McConnell, J. R., Davies, S., Sigl, M., & Plunkett, G. (2025). The 1831 CE mystery eruption identified as Zavaritskii caldera, Simushir Island (Kurils). *Proceedings of the National Academy of Sciences of the United States of America*, *122*(1). https://doi.org/10.1073/pnas.2416699122

Hynek, B., Binder, D., Citterio, M., Larsen, S. H., Abermann, J., Verhoeven, G., Ludewig, E., & Schöner, W. (2024). Accumulation by avalanches as a significant contributor to the mass balance of a peripheral glacier of Greenland. *The Cryosphere*, *18*(11), 5481–5494. https://doi.org/10.5194/tc-18-5481-2024

Joerg, P. C., & Zemp, M. (2014). Evaluating volumetric glacier change methods using airborne laser scanning data. *Geografiska Annaler, Series A: Physical Geography*, *96*(2), 135–145. https://doi.org/10.1111/geoa.12036

Juen, M., Mayer, C., Lambrecht, A., Han, H., & Liu, S. (2014). Impact of varying debris cover thickness on ablation: A case study for Koxkar Glacier in the Tien Shan. *Cryosphere*, *8*(2), 377–386. https://doi.org/10.5194/tc-8-377-2014

Kääb, A., Berthier, E., Nuth, C., Gardelle, J., & Arnaud, Y. (2012). Contrasting patterns of early twenty-first-century glacier mass change in the Himalayas. *Nature*, *488*(7412), 495–498. https://doi.org/10.1038/nature11324

Kneib, M., Dehecq, A., Brun, F., Karbou, F., Charrier, L., Leinss, S., Wagnon, P., & Maussion, F. (2024). Mapping and characterization of avalanches on mountain glaciers with Sentinel-1 satellite imagery. *Cryosphere*, *18*(6), 2809–2830. https://doi.org/10.5194/tc-18-2809-2024

Laha, S., Kumari, R., Singh, S., Mishra, A., Sharma, T., Banerjee, A., Nainwal, H. C., & Shankar, R. (2017). Evaluating the contribution of avalanching to the mass balance of Himalayan glaciers. *Annals of Glaciology*, *58*(75), 110–118. https://doi.org/10.1017/aog.2017.27

Lliboutry, L. (1974). Multivariate Statistical Analysis of Glacier Annual Balances. *Journal of Glaciology*, *13*(69), 371–392. https://doi.org/10.3189/s0022143000023169

McCarthy, M., Pritchard, H., Willis, I., & King, E. (2017). Ground-penetrating radar measurements of debris thickness on Lirung Glacier, Nepal. *Journal of Glaciology*, *63*(239), 543–555. https://doi.org/10.1017/jog.2017.18

Messmer, J., & Groos, A. R. (2024). A low-cost and open-source approach for supraglacial debris thickness mapping using UAV-based infrared thermography. *Cryosphere*, *18*(2), 719–746. https://doi.org/10.5194/tc-18-719-2024

Mihalcea, C., Mayer, C., Diolaiuti, G., Lambrecht, A., Smiraglia, C., & Tartari, G. (2006). Ice ablation and meteorological conditions on the debris-covered area of Baltoro glacier, Karakoram, Pakistan. *Annals of Glaciology*, *43*, 292–300. https://doi.org/10.3189/172756406781812104

Nicholson, L., & Benn, D. I. (2013). Properties of natural supraglacial debris in relation to modelling sub-debris ice ablation. *Earth Surface Processes and Landforms*, *38*(5), 490–501. https://doi.org/10.1002/esp.3299

Oerlemans, J. (1997). Climate Sensitivity of Franz Josef Glacier, New Zealand, as Revealed by Numerical Modeling. In *Arctic and Alpine Research* (Vol. 29, Issue 2).

Olson, M., & Rupper, S. (2019). Impacts of topographic shading on direct solar radiation for valley glaciers in complex topography. *Cryosphere*, *13*(1), 29–40. https://doi.org/10.5194/tc-13-29-2019

Østrem, G. (1959). Ice Melting under a Thin Layer of Moraine, and the Existence of Ice Cores in Moraine Ridges. *Geografiska Annaler*, *41*(4), 228–230. https://doi.org/10.1080/20014422.1959.11907953

Østrem, G., & Brugman, M. (1991). *Glacier Mass-Balance Measurements: A Manual for Field and Office Work* (Vol. 4). National Hydrology Research Institute.

Rounce, D. R., Hock, R., McNabb, R. W., Millan, R., Sommer, C., Braun, M. H., Malz, P., Maussion, F., Mouginot, J., Seehaus, T. C., & Shean, D. E. (2021). Distributed Global Debris Thickness Estimates Reveal Debris Significantly Impacts Glacier Mass Balance. *Geophysical Research Letters*, *48*(8). https://doi.org/10.1029/2020GL091311

Rubin, V. C., & Kent Ford, W. (1970). (c) 1970. The University of Chicago. All rights reserved. *The Astrophysical Journal*, *159*.

Scherler, D., Bookhagen, B., & Strecker, M. R. (2011). Hillslope-glacier coupling: The interplay of topography and glacial dynamics in High Asia. *Journal of Geophysical Research: Earth Surface*, *116*(2). https://doi.org/10.1029/2010JF001751

Schmidt, L. S., Aoalgeirsdóttir, G., Pálsson, F., Langen, P. L., Guomundsson, S., & Björnsson, H. (2019). Dynamic simulations of Vatnajökull ice cap from 1980 to 2300. In *Journal of Glaciology* (Vol. 66, Issue 255, pp. 97–112). Cambridge University Press. https://doi.org/10.1017/jog.2019.90

ShadeMap. (2024). *ShadeMap*.

Sold, L., Huss, M., Machguth, H., Joerg, P. C., Vieli, G. L., Linsbauer, A., Salzmann, N., Zemp, M., & Hoelzle, M. (2016). Mass balance re-analysis of findelengletscher, Switzerland; benefits of extensive snow accumulation measurements. *Frontiers in Earth Science*, *4*. https://doi.org/10.3389/feart.2016.00018

Sugiyama, S., Bauder, A., Zahno, C., & Funk, M. (2007). Evolution of Rhonegletscher, Switzerland, over the past 125 years and in the future: Application of an improved flowline model. *Annals of Glaciology*, *46*, 268–274. https://doi.org/10.3189/172756407782871143

Sutherland, J. L., Carrivick, J. L., Gandy, N., Shulmeister, J., Quincey, D. J., & Cornford, S. L. (2020). Proglacial Lakes Control Glacier Geometry and Behavior During Recession. *Geophysical Research Letters*, *47*(19). https://doi.org/10.1029/2020GL088865

Winstral, A., Elder, K., & Davis, R. E. (2002). Spatial Snow Modeling of Wind-Redistributed Snow Using Terrain-Based Parameters. *Journal of Hydrometeorology*, *3*(5), 524–538. https://doi.org/10.1175/1525-7541(2002)003<0524:SSMOWR>2.0.CO;2

Zekollari, H., Huss, M., Farinotti, D., & Lhermitte, S. (2022). Ice-Dynamical Glacier Evolution Modeling—A Review. In *Reviews of Geophysics* (Vol. 60, Issue 2). John Wiley and Sons Inc. https://doi.org/10.1029/2021RG000754

Zekollari, H., Huss, M., Schuster, L., Maussion, F., Rounce, D. R., Aguayo, R., Champollion, N., Compagno, L., Hugonnet, R., Marzeion, B., Mojtabavi, S., & Farinotti, D. (2024). Twenty-first century global glacier evolution under CMIP6 scenarios and the role of glacier-specific observations. *Cryosphere*, *18*(11), 5045–5066. https://doi.org/10.5194/tc-18-5045-2024

Zemp, M., Thibert, E., Huss, M., Stumm, D., Rolstad Denby, C., Nuth, C., Nussbaumer, S. U., Moholdt, G., Mercer, A., Mayer, C., Joerg, P. C., Jansson, P., Hynek, B., Fischer, A., Escher-Vetter, H., Elvehøy, H., & Andreassen, L. M. (2013). Reanalysing glacier mass balance measurement series. *Cryosphere*, *7*(4), 1227–1245. https://doi.org/10.5194/tc-7-1227-2013

Personal Declaration

I hereby declare that the submitted thesis is the result of my own, independent work. All external sources are explicitly acknowledged in the thesis.

Winterthur, 29.08.2025, Mattia Salvi